UCLouvain

FACULTE DES SCIENCES

Faculté des sciences

Evaluating the effect of a new antiviral compound on the interaction between ACE2 and the SARS-CoV-2 spike protein

Author: Deven Rubens

Supervisors: Prof. David Alsteens,
Prof. Patrice Soumillion

Readers: Prof. Corentin Claeys Bouuaert,
Prof. Thomas Michiels,
Prof. René Rezsohazy

Academic year: 2022-2023

Master's thesis presented in order to obtain the Biochemistry and Molecular and Cell Biology diploma with a research orientation in biological sciences

Acknowledgements

First of all, I would like to thank my supervisors Prof. David Alsteens and Prof. Patrice Soumillion for allowing me to do my master thesis between their two laboratories (nBioPhysics lab and Biochemistry and Genetics of Microorganism lab [BGM]).

Thank you for always listening to me when I came to you to discuss this project or future opportunities.

My presence in two laboratories allowed me to meet a lot of people who all helped me to develop this work. I like to think that this work is a collaborative work between several teams than a personal work.

I would like to thank in particular Joseph Nader (FYMO) and Damien Evrard (BGM) who supported me in many reflections and took me under their wings for my development within a laboratory.

I would also like to thank Dr. Ankita Ray and Kimberley Durlet for their support during my master thesis and their help with the experiments. Similarly, a big thank you to all the people at the nBio lab and the BGM who were available to help and discuss this project.

A mention to the whole team of master students at the BGM with whom I shared many pleasant moments. Special mention also to Théo Degand, Veronica Gonzalez Gonzalez and Marie Guijarro Guijarro for accompanying me during this master and with whom I shared many incredible memories.

I would like to thank Victoria Lievens who knew how to support me and help me in the most difficult moments from an academic and personal point of view. A very small mention to Alexander Cosslet, who has been there since primary school. Nothing more to say about him.

Thanks also to my family (QLF), whom I hope I have made proud during all these years. Thanks for the support despite years of not finding my way. I have it and I will hold on to it.

Thanks to myself and my resilience. It is important to continue to develop and heal your wounds. Next step is an internship at Cambridge University. What does the future hold?

Finally, I would also like to thank the readers of this master thesis, Prof. Corentin Claeys Bouuaert, Prof. Thomas Michiels, and Prof. René Rezsohazy for accepting to be part of the jury and for the time they dedicated to this function.

Abstract

The Severe Acute Respiratory Syndrome Coronavirus 2 (SARS-CoV-2) is a single-stranded RNA virus that emerged in December 2019 from Wuhan city (China). Since then, the epidemic caused by its spread has impacted the whole world and an impressive number of variants emerged of which seven have been considered as Variant of concern (VOC) by the World Health Organization. The illness caused by SARS-CoV-2 is the coronavirus disease 2019 (COVID-19) and has officially caused the death of almost 7 million people.

In a race against time, vaccine development has accelerated with the first large-scale production for human of RNA vaccines. However, other antiviral compounds have also been studied as concerns raised about vaccine protection against VOCs given the impressive number of mutations they carry. A better understanding of how SARS-CoV-2 enters the host cell to establish its infection and proliferation is key to developing our knowledge of this family of viruses that has already triggered epidemics twice since the beginning of the 21th century.

In order to spread, viruses need to enter a host cell and hijack their cellular machinery to replicate themselves. The SARS-CoV-2 virus enters host cells through interactions between its spike glycoprotein (S), divided into two sub-units (S1-S2), and host cell surface molecules. The main host cell surface molecule interacting with S is the angiotensin-converting enzyme 2 (ACE2) receptor although other functional receptors have been described for SARS-CoV-2. Therefore, several parties are involved in mediating the entry of SARS-CoV-2 into the host cell which means that many targets exist for the development of antiviral compounds.

In this context, recent work has identified two lactam molecules, Lactavir and pyroglutamate, as compounds with antiviral effects on SARS-CoV-2 infection. Moreover, these molecules are similar to the pyroglutamyl function present on many extracellular proteins following the cyclisation of an N-terminal glutamine, including the S protein and the ACE2 receptor.

The work carried out during this thesis focused on identifying the mechanism of action of Lactavir and its effect both on *in vitro* interactions between S1 and ACE2, and on the *in cellular* infectivity of Spike pseudotyped Vesicular Stomatitis Viruses (S*VSVs) in a human cell line (A549). Also, we aimed at gaining some insights into the importance of the N-terminal pyroglutamate (pGlu) function present on the S protein for the S1-ACE2 interaction.

Concerning the *in vitro* experiments, we verified the sequence of two commercial proteins by mass spectrometry and confirmed the sequence of S1(Val) but established that the sequence given for the S1(pGlu) protein was truncated. By using BioLayer Interferometry (BLI), we found that the addition of Lactavir has no impact on the interaction between S1 and ACE2 regardless the S1 used. Also, we measured that the presence or absence of the N-ter pGlu residue on S1 has no impact on the affinity constant of the S1-ACE2 interaction. We highlight also that Lactavir does not act as an inhibitor on ACE2 enzymatic activity.

For the *in cellular* experiments, we improved the VSV production and we determined that there are no significant effects of Lactavir on the infectivity of VSVs pseudotyped with the S from the Wuhan strain. Preliminary results with a VOC (Delta) were obtained but no conclusions can be drawn for these.

Overall, this thesis has improved our knowledge concerning the impact of Lactavir on the Spike-ACE2 interaction. These results can be used for further research to identify and characterize antiviral compounds.

Table of contents

1. Introduction 1
1.1 SARS-CoV-2 characteristics 1
1.1.1 Taxonomy 1
1.1.2 Genome characteristics 2
1.1.3 Physiopathology 3
1.1.4 Classification and variants 3
1.2 SARS-CoV-2 entry process 5
1.2.1 Life cycle and replication steps 5
1.2.2 The Spike glycoprotein 7
1.2.3 The ACE2 receptor 9
1.2.4 Others actors or attachment factors 10
1.3 Identification of a new antiviral drug 11
1.4 Pyroglutamylation process 12
1.5 Biolayer interferometry (BLI) technology: 13
1.6 Vesicular stomatitis virus (VSV) technique 16
2. Objectives and strategies 17
3. Materials and Methods 18
3.1 *In vitro* experiments 18
3.1.1 Purified compounds 18
3.1.2 Mass Spectrometry (MS) 19
3.1.3 BLI design 20
3.1.4 Enzymatic assay design 22
3.2 *In cellular* experiments 23
3.2.1 Main reagents used: 23
3.2.2 VSV production and optimisation 23
3.2.3 Infectivity assay 25
4. Results and discussion 26
4.1 *In vitro* experiment 26
4.1.1 Validation of S1 sequence by MS 26
4.1.2 Evaluation of the S1-ACE2 interaction with BLI 28
4.1.3 ACE2 inhibition assays 33
4.2 *In cellular* experiments 35
4.2.1 VSV production 35
4.2.2 Infectivity assays 35
5. Conclusion and perspectives 38
6. Appendix 41
7. Bibliography 49

List of acronyms and symbols

ACE2	Angiotensin-converting enzyme 2
ARDS	Acute respiratory distress syndrome
ASGPR1	Asialoglycoprotein receptor 1
BLI	BioLayer Interferometry
BMBL	Biosafety in Microbiological and Biomedical Laboratories
Cf	Final concentration
CH	Central helix
CT	Cytoplasmic tail
CTD1/2	C-terminal domain ½
CoVs	Coronaviruses
COVID-19	Coronavirus disease 2019
DC-SIGN	Dendritic Cell-Specific Intercellular adhesion molecule-3-Grabbing Non-integrin (DC-SIGN) also known as Cluster of Differentiation 209 (CD209)
E	Enveloppe protein
ER	Endoplasmic reticulum
FFPR	Fusion-peptide proximal region
FP	Fusion peptide
HCoVs	Human coronaviruses
HIV	Human immunodeficiency viruses-1
HR1/2	Heptad repeat ½
HS	Heparan sulfate
isoQC/gQC	Golgi resident glutaminyl cyclase
ICU	Intensive care units

Ifs	Interferons
k_a	Association rate constant
k_d	Dissociation rate constant
K_D	Affinity constant or equilibrium dissociation constant
kDa	kilodalton
KREMEN1	Kremen protein 1
L	Large polymerase protein
L-SIGN	Lymphocytes-Specific Intercellular adhesion molecule-3-Grabbing Non-integrin (L-SIGN) also known as Cluster of Differentiation 209 L (CD209L)
LCM	Lymphocytic choriomeningitis virus
M	Membrane protein or Matrix protein
MERS-CoV	Middle east respiratory syndrome coronavirus
MLV	Murine leukemia virus
nsp	Non-structural proteins
N	Nucleocapsid
N-RNA	Nucleoprotein coated with RNA
NTD	N-ter domain
NRP1	Neuropilin-1
ORF	Open reading frame
pp	Polyprotein
pGlu/pE	Pyroglutamate
P	Phosphoprotein
RAS	Renin-angiotensin-aldosterone system
RBD	Receptor Binding Domain

RBM	Receptor Binding Motif
RG	Risk group
RNP	Ribonucleoprotein
RT-LF	Real-time and label free
RTC	Replication and transcription complex
ssRNA	Single stranded RNA
sQC/QC	Secretory glutaminyl cyclase
S	Spike protein
SARS-CoV	Severe acute respiratory syndrome coronavirus
SARS-CoV-2	severe acute respiratory syndrome coronavirus 2
SIV	Simian immnodeficiency virus
SPR	Surface plasmon resonance
SRB1	Scavenger receptor class B member 1
TM	Transmembrane domain
TMPRSS2	Transmembrane protease serine 2
TRF	Thyrotropin-releasing factor
VOI	Variant of interest
VOC	Variant of concern
VUM	Variant under monitoring
VSV	Vesicular Stomatitis virus
WHO	World Health Organization

1. Introduction

The introduction aims at providing the important concepts related to this work. The first part of the introduction describes the severe acute respiratory syndrome coronavirus 2 (SARS-CoV-2) characteristics including taxonomy, genome characteristics, physiopathology of the coronavirus disease 2019 (COVID-19) and variants classification. The second part summarizes the SARS-CoV-2 entry process with its life cycle, replication steps and necessary protagonists. Then the emphasis is placed on the identification of a new antiviral drug as well as the pyroglutamylation process. Finally, the basic principles of the *in vitro* and *in cellular* techniques used during this master thesis are explained.

1.1 SARS-CoV-2 characteristics

1.1.1 Taxonomy

Coronaviruses (CoVs) are enveloped, positive- and single-stranded RNA (ssRNA) viruses that form a family of important pathogens for humans, mammals such as livestock or domestic animals and avian species. [1–3] The *Coronaviridae* family is within the order of *Nidovirales* and the suborder of *Cornidovirineae*. The associated subfamilies are *Letovirinae*, *Pitovirinae* and *Orthocoronavirinae* that can be further divided in four genera: *alphacoronavirus*, *betacoronavirus*, *gammacoronavirus* and *deltacoronavirus* (See Figure 1). [4] The two first genera are known to exclusively infect mammalian species and their intermediate hosts, which carries the virus without being too affected, are rodents and bats while the two latter have a larger host spectrum and their intermediate hosts are birds. [1–3]

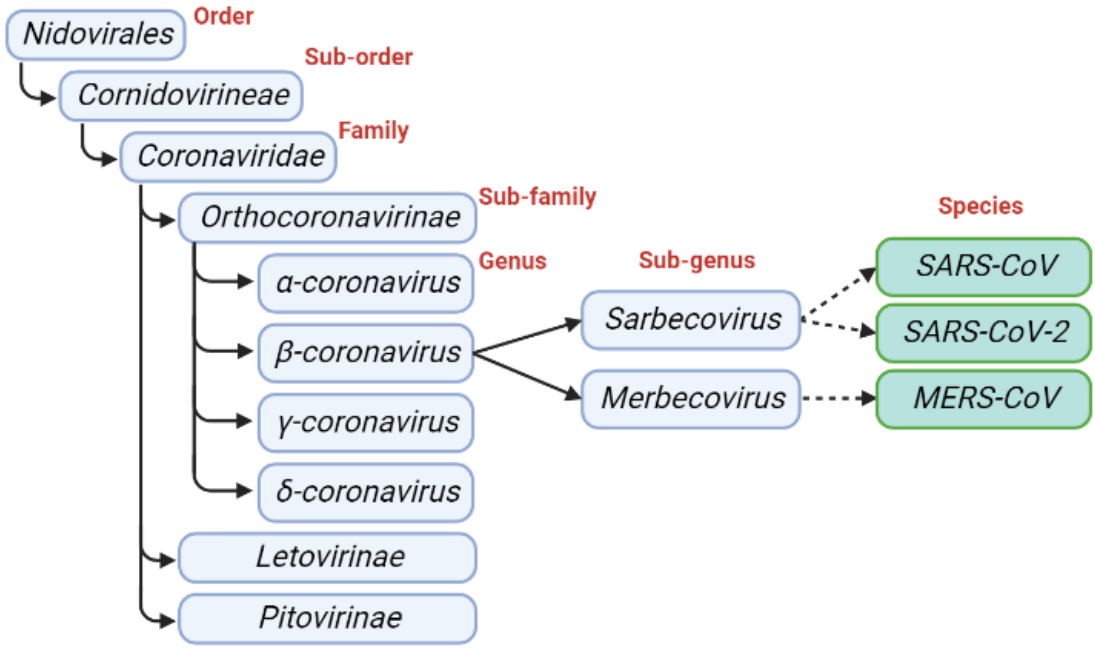

Figure 1 : Representation of a taxonomic tree for the SARS-CoV, SARS-CoV-2 and MERS-CoV species of viruses. Created with BioRender based on International Committee on Taxonomy of Viruses (ICTV)[4]

To date, seven human coronaviruses (HCoVs) have been characterized with four of them causing mild-to-moderate respiratory infections (HCoV-NL63, HCoV-229E, HCoV-HKU1 and HCoV-OC43). Since 2002, three highly pathogenic coronaviruses causing severe respiratory pathologies with a significant mortality rate have emerged. In 2002, severe acute respiratory syndrome coronavirus (SARS-CoV) has appeared in China and spread to 29 countries while in 2012, the middle east respiratory syndrome coronavirus (MERS-CoV) popped up in Saudi Arabia and spread to 27 countries. More recently, in December 2019, the SARS-CoV-2 was discovered in the city of Wuhan in China and developed in a pandemic all over the world in less than four months. The sequence identity shared between SARS-CoV-2 and SARS-CoV is 75-80% which accelerated the research and development of a rapid medical answer.

Those three viruses are part of the *betacoronavirus* genus and are similar concerning the general genome organization and life cycle but their receptors and internalization manner may differ from one to another. [2,3,5,6] The initial reservoir of SARS-CoV-2 is not unambiguously identified but it is known that bats and pangolin are reservoirs for alpha- and beta-coronaviruses. Similar coronaviruses sharing up to 96.2% of genome sequence with the SARS-CoV-2 genome have been detected in bats population near the initial epicentre of the pandemic (RaTG13).[2,3,5–7] However, it is unknown if there was an animal intermediate host allowing the evolution of the virus before infecting humans and, moreover which animal was the intermediate host. Wildlife animals and domesticated or laboratory animals are two possible trails of intermediate hosts after reports attested SARS-CoV-2 infection in pangolin, dogs, cats and ferrets. [2,8,9]

1.1.2 Genome characteristics

SARS-CoV-2 nucleocapsid (N) contains a ~30kb positive ssRNA genome capped in 5', polyadenylated in 3' and every open reading frame (ORFs) is flanked by 5' and 3' untranslated regions. Two-third of the ORFs encodes for non-structural proteins (nsp1-16) involved in virus replication and assembly while the last third encodes for four structural proteins (nucleocapsid, membrane (M), envelope (E), spike proteins (S)) and other accessory proteins (See Figure 2). The ORFs encoding for the accessory proteins are interspersed between the ORFs encoding the structural proteins. The accessory genes show high variability among coronaviruses and are non-essential for the viral replication but are supposed to have an important role in the host cells. For instance, SARS-CoV-2 genome contains accessory genes involved in the disruption of the cellular machinery with consequences such as apoptosis of the infected cell or inhibition of interferons (IFs) and host antiviral response. [2,6]

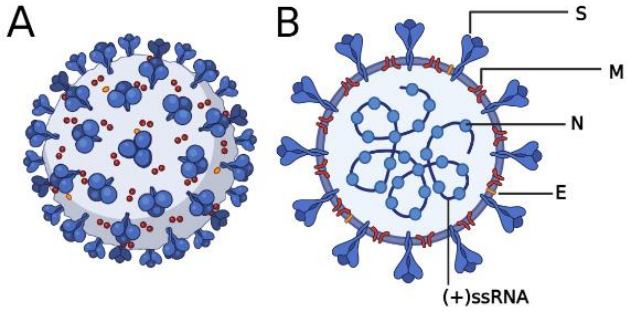

Figure 2 : Representation of the SARS-CoV-2 virion. A) 3D graphical representation B) Cross-section representation with associated elements (see Genome characteristics). Created with BioRender.

1.1.3 Physiopathology

The infection by SARS-CoV-2 leads to respiratory pathologies and lung injuries call coronavirus disease 2019 (COVID-19). The typical symptoms are fatigue, dry cough and fever that may lead, in severe case, to pneumonia, dyspnea, acute respiratory distress syndrome (ARDS) and/or multi-organ failure resulting in the necessity use of intensive care units (ICU). The incubation period last for 1 to 14 days (most commonly being around 5 days) and a severe disease develops around eight days after illness onset and the death arise around 16 days after onset.[2,8,9] The bronchial epithelial cells, pneumocytes and upper respiratory tract cells are the main target of the SARS-CoV-2 virus due to the high expression of proteins related to the infection mechanism (See section 1.2.2 and 1.2.3).[7]

Asymptomatic and symptomatic patients are the main source of infection through aerosol spread even though the virus is sensible to the environment where alteration of the envelope occurs leading to a decrease in the effectiveness of cell entry. [2,10] All age groups in the population are susceptible to SARS-CoV-2 infection, but the clinical need differs by age. The median age of infection is around 50 years and before that, the infected person is more likely to be asymptomatic (<10 years) or to develop a mild disease (from 10 to <50 years). Over 60 years old, the infected person is more likely to develop a severe disease and after 68 years to develop a critical disease leading to death.[2,8,9]

To date, there are some drug treatment for COVID-19 such as remdesivir, molnupiravir or paxlovid to manage the symptoms and reducing the risk of being seriously ill. However, vaccination is considered as the main tool to control this disease in the long-term.[11–13]

1.1.4 Classification and variants

The original strain of SARS-CoV-2 from Wuhan has undergone several genetic variations during its spread all over the globe and the World Health Organization (WHO) labelled the most threatening variants along with the Greek alphabet instead of the scientific names produced by GISAID, Nextstrain and Pango. This labelling has a purpose of using non-stigmatising and easy-to-pronounce terms. [12,14]

Variants of interest (VOI), variants or concern (VOC) and variants under monitoring (VUM) are highly supervised internationally and this classification is adjusted periodically to represent the evolution of the pandemic. A VOI is designated if it has been demonstrated that he no longer poses a major risk to global public health compared to other SARS-CoV-2 variants. A VOC is a variant that shows an increase in transmissibility or in virulence or alternatively a decrease in the effectiveness of the public health system or the social measures (vaccines, therapeutics and diagnostics). In addition, a VUM is a variant with suspected threatening genetic changes that can affect virus characteristics and that may pose a risk in the future.[5,12]

To this date, seven variants of SARS-CoV-2 virus received a lot of attention and were at one time on the list of VOCs. Following the Greek alphabet, they are identified as Alpha (B.1.1.7), Beta (B.1.351), Gamma (P.1), Delta (B.1.617.2), Lambda (C.37), Mu (B.1.621) and Omicron (B.1.1.529). The latter and some of its descendent lineages are the last variants classified as a VOC. Omicron variant is the current dominant variant circulating globally and it has led to significant subvariants emerging from intra-Omicron evolution. An increasing diversity of this VOC can be hazardous to the global threat and it explains why the WHO developed a specific category regrouping every Omicron subvariants under monitoring.[12]

In the context of this work, I worked with the S from the initial Wuhan strain and from the Delta and Omicron variants:

The Delta variant (B.1.617.2) possess impressive features with 23 new mutations compared to the alpha strain. It emerged in India in December 2020 and spread out faster than previous variants at that time (See Figure 3 for Belgium example). This variant is more pathogenic because its S protein binds with higher affinity to ACE2 receptor, thanks to the L452R mutation [15], and escape the immune system due to E484Q and T478K mutations.[16–18] Moreover, patients infected with the Delta variant required more frequently hospitalization in intensive care unit (ICU) due to more severe symptoms.

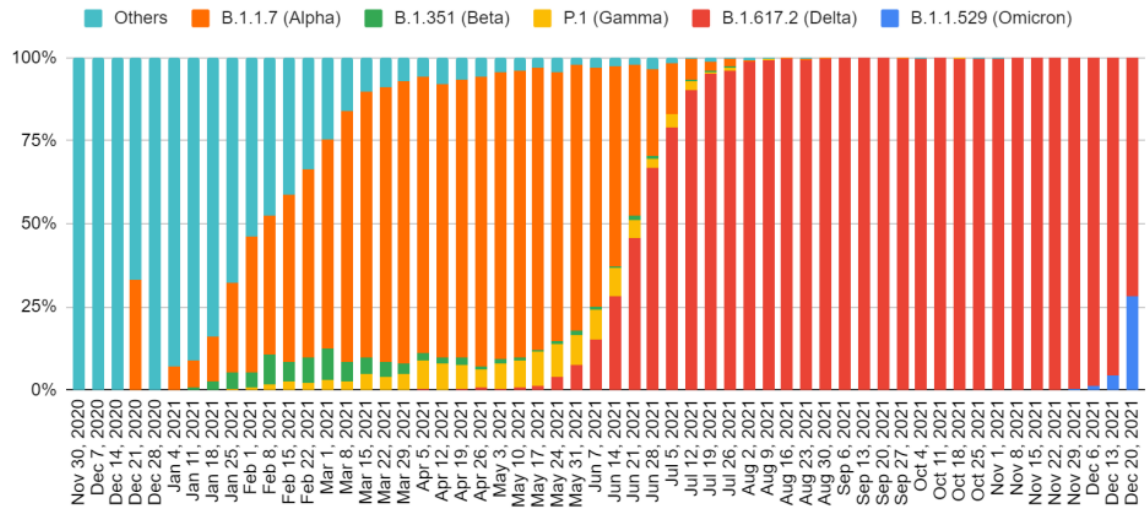

Figure 3 : Weekly representation of the frequency of VOC in Belgium for 2021 by using a baseline surveillance network using whole genome sequencing (WGS) approach. VOCs take over from each other as they develop. The Omicron variant started to spread in Belgium from 24/11/2021. Figure from Laenen et al. (2022)[19]

The Omicron variant (B.1.1.529) emerged in South Africa in November 2021 and has an unusual high number of 32 mutations in its S protein, 15 of them being located in the receptor binding domain (RBD). This variant enhance its transmissibility through three approaches: enhance ACE2 binding (Q498R, N501Y), enhance cleavage at the S1/S2 junction (See Section 1.2.2) (H655Y, N679K, P681H) and increasing viral load (R203K and G203R).[5,20] Currently, this variant and its numerous sub-lineages are dominant over all other variants and followed by the WHO with care. Omicron was reported to be more frequent in the younger age range while having a lower risk of hospitalization and death than with the previous variants.

The global response in creating vaccines has helped to slow the number of infections and the spread of COVID-19, but the question of vaccine efficacy in relation to different variants arose as soon as variants with many mutations appeared. The promise of being able to modify the RNA sequences of mRNA-based-vaccines according to virus mutations has also been a major argument for the development of this industry and the scale-up of it allowed the distribution of millions of doses in a record time compared to the classical vaccine techniques such as viral-vectored vaccines, inactivated virus-bases vaccines and recombinant proteins.[11] Fortunately, all COVID-19 vaccines have a high efficacy against the Wuhan strain (89.1%) and the VOCs (Delta: 74-80.1%, Omicron: 88%) after two doses of SARS-CoV-2 vaccination.[5,21,22]

1.2 SARS-CoV-2 entry process

This section covers the life cycle of the SARS-CoV-2 virus and the replication steps after membrane fusion. A detailed description of the spike glycoprotein and ACE2 receptor as well as other actors implicated will conclude this section.

1.2.1 Life cycle and replication steps

Entry of SARS-CoV-2 into cells is mediated by the transmembrane glycoprotein S which forms homotrimers (See Section 1.2.2) and by binding to the angiotensin-converting enzyme 2 (ACE2) receptor on the host cell surface (See Section 1.2.3) [23–26]. The crossing of the plasma membrane is a complex phenomenon due to the amphipathic nature of the lipid bilayer. Concerning viral entry, endosomal entry (See Figure 5.1A) and cell surface entry (See Figure 5.1B) are the two main modes known by the scientific community. For SARS-CoV-2, the endosomal entry pathway requires binding to ACE2 at the cell surface inducing endocytosis of the virions. Within the acidic environment of the endolysosome (See Figure 5.1C), the cathepsin L proceed to cleave the S2' site and induce fusion of the viral and endolysosome membranes (See Figure 5.1D).[24]

The cell surface entry pathway requires binding to ACE2 at the cell surface and the transmembrane protease serine 2 (TMPRSS2) to cleave the S2' site and induce the fusion of the viral and cell membranes (See Figure 5.1A).[24] Surprisingly, the Omicron variant expresses suboptimal cleavage of the S1/S2 site and a reduced ability to utilise TMPRSS2 due to multiple mutations on its S protein. Thus, this variant is associated with a shift in cell tropism as it needs less the expression of TMPRSS2 to infect a cell.[27]

Inside the infected cell, the viral gene expression starts with the translation of *orf1a* and *orf1b* from the positive strand RNA genome (See Figure 5.3). The polyprotein1a (pp1a) is encoded by ORF1a while polyprotein1ab (pp1ab) is formed by continuous translation of ORF1a and ORF1b due to a ribosomal programmed frameshift. This leads to a stoichiometry between pp1a and pp1ab (1,4-2,2 pp1a for 1 pp1ab) and to the release of sixteen nsp after proteolytic cleavage (See Figure 4)

This cleavage enables nsp1 to target the host cell machinery, nsp 2-11 to provide necessary supporting function to the viral replication and transcription complex (RTC) in addition to nsp 12-16 that compose this complex having an RNA proofreading function based on RNA-modifying and RNA-processing enzymes (See Figure 5.4).

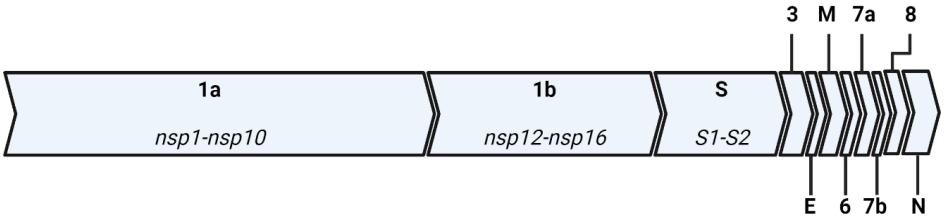

Figure 4 : Representation of the open reading frames (ORFs) of the SARS-CoV-2 genome. Created on BioRender.

The establishment of the viral RTC is one limiting step for virus replication which starts with the synthesis of negative-strand copies of the viral genome that serves as direct templates for the production of full-length new positive-strand genomes (See Figure 5.5). The translation of those will either generate more RTCs or be packaged in new virions thanks to the structural proteins produced in the host endoplasmic reticulum (ER) and the golgi apparatus (See Figure 5.6). The nucleocapsid and the structural proteins will be assembled and be ready to bud from the infected cell to infect other cells (See Figure 5.7 & 5.8).

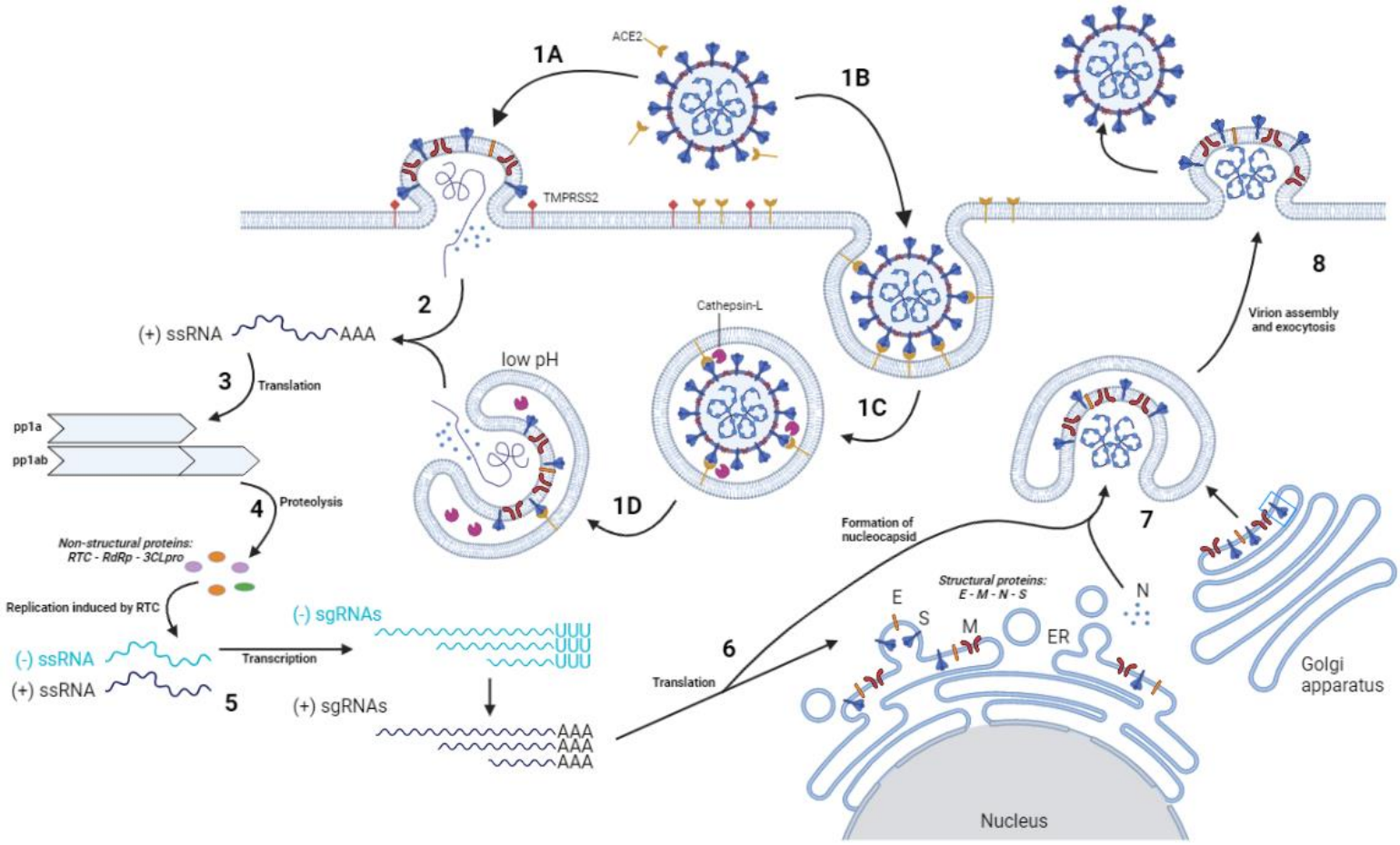

Figure 5 : Replication cycle of SARS-CoV-2 virus. ***1.*** *After binding to the host cell membrane, two main entry pathways are possible* ***2&3.*** *After penetrating into the host cell, the SARS-CoV-2 virus will release its positive ssRNA that will be partially translated into pp1a and pp1ab.* ***4.*** *The nsp will form the RTC after proteolysis and enables the full gRNA replication in a negative strand.* ***5.*** *This negative gRNA will be use as a template for the transcription and generates several negative subgenomic RNA (sgRNAs).* ***6.*** *Those negative sgRNAs will be translated into positive sgRNAs and either form the nucleocapsid of future viruses (virions) or processed in the ER-Golgi system of the host cell to form the structural proteins (sp) of the virions.* ***7&8.*** *In any case, the sp will assemble and incorporate the nucleocapsid before budding and being released to infect other cells. [RTC= Replication and transcription complex / 3CLpro = 3C-like protease / RdRp = RNA-dependant RNA polymerases] Created on BioRender and base on Hu et al. (2021) [8]*

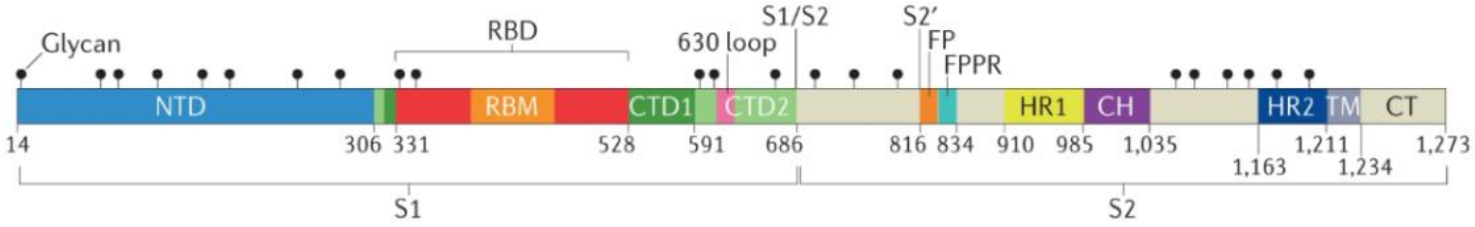

Figure 6 : Representation of the full-length SARS-CoV-2 S protein. Black circle represents the N-glycans sites with a high occupancy (>95%) while O-glycans sites are not represented. The O-glycosylation sites are numerous but only two of them shows a relative high occupancy (T323 and S325) on the S protein.[28] Figure from Jackson et al. (2022)[24]

1.2.2 The Spike glycoprotein

The homotrimer S protein of SARS-CoV-2 is composed of three monomeric type I membrane protein heavily glycosylated with 22 N-linked glycans and an approximate size of 180 kilodalton (kDa). The exact number of N-/O-glycosylation sites vary according to the mutations pattern in the different variants. [28–30] Previous studies shows that those sugars have a real importance in the interaction between the S protein and other receptors such as DC-/L-SIGN[1]. On the other hand, those glycosylation serves as a shield to mask the protein from antibodies and protect the virus from the immune response.[28–32]

Each S protein (1273 residues) consists of a cytoplasmic tail, a transmembrane domain and two subunits which are S1 and S2. The S1 subunit, from residue 14 to 686, comprises the N-terminal domain (NTD), the RBD and two C-terminal domains (CTD1 and CTD2) composed of β-strands. In the Wuhan strain, CTD2 possess an important disordered structure designated as the 630 loop (from residues 620 to 640) when the residue 614 is an aspartic acid (D).[24,33,34] A major difference between the Wuhan strain and other VOCs is the presence of a D614G substitution which stabilizes greatly the S trimer compared to the Wuhan trimer. The ordered 630 loop enhance ACE2-binding affinity and the entry efficiency of the virus.[24,33–35]

The RBD emerges from antiparallel β-strands constituting the two CTDs which intrinsically links those three partners. The RBD recognizes specifically the ACE2 receptor via the receptor binding motif (RBM) and, therefore, is a critical target for antiviral compounds and antibodies [26,36]. However, the NTD can also be targeted for infection neutralisation [23,37,38]. Each RBD can be found in a closed or open conformation (See Figure 7). The RBDs in closed conformation are gathered in the centre of the trimer, occluding the RBM and making it unreachable for the ACE2 receptor. The RBM is exposed only in the open conformation while CDT1 and NTD moves to accommodate this exposition. [24,39] The transition from close to open conformation is made through a semi-open state capable of binding ACE2 and stabilizing the RBD in the final open conformation.[40,41]

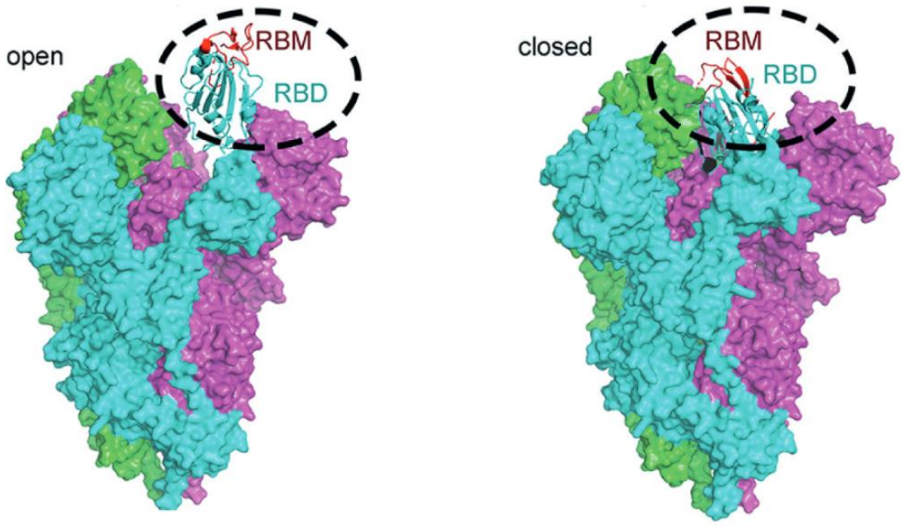

Figure 7 : Cryo-EM structure of the SARS-CoV-2 S protein in the open and closed conformations. In the open state, there is only one open RBD domain. Each of the monomer is depicted in a different color (green, cyan and magnet). RBM and RBD are shown respectively in red and cyan cartoon. PDB accession codes: open state (6VYB) and close state (6VXX). Modified from Ning et al (2021)[41]

[1] Dendritic Cell-Specific Intercellular adhesion molecule-3-Grabbing Non-integrin (DC-SIGN) also known as Cluster of Differentiation 209 (CD209)/Lymphocytes-Specific Intercellular adhesion molecule-3-Grabbing Non-integrin (L-SIGN) also known as Cluster of Differentiation 209 L (CD209L)

The S2 subunit, from residue 686 to 1273, comprises a hydrophobic fusion peptide (FP), a structural element known as fusion-peptide proximal region (FFPR), a central helix (CH) between two heptad repeats (HR1, HR2), a transmembrane domain (TM) and a cytoplasmic tail (CT) (See Figure 6). The purpose of the S1 subunit is to bind the receptor(s) on the host cell while the function of the S2 subunit is to fuse the virus and host cell membranes.[24,26]

This huge S protein will go through posttranslational cleavages by host cell proteases at two major cleavage sites: the S1/S2 site, at the junction between the S1 and S2 subunits, and the S2' site in the S2 subunit (See Figure 6).[24,34,42–45]

The first is a multibasic site (Arg-Arg-Ala-Arg) also called furin-like cleavage site which is absent in SARS-CoV and other coronaviruses. The cleavage by furin of this site is also called "priming" of the S protein because it happens during the biosynthesis of the S protein and the virion formation. This cleavage destabilises the S protein and the S1 and S2 subunits will held together by noncovalent interactions and this is suspected to promote the binding to Ace2. [23,24,34,46]

The second is a cleavage site recognized by either the TMPRSS2 at the cell surface or by cathepsins in the endolysosome. TMPRSS2 is present in the respiratory, gastro-intestinal and urogenital epithelium and its importance in respiratory virus infection like SARS or influenza virus is well known.[24,47,48]

The cleavage of the S2' site occurs after the S protein binds to the receptor and not during the biosynthesis nor the intracellular transport. More importantly, the cleavage of FCS and S2' is mandatory for coronavirus infection. This cleavage results in large-scale conformational changes for the S2 subunit between prefusion and postfusion conformation depending on the detachment of the S1 subunit (See Figure 8)

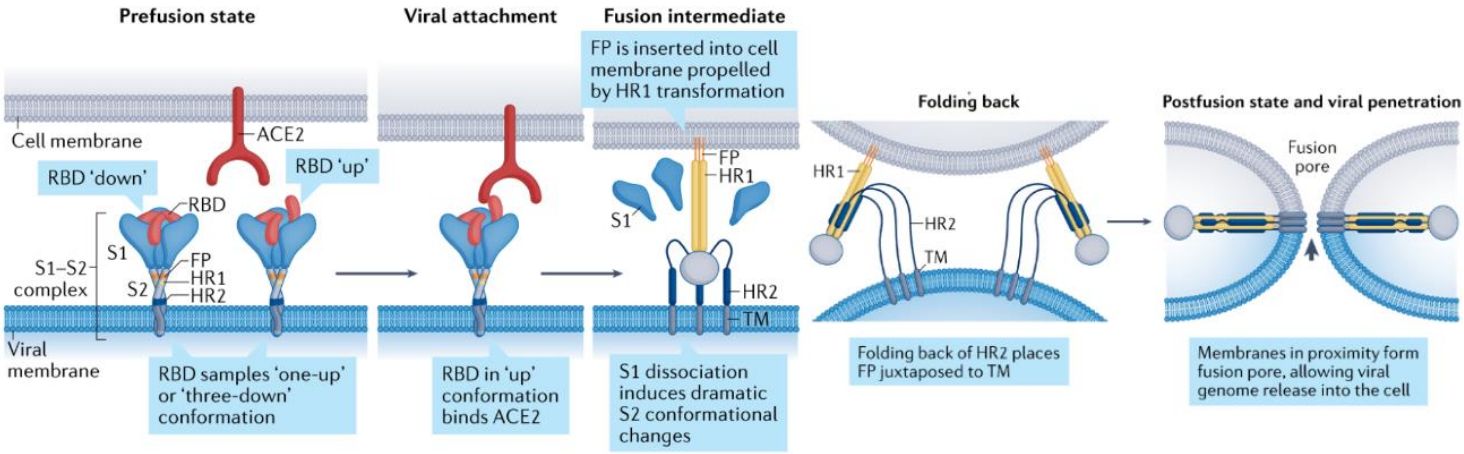

Figure 8 : Schematic representation of the transition between the prefusion conformation to the postfusion conformation. The RBDs of the prefusion S trimer are alterning between the "down" (close) and "up" (open) conformations. Since one "up" RBDs binds the ACE2 receptor, it will expose the S2' cleavage site to TMPRSS2 cleavage, allowing the release of conformational constraints on the FP and a cascade of refolding events in S2. The refolding of HR1 will trigger the penetration of FP in the host cell membrane while the S1 subunit will dissociate from the S2 subunit. HR2 rearrangements will lead to postfusion structure of S2, bringing the two membranes together and facilitating the fusion of membranes and viral entry.[24,44] Modified from Jackson et al. (2022).

After cleavage, the HR1 will refold and insert the FP through the target cell membrane. This FP (residues 816-857) contains many hydrophobic, alanine and glycine residues, as well as a disulfide bond and is capable of penetrating into the host bilayer. The insertion of the FP is supposedly the same as with other coronaviruses. Thanks to this insertion, a central three-stranded helix (HR1) will be circled with three single-stranded helixes (HR2) forming a fusogenic hexameric core structure called six-helix bundle structure (6-HB).[34,49] This stable postfusion structure will bring together the host membrane and the viral membrane facilitating the membrane fusion and creating fusion pores (See Figure 8).[50] Several studies have also demonstrated the ability of the S1 subunit of the S protein to disrupt the lipid bilayer of the host membrane and thus facilitate virus penetration. These disruptions occur through non-specific interactions that alter the composition of the bilayer. [51,52]

1.2.3 The ACE2 receptor

ACE2 is an acid carboxypeptidase removing a single amino acid from the C-terminus of its substrates. It is composed of 805 amino acids and its first half contains a single metallopeptidase domain with a zinc-binding motif (HEXXH) at the catalytic site. The second half is the C-terminal part of the enzyme including the transmembrane domain. The physiological role of ACE2 is to convert angiotensin-I and angiotensin-II into angiotensin-(1-9) and angiotensin-(1-7) respectively. This enzyme is involved in the renin-angiotensin-aldosterone system (RAS) and the downregulation of ACE2 during SARS-CoV-2 infection is allegedly implied in disease severity due to the similarities between SARS-CoV and SARS-CoV-2.[24,53]

The interaction between the RBD of S protein and ACE2 has been described by using cryo-electron microscopy[54], dynamic simulations[55] and atomic force microscopy[56] among other techniques. This interaction is based on a network of hydrophilic interactions involving the side chains of 20 residues from ACE2 and 17 residues from the RBD (See Figure 9).

The interplay between the ACE2 receptor and the SARS-CoV-2 and SARS-CoV RBDs are almost identical even though several residues in the RBD of new VOCs have mutated.[57,58] An interesting paradox must be noted, despite several mutations and an extra ACE2-interacting residue (Lys417), enhancing the affinity of the RBD for ACE2, the SARS-CoV-2 S trimer does not bind ACE2 as effectively as the SARS-CoV S trimer.[24,25,59]

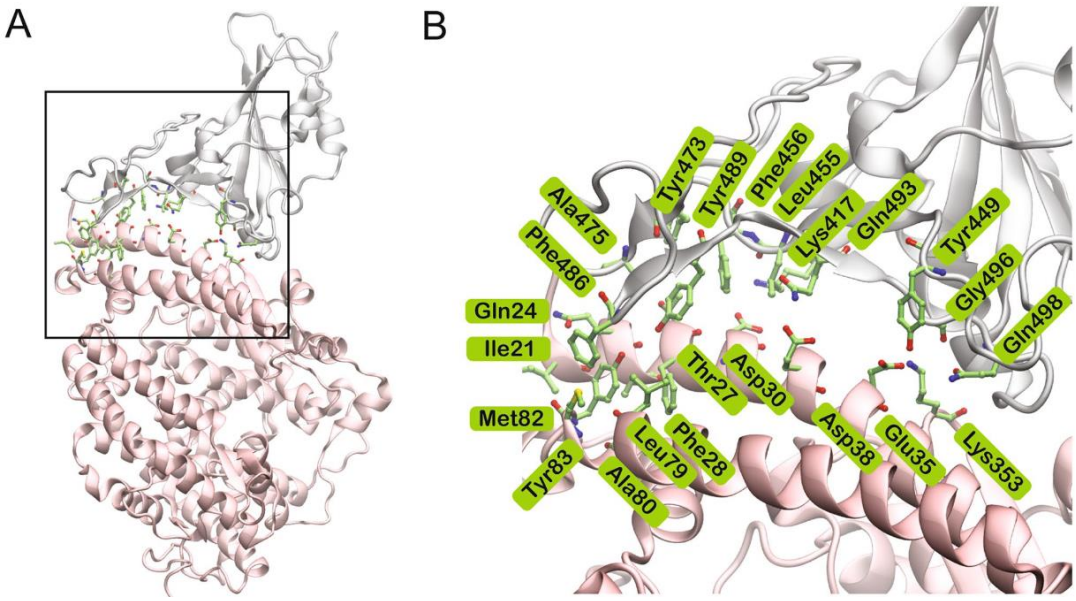

Figure 9 : A) Structure of the RBD from SARS-CoV-2 (grey) bound to ACE2 (pink). B) Enlarged box showing the main interacting residues in the interface. From Vijayan & Ali (2020)[55]

The distribution of ACE2 expression throughout the respiratory tract follows the SARS-CoV-2 infection gradient with a high expression in the nasal ciliated cells being infected during the early stage of infection, followed by the upper bronchial epiderma and ending with a lowest expression in the type II alveolar cells. The highest expression of ACE2 are in the thyroid, the heart muscle, kidneys, the small intestine, and the colon. [53,60–62] Those viral growth sites are consistent with the observed transmission of coronaviruses via the faecal-oral route in addition to the respiratory route.[24]

1.2.4 Others actors or attachment factors

Since SARS-CoV-2 infects many organs, alternative or cooperating candidate receptors are investigated as contributors to viral dissemination in vivo. This section briefly describes the ones that have been established as biologically relevant. We can classify them in two categories: cell attachment factors for SARS-CoV-2 virus and alternatives receptors to ACE2.[3]

The first category regroups receptors known to bind the S protein and whose depletion or increased expression impacts the SARS-CoV-2 infection **in presence** of ACE2. Those co-factors are heparan sulfate (HS)[63,64], scavenger receptor class B member 1 (SRB1)[65], C-type lectins (DC-SIGN/L-SIGN)[32,66–68] and neuropilin-1 (NRP1)[69,70].

The second category contains functional receptors enabling SARS-CoV-2 infection **in absence** of ACE2. Those are Kremen protein 1 (KREMEN1)[2] and asialoglycoprotein receptor 1 (ASGPR1)[71]

Regardless of the receptor, there is a need for more studies on the specificity of these receptors in their interactions with the SARS-CoV-2 virus in order to understand more precisely the essential first steps of virus attachment to the cell membrane. This, together with the distribution of all these receptors within the organs, will probably allow us to better understand the broad infectious spectrum of the virus (See Section 1.1.4).

Box 1: Cell lines definition and $TCID_{50}$ measurement

Caco-2 is an immortalized cell line of colorectal adenocarcinoma cells and is used as a model of the intestinal barrier as it differentiates spontaneously in a heterogeneous population of intestinal epithelial cells.[72]

Calu-3 is an immortalized cell line of lung adenocarcinoma cells and used as a model of the human epithelial airway.[73]

Vero cell is a lineage of cell isolated from kidney epithelial cells from an African green monkey. They are widely used as host cells for growing viruses due to their interferon deficiency.[74]

HEK293 is an immortalised cell line of human embryonic kidney 293. They are easy to grow in culture and to transfect. The HEK293T variant is more efficiently transfectable with DNA.[75]

A549 is an immortalized cell line of adenocarcinomic human alveolar basal epithelial cells used as a model of alveolar type II pulmonary epithelium.[76]

$TCID_{50}$ is the median tissue culture infectious dose and assess the threshold where the amount of virus dilution required to induce a cytopathic effect in 50% of cultured host cells is reached. Based on this, it is possible to calculate the Infectious Unit per milliliter (IU/mL) of the virus solution which represents the number of virus particle capable to infect a host cell.

[2] Kremen (kringle containing protein marking the eye and the nose) proteins

1.3 Identification of a new antiviral drug

A new antiviral molecule of interest has been discovered in the research group of Pr. Patrice Soumillion. It was named Lactavir deriving from its lactam structure paired with its antiviral properties.

Lactavir is generated by intramolecular condensation of carbocysteine (S-(carboxymethyl)-*L*-cysteine), a simple amino acid used in some mucolytic syrups (See Figure 10). Suspecting a COVID-19 illness, a researcher in the group was surprised his fast recovery after taking up he syrup. Literature analysis revealed some sparse data reporting antiviral effect of carbocysteines and a collaboration with Prof. Steeve Boulant in Heidelberg (Germany) was then initiated.

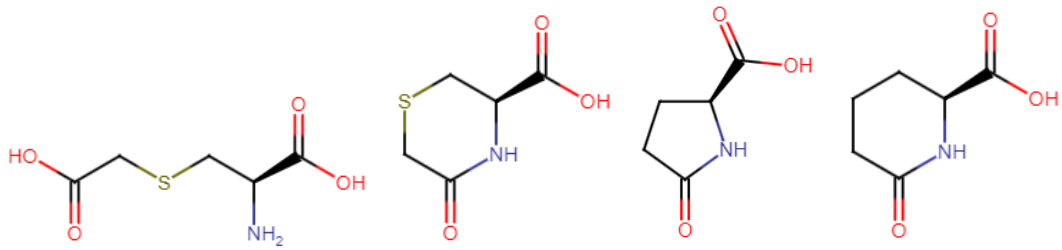

Figure 10 : From left to right: structure of carbocysteine, Lactavir, pyroglutamate and Lactam3.

As a first step, the effect of Lactavir on SARS-CoV-2 infection of two types of cells were assessed (Caco-2 and Calu-3). Those experiments highlight the fact that carbocysteine is not affecting the virus infectivity while Lactavir was able to reduce SARS-CoV-2 infectivity by 20-30% at a concentration as low as 50nM. However, antiviral effect was not observed when using Vero cells. SARS-CoV-2 virus is known to enter by the endosomal pathway in Vero cells while it is fusing to the plasma membrane in the two other tested cell types (Caco-2 and Calu-3). As a result, those experiments provide some clues on the mode of action of the antiviral compound and it suggest an activity during the membrane fusion steps (See Appendix 1).

In an effort to better understand the mechanism of action of the Lactavir, two other lactams were found with similar antiviral activity. These are pyroglutamate (pGlu/pE) and Lactam 3 which are Lactavir without the sulphur or with a CH_2 instead of a sulphur atom respectively (See Figure 10).

In a second step, the virus replication after 24h drug incubation on primary bronchial and nasal cells was assessed by using qPCR and TCID50 tests. This allowed us to confirm that carbocysteine does not have an inhibition effect on viral replication while Lactavir and other similar compounds (pGlu and Lactam 3) caused a strong inhibition effect of almost 50% for the qPCR test and a diminution in virus production up to three orders magnitude (See Appendix 2A & 2B).

Lastly, the capacity of Lactavir to inhibit syncytia formation due to the S protein fusogenic properties was tested. A syncytium is a multinucleate cell resulting from multiple cell fusions sharing a single cytoplasm. In the case of SARS-CoV-2 infection, infected cells can express the S protein at their plasma membrane and therefore bind and fuse to other cells leading to syncytia formation. [77] The results show a significant diminution of cell fusion when treated with micromolar Lactavir concentration confirming the putative impact of the antiviral compound in viral membrane fusion mechanism (See Appendix 2C).

1.4 Pyroglutamylation process

The pyroglutamate (pGlu/pE) formation is a common and well-known post-translational modification at the N-terminus of peptides and proteins. It implies a glutamate (Glu) or a glutamine (Gln) N-ter residue that will undergo a cyclization releasing H_2O (for Glu) or NH_3 (for Gln) (See Figure 11).[78–80] The cyclization will form a γ-lactam (five membered ring cyclic amide) at the N-terminus extremity. Although cyclisation can occur spontaneously at a low rate, in vivo pyroglutamylation of both Glu and Gln is catalysed by two types of glutaminyl cyclases.[78,79,81]

The first one, a Golgi resident glutaminyl cyclase named isoQC or gQC catalyzes the pGlu formation after cleavage of the protein peptide signal. The second one, secretory glutaminyl cyclase (QC/sQC), is present extracellularly.[81]

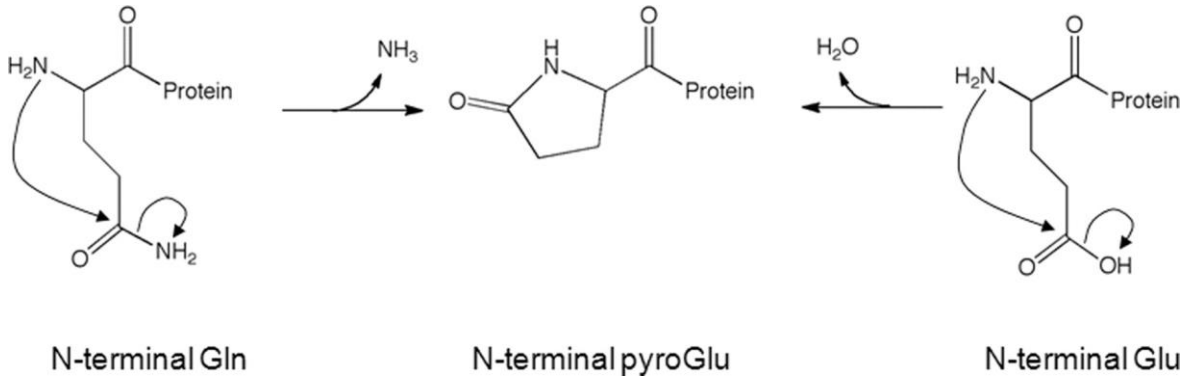

Figure 11 : Schematic representation of a N-terminal pyroglutamate from a glutamine residue (Gln) or from a glutamate residue (Glu). Figure from Liu et al. (2011)[78]

The pyroglutamyl residue is present on numerous extracellular and membrane anchored proteins and, just by looking at the first residue after signal peptide cleavage, we can assume the potential presence or absence of this chemical function.

This post-translational modification is important for a wide range of proteins from the CX3CL1 mediating adhesion and cell migration in the inflammatory process[82] to mammalian thyrotropin-releasing factor (TRF) receptor recognition specificity.[83].

In our study, the sequence of the S protein contains a signal peptide from 1 to 13 residues and the 14th residue is a glutamine.[84] The sequence of the ACE2 contains a signal peptide from 1 to 17 residues and the 18th residue is also a glutamine[84]. Therefore, we can assume that both protein S and the ACE2 receptor are pyroglutamylated by the isoQC/gQC *in cellular* when expressed in mammalian cells while TMPRSS2 is not.

1.5 Biolayer interferometry (BLI) technology:

With the huge development of the biopharmaceutical industry, specifics tools to characterize biophysical and kinetics properties of molecular interactions are becoming more and more important and interesting for a higher-throughput analysis. [85–88] In this context, real-time and label free (RT-LF) platforms are gaining ground against more classical techniques using labelling reagents.[85,89] A RT-LF platform makes easy the measurement of association/dissociation rates (k_a/k_d) and equilibrium dissociation constant (K_D) of ligand-analyte interaction without using labelling reagents. It helps reducing the time to set up the experiment and it minimizes the potential impact of a label on the binding interaction. [85–88]

There are two main well-known RT-LF platform:

1) Surface Plasmon Resonance (SPR) in which the ligand is immobilized on the surface of a sensor while the solution containing the analyte will flow in contact with the ligand through a microfluidic system. [87,88,90]
2) Biolayer Interferometry (BLI) technology is a platform that allows the analysis of crude material without worrying about clogging because it does not require the use of a microfluidic system. [85,88] It uses biosensors coated with immobilized ligand that are dipped into wells containing soluble material including analytes without any washing step needed such as in filter binding or pull-down assay. This allows the characterization of transient and/or very weak interactions while not disturbing the reaction equilibrium. [85–88,90,91]

The BLI technology consists of the analysis of the reflection of an incident polychromatic white light beam sent through a specific fibre-optic disposable biosensor. The biosensor tip is industrially coated with a capture tag (Ni-NTA, ProteinA, Streptavidin…) allowing the immobilization of a ligand equipped with a linking tag (His tag, Fc domain, biotin…) capable of interaction with a free analyte in solution.

The white light is directed towards two interfaces separated by a thin layer at the tip of the optical fibre. The first interface is an internal reference layer and the second one is the biolayer itself which is the interface between the immobilized protein and the surrounding solution at the surface of the tip (See Figure 12).

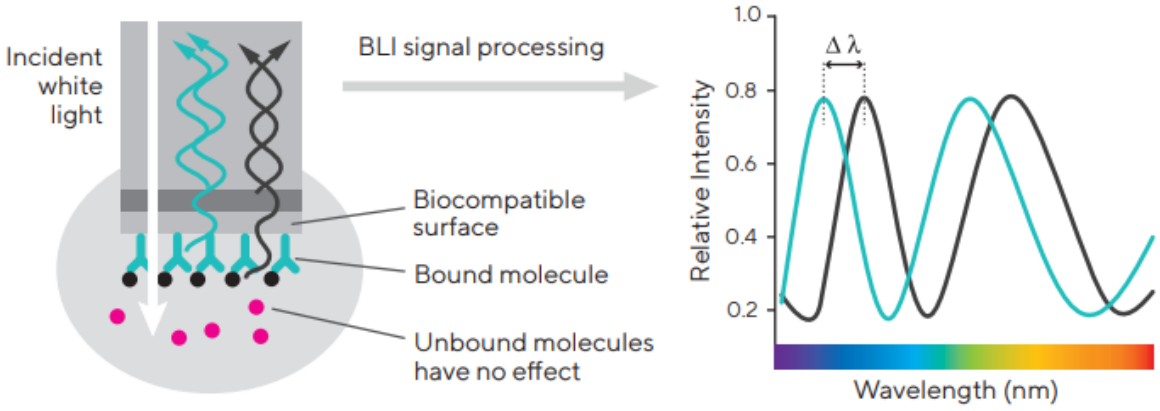

Figure 12 : Focus on the optical fiber of the biosensor tip and the BLI signal process. See main text for more information. From Sartorius

The light reflected along the optical fibre will be collected by a spectrometer where some wavelengths will show constructive interference and others destructive interference. The binding of an analyte to an immobilized ligand on the biolayer will change the optical thickness of the molecular layer (in nm) at the tip of the biosensor and cause a change in the phase of the reflected light. The resulted spectral shift in the interference pattern ($\Delta\lambda$ in nm) can be monitored over time allowing to derive kinetic information about the interaction mechanism. This interaction can be further detailed by testing modified analyte or by changing analysis parameters such as buffer, pH, analyte concentration or temperature. [85]

The different steps of a typical BLI assay are described in Figure 13. The biosensor is moved from one well to another by a robotic arm and the sample plate is constantly in orbital motion to avoid the effects of diffusion on kinetic measurements and to induce flow across the stationary biosensor surface. This technology is non-destructive for the sample and there is no need to label or modify the sample protein.

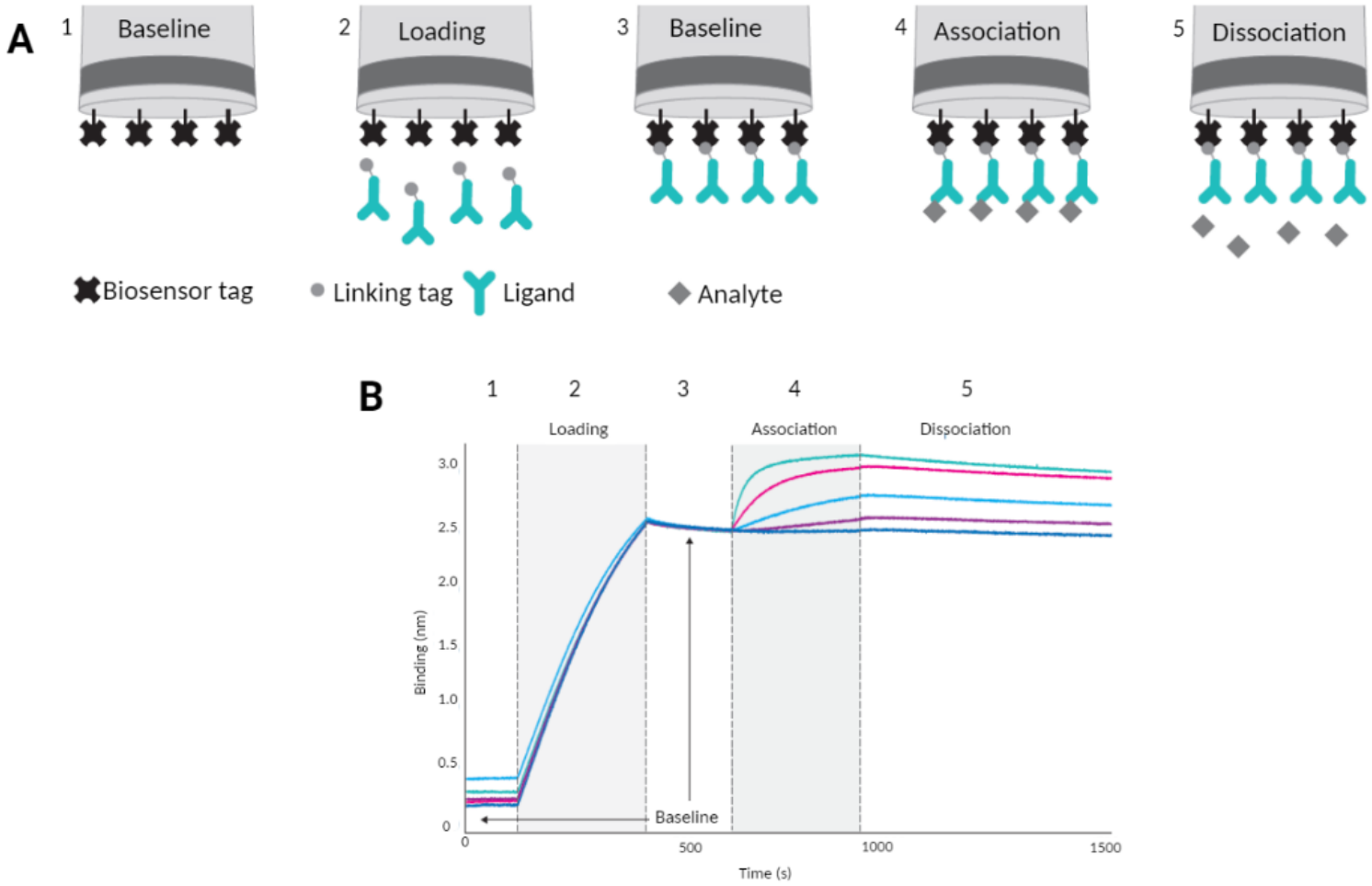

Figure 13 : ***A)*** *Representation of the biosensor surface during the five classical steps during a BLI experiment with Ni-NTA or Protein A biosensors.* ***B)*** *Typical data acquisition with the program from Sartorius.* ***1)First baseline:*** *This step is necessary to ensure that there is no signal drift and to make sure that the biosensor used and the buffer solution used do not interact.* ***2)Loading step:*** *The loading step is where the biosensors are dipped into a well containing the ligand in solution that will interact with the tag on the surface of the biosensor.* ***3)Second baseline:*** *Biosensors coated with the ligand are dipped in a buffer solution to assess any drifts and identify the shift (in nm) induced by the loading of ligand.* ***4)Association step:*** *Biosensors linked with the ligand are dipped into wells containing the analyte in solution and the two interactants (ligand-analyte) are free to associate with each other providing us information over the dynamics of the binding interaction.****5) Dissociation step:*** *During the dissociation phase, the biosensors are dipped in a buffer solution and the signal is monitored as the complexes break down over time.*

Box 2: Definition of the kinetic parameters of a protein-protein interaction

Association rate constant (k_a [$M^{-1}.s^{-1}$]) determines the concentration of AB complex formed par second in a 1 molar solution of A and B.

Dissociation rate constant (k_d [s^{-1}]) determines the fraction of complexes dissociating per second. It is a good indicator of the stability of the interaction; the smaller is the k_d, the more stable is the complex.

Affinity constant **or** equilibrium dissociation constant (K_D [M]) represents the ratio of the dissociation rate constant (k_d) on the association rate constant (k_a).

By using BLI technique, we can characterize protein-protein interaction but we have to be careful with the terms used. The first interaction partner is the ligand that will be load on the biosensor and immobilized while the analyte is the second partner and is free in solution. Both are interaction partners and the best way to assess the interaction is to perform the experiment two times with every partner in the immobilized position.

If it is assumed that one ligand molecule (A) interacts with one analyte molecule (B) independently and conversely, then the binding model is a simple 1:1 interaction involving an association rate constant "k_a" and a dissociation rate constant "k_d" at equilibrium (See Equation 1). The complex (AB) formation follows a pseudo-first-order kinetics where the association rate constant "k_a", the dissociation rate constant "k_d" and the concentration of the unbound analyte are establishing the observed rate constant "k_{obs}" which reflects the combined association and dissociation of two binding partners (See Equation 2).

By using equations fitting the association and dissociation curves obtained during the experiment (See Figure 13B steps 4 and 5), it is possible to determine first the "k_d" from the dissociation curve because the concentration of analyte is equal to zero during this step based on Equation 2, "k_d" is then equal to "k_{obs}". Next, we can further can evaluate the "k_a" from the association curve by using the pre-calculated "k_d" value in Equation 3.

Using "k_d" and "k_a" previously obtained, we can determine the equilibrium dissociation constant "K_D" of the protein-protein interaction (See Equation 4).

Equation 1 : Molecular interaction at equilibrium

$$A + B \underset{k_d}{\overset{k_a}{\rightleftharpoons}} AB$$

Equation 2 : Details of the observed rate constant

$$k_{obs} = k_a \times [\text{Analyte}] + k_d$$

Equation 3 : Details of the association constant k_a

$$k_a = \frac{k_{obs} - k_d}{[Analyte]}$$

Equation 4 : Details of the affinity constant K_D

$$K_D = \frac{[A]x[B]}{[AB]} = \frac{k_d}{k_a}$$

The "K_D" is a measurement of the strength of the bound established between the ligand and the analyte. A small "K_D" indicates a tight interaction between the analyte and the ligand. Moreover, it corresponds to the concentration of analyte at which half of the ligand binding sites are occupied at equilibrium if the analyte is in large access compared to the bounded ligand. It is mandatory to know the concentration of analyte to be able to calculate the "K_D" and the "k_a" but not for the "k_d" that is concentration independent. The "k_d" can be useful for classifying solutions of analyte of unknown concentration based on off-rate.

1.6 Vesicular stomatitis virus (VSV) technique

Following the recommendation of *Biosafety in Microbiological and Biomedical Laboratories (BMBL)*, an existing classification includes 4 possible risk groups (RG) (See Appendix 3).[92]

Viruses belonging to RG 3 (such as SARS-CoV-2, lymphocytic choriomeningitis virus (LCM) or retroviruses like human immunodeficiency viruses-1 [HIV] and simian immunodeficiency virus [SIV]) are a major threat for human and animal health and the democratisation of their study in less dangerous conditions can only be beneficial. [93] One way to overcome their dangerousness in the lab is by pseudotyping the envelope of a non-pathogenic virus with a protein from the pathogenic one (such as the Spike protein). The outcome is a pseudovirus which is a recombinant viral particle composed of envelope proteins derived from the pathogen and modified genes so that they are incapable to produce surface proteins on their own. They can infect susceptible cells, but they will be unable to produce viable viruses due to the lack of genes for their surface proteins. [93] Thanks to that, it is possible to safely handle pseudoviruses in BSL-2 laboratories. [93,94]

To prepare envelope-pseudotyped viruses, there are several possible vectors (also called packaging systems) coming from retroviruses like the lentivirus (derived from HIV-1), the murine leukemia virus (MLV) or the vesicular stomatitis virus (VSV).[94] In our case, a previous researcher at the nanoBioPhysics lab was already working with the VSV packaging system which is known as a versatile tool to produce pseudotyped viruses. For example, this system has already been used for the study of envelope proteins from different viruses like Ebola Virus, Hepatitis C virus, etc. [93–95] The VSV particle is bullet-shaped and possess a lipid envelope including trimeric glycoprotein (protein G). There is a helical nucleocapsid protein, also known as ribonucleoprotein (RNP) and coated with RNA (N-RNA), associated with large polymerase protein (L) and accessory phosphoprotein (P) in the centre of the viral particle. The last structural component is the matrix protein (M) located underneath the membrane and associated with the N-RNA (See Figure 14). The RNA genome of the VSV is unsegmented and possess a negative polarity which, if naked, is not infectious.[93,95]

In the context of this work about the SARS-CoV-2 virus, I will use VSVs whose gene encoding G protein, essential for their ability to infect cells, is deleted (VSVs-ΔG). Those VSVs-ΔG will be pseudotyped with the S protein of SARS-CoV-2 (S*VSVs-ΔG) and their capacity to infect mammalian cells through the fusogenic activity of the S protein will be evaluated.

Box 2: Main replication steps of VSVs

The viral replication cycle of the VSV can be separated in three steps but should be considered as a continuum of events.

1) Attachment, entry and uncoating of VSV in the host cell

Due to his wide capacity of infection, it is supposed that the VSV may be able to attach multiple surface molecules due to its G protein. It will be internalized via clathrin-dependent endocytosis and hand over to an early endosome where a pH threshold will spark a conformational change promoting the viral and host cell membranes fusion.

2) Replication cycle of VSV in host cytoplasm

The host translation machinery is used to translate the viral mRNAs and each of the viral protein plays a specific role in the hijacking of the host cellular machinery.[96]

3) Assembly and budding of the VSV from the host cell

Acquisition of a lipid envelope coated with G proteins.

For more information, see Whelan S.P.J. (2008)[96]

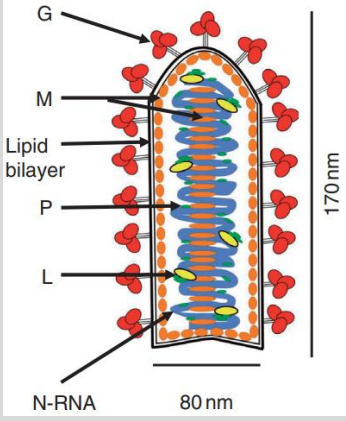

Figure 14 : Representation of a VSV virion. See main text for legend. Image from Whelan S.P.J.

2. Objectives and strategies

This master thesis is inspired by preliminary results obtained by Prof. Soumillion in collaboration with the team of Prof. Steeve Boulant when he was at the University Hospital of Heidelberg.

Together, they discovered that small delta- and gamma-lactams, including Lactavir and pyroglutamate, are endowed with antiviral activity against SARS-CoV-2 (See Section 1.3). Even if antiviral activity is clearly demonstrated and points toward a reduced membrane fusion, the mechanism underlying the observed effect is not precisely understood.

Given the presence of a pyroglutamyl residue at the N-terminus of both S protein and the ACE2 receptor, the aim of this work is to investigate a possible link with the activity of the small lactams.

Three objectives will be pursued in this master thesis:

1) Evaluate a possible implication of the pyroglutamyl residue of S protein in its *in vitro* interaction with the ACE2 receptor as well as the potential impact of Lactavir on this interaction.
2) Identify a possible inhibition of ACE2 enzymatic activity by Lactavir since this compound can be considered as a mimick of a C-terminus and ACE2 is a carboxypeptidase.
3) Develop the pseudotyped VSV technique by using S*VSV-ΔG and assess the impact of Lactavir on *in cellular* conditions.

To complete the first objective, we will perform BLI assays which will enable us to highlight two features concerning the ACE2-S1 interaction. The first feature is to detect if the presence or absence of pGlu at the N-ter part of the S1 protein has an impact on the binding affinity between the ACE2 receptor and S1. The second feature is to assess if the addition of Lactavir in the *in vitro* environment has an impact on the binding affinity of the interaction.

The second objective will be completed by realising ACE2 activity assays in the presence of Lactavir and look for a potential inhibition.

For the last objective, we aim to optimise the VSV production and to pseudotype them with three variants of S proteins (Wuhan, Delta and Omicron) and to test their infectivity on A549 cells over-expressing ACE2 and TMPRSS2. The infectivity of those pseudotyped VSVs will be assessed in presence of a gradient of Lactavir. The use of SARS-CoV-2 variants also aims to identify whether either would be more sensitive to the antiviral compound in order to better understand the action mechanism of the latter.

3. Materials and Methods

3.1 *In vitro* experiments

3.1.1 Purified compounds

Human angiotensin-converting enzyme 2

The purified ACE2 protein used for each of our experiment is a Human ACE2, Fc Tag expressed from HEK293 cells by AcroBiosystems (Cat. No. ACE2-H5257). The company gives us several information which are that the predicted N-terminal part of the protein is a Gln18 and the C-terminal part carries a human IgG1 Fc tag. They calculated a molecular weight (MW) of 100 kDa and an SDS-Page under reducing condition of the sample migrate around 125-150 kDa due to glycosylation (See Annexed document).

50µg of powder was firstly solubilized in 83µL of demineralised sterile water to obtain a solution at 600µg/mL. 50 µL aliquots at 100µg/mL were made and stored at -80°C as indicated by the supplier.

SARS-CoV-2 S1 subunit (Gln14)

The purified S protein used for each of our experiment is the subunit 1 of the SARS-CoV-2 virus expressed from HEK293 cells by Genscript (Cat. No. Z03501). The company gives us several information which are that the predicted N-terminal part of the S1 is a Gln14 and the C-terminal part carries no tag. They calculated a MW of 78.3 kDa and an SDS-Page under reducing condition of the sample migrate around 100 kDa due to glycosylation (See Annexed document).

100µg of powder was firstly solubilized in 69µL of demineralised sterile water to obtain a solution at 1,45mg/mL. 50 µL aliquots at 100µg/mL were made and stored at -80°C as indicated by the supplier.

His-tagged SARS-CoV-2 S1 subunit (Val16)

The purified S protein used for each of our experiment is the subunit 1 of the SARS-CoV-2 virus, His tag expressed from HEK293 cells by Genscript (Cat. No. Z03485). The company gives us several information which are that the predicted N-terminal part of the S1 is a Val16 and the C-terminal part carries a polyHis tag. They calculated a MW of 79 kDa and an SDS-Page under reducing condition of the sample migrate around 100-110 kDa due to glycosylation (See Annexed document).

100µg of powder was firstly solubilized in 69µL of demineralised sterile water to obtain a solution at 1,45mg/mL. 50 µL aliquots at 100µg/mL were made and stored at -80°C as indicated by the supplier.

Lactavir

Lactavir's chemical name is (3R)-5-oxothiomorpholine-3-carboxylic acid and it was purchased at Enamine (Catalog ID: EN300-657320; CAS number: 62305-89-9). The formula of this product is $C_5H_7NO_3S$ and the calculated MW is 161.2 kDa (See Annexed document). 50,5 mg of powder was solubilized in 25,26 mL of demineralised water to obtain a solution at 20mM stored at -20°C.

3.1.2 Mass Spectrometry (MS)

Preparation for in solution samples:

Chloroform-methanol precipitation: Each sample was transferred to 0.5 mL polypropylene Protein LoBind Eppendorf tubes and precipitated with chloroform-methanol method. [97]

In-solution trypsin digestion: 20µl of 100 mM TEAB (triethylammonium bicarbonate) were added to reach pH 8.5. Proteins were reduced by 5mM DTT (dithiothreitol) and alkylated by 15 mM iodoacetamide. Proteolysis was performed with 0.5 µg of trypsin and allowed to continue overnight at 37°C. Each sample was dried under vacuum with Savant Speed Vac Concentrator.

Peptide separation using nanoUPLC: Before peptide separation, the samples were dissolved in 20 µl of 0.1 % (v/v) formic acid and 2% (v/v) acetonitrile (ACN). Peptide mixture was separated by reverse phase chromatography on a NanoACQUITY UPLC MClass system (Waters) working with MassLynx V4.1 (Waters) software. 200ng of digested proteins were injected on a trap C18, 100Å 5 µm, 180 µm x 20 mm column (Waters) and desalted using isocratic conditions with at a flow rate of 15 µL/min using a 99% formic acid and 1% (v/v) ACN buffer for 3 min. Peptide mixture was subjected to reverse phase chromatography on a C18, 100Å 1.8 µm, 75 µm x 150 mm column (Waters) PepMap for 130 min at 35°C at a flow rate of 300 nL/min using a two part linear gradient from 1% (v/v) ACN, 0.1 % formic acid to 35 % (v/v)) ACN, 0.1 % formic acid for 90 min and from 35% (v/v) ACN, 0.1 % formic acid to 85 % (v/v)) ACN, 0.1 % formic acid for 10 min. The column was re-equilibrated at initial conditions after washing 30 min at 85% (v/v) ACN, 0.1 % formic acid at a flow rate of 300 nL/min. For online LC-MS analysis, the nanoUPLC was coupled to the mass spectrometer through a nano-electrospray ionization (nanoESI) source emitter.

LC-QTOF-MS/MS Analysis (DDA): DDA(Data Dependent Analysis) analysis were performed on an SYNAPT G2-Si high definition mass spectrometer (Waters) equipped with a NanoLockSpray dual electrospray ion source (Waters).Precut fused silica PicoTip^{R} Emitters for nanoelectrospray, outer diameters : 360 µm; inner diameter: 20 µm; 10 µm tip; 2.5" length (Waters) were used for samples and Precut fused silica TicoTip^{R} Emitters for nanoelectrospray, outer diameters : 360 µm; inner diameter: 20 µm; 2.5" length (Waters) were used for the lock mass.solution. The eluent was sprayed at a spray voltage of 2.8 kV with a sampling cone voltage of 25 V and a source offset of 30 V. The source temperature was set to 80°C. The cone gas flow was 20 liters/h with a nano flow gas pressure of 0.4 bar and the purge gas was turned off. The SYNAPT G2Si instrument was operated in DDA (data-dependent mode), automatically switching between MS and MS2. Full scan MS and MS2 spectra (*m/z* 400 - 2000) were acquired from 2 min after injection to 30 min in resolution mode (20,000 resolution FWHM at *m/z* 400) with a scan time of 0.1 sec. Tandem mass spectra of up to 10 precursors were generated in the trapping region of the ion mobility cell by using a collision energy ramp from 17/19 V (low mass, start/end) to up to 65/75 V (high mass,start/end). Charged ions (+2, +3, +4) are selected to be submitted to the MSMS fragmentation over the m/z range from 50 to 2000 with a scan time of 0.25 sec. For the post-acquisition lock mass correction of the data in the MS method, the doubly charged monoisotopic ion of [Glu^{1}]-fibrinopeptide B was used at 100 fmol/µl using the reference sprayer of the nanoESI source with a frequency of 30 s at 0.5µl/min into the mass spectrometer.

ESI-QTOF data processing: Data were processed with UNIFI (Waters) using spike protein sequence from the company. Carbamidomethylation, as the variable Cysteine modification, oxidation as the variable Methionine modification and Pyro-glu from Q as Glutamin modification. Trypsin as the digestion enzyme were selected and one miss cleavage allowed. MassLynx V4.1 (Waters) software was used to search charged peptides and to compare spectra.

3.1.3 BLI design

The BLI machine used during this master thesis is an Octet® R2 Protein Analysis System from Sartorius company and the biosensors used were purchased from the same company (Ni-NTA item no.:18-5101; ProA item no.:18-5010). Due to the high costs of biosensors, we initially used Ni-NTA biosensors due to their easy capacity of regeneration by treating them with an acidic solution (10mM glycine - pH 1.7) followed by a neutralization into Phosphate Buffer Saline (PBS: 10mM Na_2HPO_4; 2mM KH_2PO_4; 2,7mM KCl) for both 5 seconds. After three cycles of this treatment, the NTA biosensor is incubated with a $NiCl_2$ solution (10mM $NiCl_2$ in H_2O). The Ni-NTA biosensor allowed us to perform experiments with the S1-His as ligand and the ACE2-Fc as analyte.

Due to lack of consistency, we invert the ligand and the analyte by using Protein A biosensors for immobilizing the ACE2-Fc protein. The strong interaction between protein A and the Fc-tag is more specific and does not rely on an electrostatic interaction as in the case of Ni-NTA biosensors with the His tag.

For these experiments, the set up was shorter to maximize the reproducibility, diminish the impact of evaporation and with new biosensors to avoid the potential impact on the regeneration on the biosensor. Due to the high concentration of ACE2-Fc used, we reused them to perform experiments on a maximum of three days (two cycles of freezing and thawing). In this type of experiments, the concentrations are expressed in nanomolar and thus the four concentration of analytes used were ±316nM (25µg/mL), ±253,2nM (20µg/mL), ±126,6nM (10µg/mL), ±63,29nM (5µg/mL) and referred later on by 316nM, 253,2nM, 126,6nM and 63,29nM.

A first experiment includes a range of analyte (S1Val or S1pGlu) concentration from 63,29nM to 316nM and is performed in triplicate (See Figure 15) to analyse a potential difference in the binding affinity of the S1Val and the S1pGlu with the ACE2 receptor.

Table 1 : Organization of the experiment testing the interaction between S1Val or S1pGlu with ACE2 receptor.

One set = 2 rows					
Steps/row	Baseline (1)	Loading (2)	Baseline (3)	Association (4)	Dissociation (5)
Time (s)/well	250	600	60	300	300
Total time per set	~25 minutes				

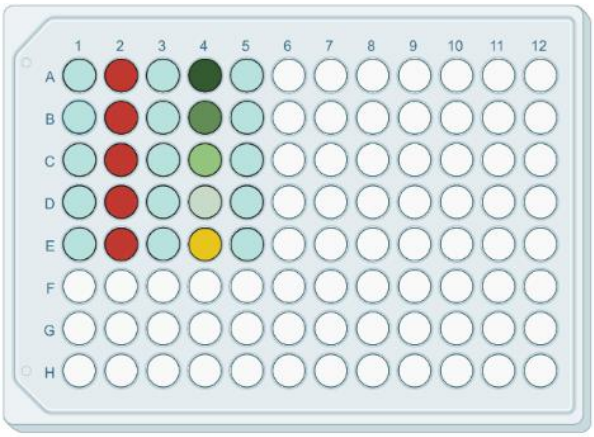

Figure 15 : Experimental repartition in a plate for the experiment described in Table 1.
Light cyan: PBS buffer; Red: ACE2 receptor (50µg/mL or 632nM); Dark green to light green: Decreasing concentration range of either S1Val or S1pGlu (316nM – 63,29nM); Yellow: reference sensor without analyte.

A second experiment, also done in triplicate, involved a fixed concentration of analyte (253,2nM) with a range of Lactavir concentration (1mM – 100µM – 10µM – 1µM – 0.1µM) to assess the potential impact on the binding affinity of the S1Val or S1pGlu with the ACE2 receptor.

To design our experiments, we used the BLI Octet Discovery 12.2 software and the Octet Analysis 12.2 software to process them. Throughout the experiment, measurements are recorded every 0.2s and plotted on a global graph as shown in Figure 13b. We processed our experiments by correcting our data by aligning the Y axis to the start of association step with an inter-step correction aligned on the dissociation step and by filtering the whole with the Savitzky-Golay filter to smooth our curve and extract the successive derivatives.

For the specificity of the kinetic analysis, we have to focus the analysis software on the association/dissociation steps with a classical binding model of 1:1 and choose a global (group) fitting of the data. For example, one set of the kinetic graph of ACE2 - S1(Val) is presented in Figure 21A while the Figure 21B represent the kinetic graph for the triplicate experiment of this interaction.

3.1.4 Enzymatic assay design

The fluorogenic ACE2 substrate used is a synthetic substrate Mca-APK(Dnp)-OH from AnaSpec (Catalog#AS-60757 – Lot#2155954) with a molecular weight of 696.7 g/mol. This ACE2 substrate is a FRET peptide using 2,4-dinitrophenyl (Dnp) to quench the fluorescence of methoxycoumarin (Mca) (See Figure 16). Whenever the substrate is cleaved by the enzyme, the interaction is broken and the fluorescence of Mca increases. The peptide was reconstituted by adding 100µL 1%NH_4OH to 1mg powder and dilute in 900µL PBS to obtain a 1mg/mL solution. Aliquots of 100µL at 1,43mM were stored at -20°C as recommended by the supplier. Before use, each aliquot was thaw at room temperature and further diluted with buffer assay without $ZnCl_2$ to obtain a 1mM solution.

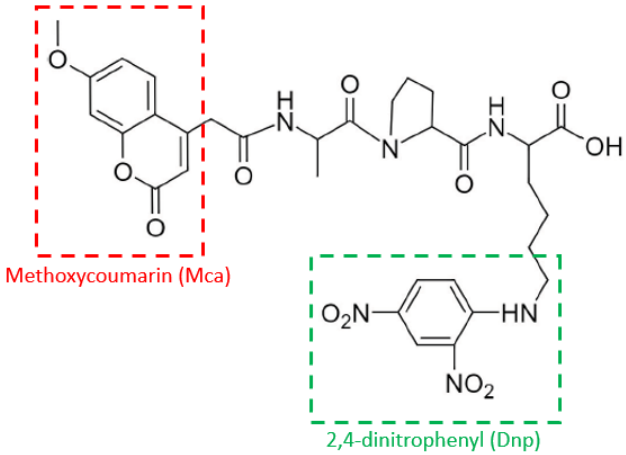

Figure 16 : Chemical structure of the fluorescent ACE2 substrate Mca-APK(Dnp)-OH.

The assay buffer is composed of 0,05M MES, 0,3M NaCl at pH 6.8. Solutions containing assay buffer and various concentrations of $ZnCl_2$ (10µM and 100µM) were also prepared and pH was verified to stay at pH 6.8. All of those solutions were stocked at 4°C and warmed to room temperature before use. Lactavir solutions and ACE2 aliquots were prepared using demineralised water and stored at -20°C. Before use, those solutions were thaw at room temperature.

The enzymatic activity of the ACE2 enzyme with a fluorescent peptide was monitored in Greiner 96 black microtiter plate using a Tecan Infinite 200Pro. The parameters used on the Tecan were determined with first experiments by using an automatic detection to establish the best gain (65) and Z-position (17800µm). The kinetic duration is 45 minutes with an interval time of 10 seconds at 35°C. The mode used is top reading fluorescence with an excitation wavelength of 325nm (bandwidth=9nm), an emission wavelength of 393nm (bandwidth=20nm) and an integration time of 20µs for 25 flashes.

The protocol used for the enzymatic assay is the following. First, preparation of each well by adding 5µL of 1mM peptide (50µM final concentration (C_f)), 45µL of assay buffer and 10µL of Lactavir (variable concentrations) or 10µL demineralised water for controls. Second, initiation of the reaction by adding 50µL of 100nM ACE2 enzyme (50nM C_f) or assay buffer for controls. Finally, start of fluorescence measurements within one minute after addition of ACE2.

A maximum of six conditions were tested simultaneously in order not to create too much variation between the different wells. However, four conditions seem to be the best compromise for this kind of experiment.

3.2 *In cellular* experiments

3.2.1 Main reagents used:

Gibco™ Dulbecco's Modified Eagle Medium (DMEM) (Catalog number :11965092) is enriched in glucose, L-glutamine and phenol red but without sodium pyruvate nor HEPES.

Gibco™ Advanced DMEM (Catalog number: 12491015) is enriched in glucose, sodium pyruvate, non-essential amino acids and phenol red but without L-glutamine.

Gibco™ Dulbecco's Phosphate Buffered Saline (DPBS) (Catalog number: 14190250) is enriched with calcium, magnesium, glucose and sodium pyruvate but without phenol red.

Gibco™ Fetal Bovine Serum (FBS) (Catalog number: 16000044) is deactivated at 56°C for 30min. and then frozen by 25mL aliquots for later use.

Gibco™ Trypsin-EDTA (0.5% - no phenol red) (Catalog number: 15400054) is made from trypsin powder derived from porcine pancreas and contains EDTA but no phenol red. The solution used is diluted 10x from this stock.

Sigma-Aldrich Penicillin-Streptomycin (P/S) (SKU: P4333-100mL) is a stabilized solution with 10.000 units penicillin and 10mg streptomycin/mL, 0,1µm filtered and suitable for cell culture.

pCG1 corresponds to the S protein of the Wuhan strain (See Appendix 4)

pUNO1 corresponds to the S protein of the Delta variant strain (See Appendix 5)

pLV corresponds to the S protein of the Omicron variant strain (See Appendix 6)

3.2.2 VSV production and optimisation

The VSV pseudotyping and production is a long process taking up to a week to do. This subpart was mainly realised by Kimberley Durlet who is working in the laboratory of Prof. Alsteens. The main steps are summarised in Figure 17 while the optimised protocol is the follow:

Day 1 – seeding: Seeding 240.000 HEK-293T cells in 6 well plate in 2ml medium

Day 2 – Transfection: Transfection with 8µg of plasmid containing the glycoprotein of interest

Preparation of a mix containing: 1100 ng spike expression vector + 100 ng DsRed expression vector per well to infect in 50µL of OPTIMEM. Add 50µL of OPTIMEM containing 4µg of Polyethylenimine per well to infect and mix gently. Incubate the mix for 15 min at room temperature. Add 100µL of the mix to each well containing cells ready to be transfected.

Day 3 – Transduction: Check transfection efficacy after 24h post-transfection with optical microscope with DsRed filter (should be min 50%). Discard the supernatant carefully and transduce with 100µL VSV-ΔG (1:100) in 1mL DMEM (without FBS without F/S). Incubate during 1h at 37°C then remove medium and wash carefully 1x with PBS. Add 2mL DMEM (+ 5%FBS, PS, Gln, Na-Pyruvate and NEAA) containing anti VSV-G antibody (1:1000) (except for VSV-G production). Incubation at 37°C and 5% CO2 overnight (o/n).

Day 4 – Collection and storage: Check transduction efficacy after 24h post-transduction with optical microscope with GFP filter. Collect supernatant and clear cell debris by 10 min centrifugation at 1250xg. Aliquot, snap freeze and store at -80°C **or** keep at 4°C for direct use (can be stored at 4°C for 1-2 weeks) **or** perform polyethylene glycol (PEG) precipitation (add 25%PEG to cleared medium for a final PEG concentration of 8%, incubate 4 hours or o/n at 4°C while gently shaking or rotating, centrifuge for 30 min at 3000xg, resuspend pellet in 1 ml DMEM (+5% FCS, PS, Gln, Na-Pyruvate and NEAA) and aliquot, snap freeze and store at -80°C).

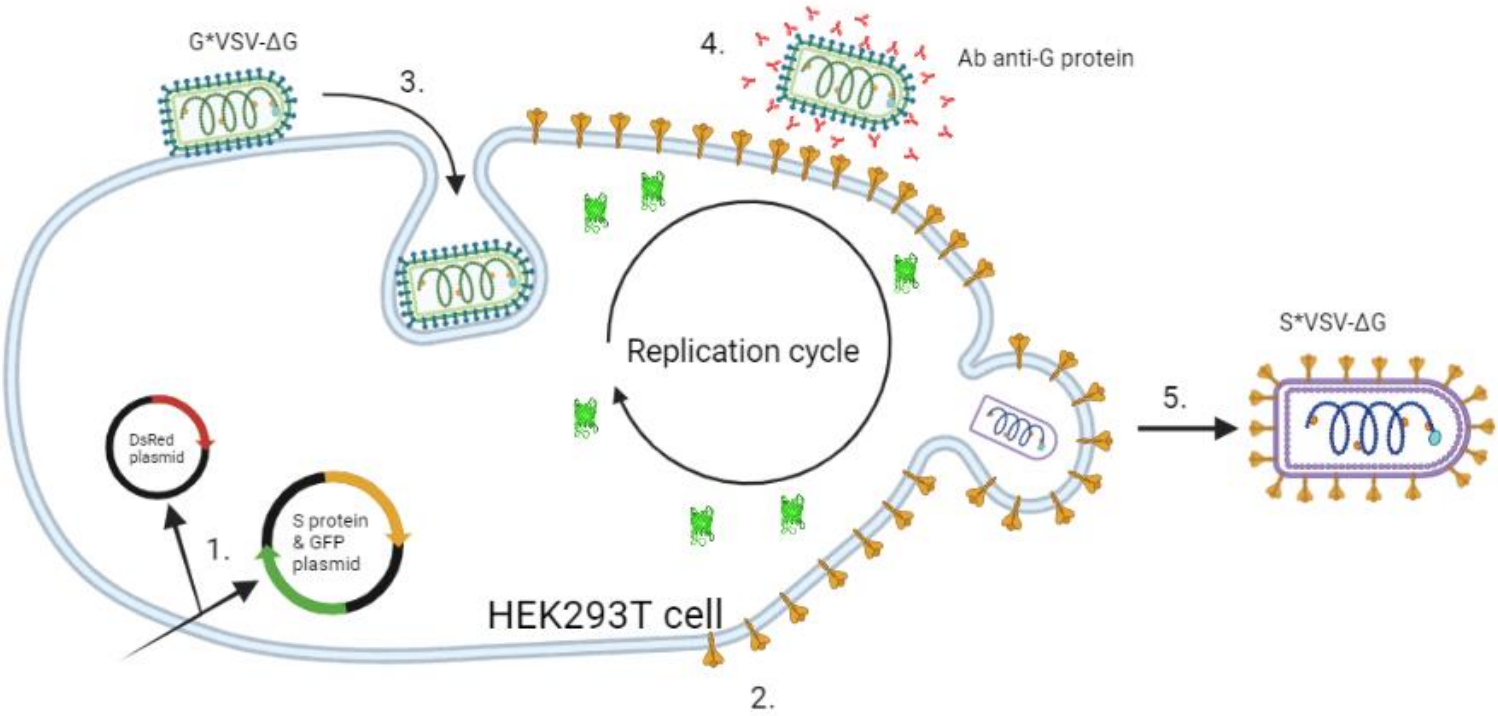

*Figure 17 : **1.** Transfection of HEK293T cells with two plasmids simultaneously. One of them contains the gene for a red fluorescent protein (DsRed) and the second one contains a gene for the green fluorescent protein (GFP) and a gene for the S protein. During the transfection, the second plasmid is 10 times more present than the first one. Thanks to this, if our cell emits red fluorescence, the probability for this cell to assimilate the second plasmid is really high. **2.** There is a high expression of the S protein at the cell surface. **3.** Transduction of HEK293T cells by G*VSV-ΔG capable of only one infection due to the deleted gene for the G protein. The VSV-ΔG can use the host cellular machinery to perform its replication cycle and while the newly formed virion is budding, it will be coated with the content of the membrane surface of the HEK293T cell (S protein in our case). **4.** After 1h of incubation, antibodies (Ab) directed against the G protein will recognise only that protein and prevent further transduction of unbound G*VSV-ΔG that could be present in the supernatant. **5.** Harvesting of S*VSV-ΔG from the supernatant.*

3.2.3 Infectivity assay

The A549cells on which the infectivity assays are performed are cultivated in T75 flasks with an adequate medium (DMEM+10%FBS+1%P/S) in an incubator (37°C, 5% CO2). At a confluence between 75% and 90%, we have to pass them and dilute them in another T75 flask. To do so, we suck up the medium with a fluid aspiration system (VacuuBrand® BVC professional-Article number: 20727400) while leaving the adherent cells on the bottom surface of our flask. We wash those cells at least once by using 5mL of PBS then suck it up also. We detach the cells from the flask using 2mL of Trypsin (1x) and leave it on for about ten minutes while checking the proportion of detached cells under the optical microscope. After the cells detach and float freely, we take a precise volume and dilute it in a variable volume to reach the desired dilution rate. It is really important to avoid the culture of cells at high confluence because it can impact their developmental process and induce a differentiation of them. The A549cells used are expressing the ACE2 receptor and TMPRSS2 enzyme (ACE2+TMPRSS2).

To realize a $TCID_{50}$ test, we seed on Greiner 96 transparent microtiter plate with 100µL/well of A549 cells (ACE2+TMPRSS2) at a concentration of 120 000 - 150 000 cells/mL in DMEM (+10%FBS+1%P/S). The concentration is calculated using LUNA-II™ Automated Cell Counter. Those plates rest o/n to let cells adhere to the bottom surface. Prior the addition of the infectious agent, the medium is sucked up and replaced with 150µL Advanced DMEM (without FBS nor P/S) except for the first column where the final volume of 200µL must be added as a negative control. The second column is infected with 50µL of S*VSV-ΔG and a serial dilution is done for the whole plate (dilution factor of 4 or 10 if high concentration of VSV). The dilution factor can vary depending on the concentration of the batch but the smaller it is, the higher the accuracy of the $TCID_{50}$.

To realize an infectivity assay, we seed one or multiple plates of 96 wells in the same manner as for a $TCID_{50}$ test and we let them o/n. The medium is sucked up and replaced with 150µL Advanced DMEM (without FBS nor P/S) and if external compounds are studied during the test, they must be put into solution and incubated with the cells for at least 1 hour. To infect a plate, 50µL of S*VSV-ΔG are added to each well for a variable length (between 18h and 24h). It is particularly important to have plates with both negative (only medium added) and positive control (virus added without external compounds).

After this incubation period, the plates are either washed two times by using PBS and scanned or scanned with the media using the Amersham Typhoon. The scans are analysed by using ImageJ to obtain images and by ImageQuantTL software to quantify the intensity of fluorescence of our samples. Washing steps result in scans with less background effect and nicer images. An example of the scan obtained is provided in Appendix Figure 7.

4. Results and discussion

This chapter will present and discuss the results obtained during this work. We worked by using two axes: *in vitro* experiments and *in cellular* experiments.

For the first axis, we validated first the S1 sequences used by MS and performed BLI experiments to evaluate the impact or not of Lactavir on S1-ACE2 interaction. We finished by evaluating the potential effect of Lactavir on ACE2 enzymatic activity by performing ACE2 inhibition assays. The second axis was studied by producing VSV and by performing infectivity assays with pseudotyped VSVs on A549 cells in presence of Lactavir to assess its antiviral effect.

4.1 *In vitro* experiment

4.1.1 Validation of S1 sequence by MS

Two purified S1 proteins, called S1(Val) and S1(pGlu), were purchased to perform our BLI experiments and we first wanted to validate their sequence by MS to check for the presence or absence of N-terminal pyroglutamate. Indeed, while S1(pGlu) should have a wild type pyroglutamylated N-terminus, the S1(Val) is truncated by two residues and should not have this feature.

In a first step, we digest the protein using trypsin to cut the protein in smaller peptides just after Arginine (R) and Lysine residues (K) and by calculating each peptide weight, we can highlight them in the MS spectrum. Based on the sequences given by the company, S1(Val) and S1(pGlu) should generate N-terminal hexa- and octa-peptides (peptides **1a** and **1b**, Figure 18) with 703.41 and 974.48 Da as expected masses ($(M+H)^+$) respectively. 40 Da should be added to the expected mass of peptide **1b** because of both Gln14 pyroglutamylation (-17 Da) and Cys15 alkylation by iodoacetamide (+57 Da, proteins are reduced and alkylated prior to trypsin treatment).

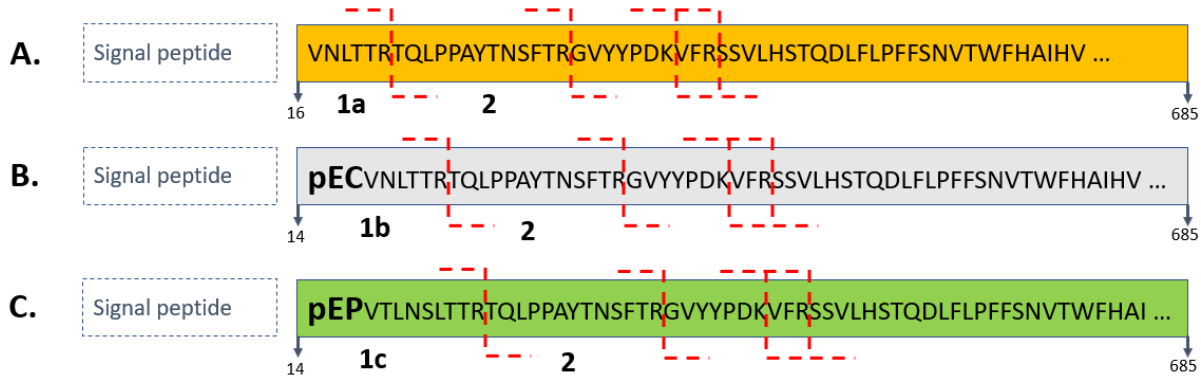

*Figure 18 : Representation of the expected N-terminal primary sequence of S1 proteins. Red dashes represent the trypsin cleavage sites (after Lys and Arg). **A)** Sequence for the S1(Valine) with a specific N-ter part (**1a**) and a second peptide similar in both proteins (**2**). **B)** Theoretical sequence for the S1(pGlu) with a specific N-ter part (**1b**) and the second peptide (**2**). **C)** Unexpected sequence for the S1(pGlu) with a specific N-ter part (**1c**) and the second peptide (**2**).*

To attest that our analysis worked, we were able to identify many S1 peptides in both samples, including the peptide **2** (residues 22-34) of the S1 protein (See Appendix 8). Due to a miscleavage of the S1(Val), a longer peptide **1a-2** (16-34) was also identified on the MS spectrum (See Appendix 9). We examined our S1(pGlu) sample to attest the absence of this peptide and highlight its unique presence in the S1(Val) sample (See Appendix 10).

For S1(pGlu), peptides **1b** or **1b-2**, with and without pyroglutamylation were not detected. However, by visual comparison of MS spectra, an abundant peptide present in the S1(pGlu) sample and absent in the S1(Val) sample, and featuring an expected LTTR C-terminal signature in the fragmentation spectrum was observed. Its 1211,7 Da molecular weight is unexpected and the peptide is detected with two distinct charged states (+3 or +2) (See Appendix 11). Interestingly, the same peptide was found at two different elution times with different +3/+2 ratios.

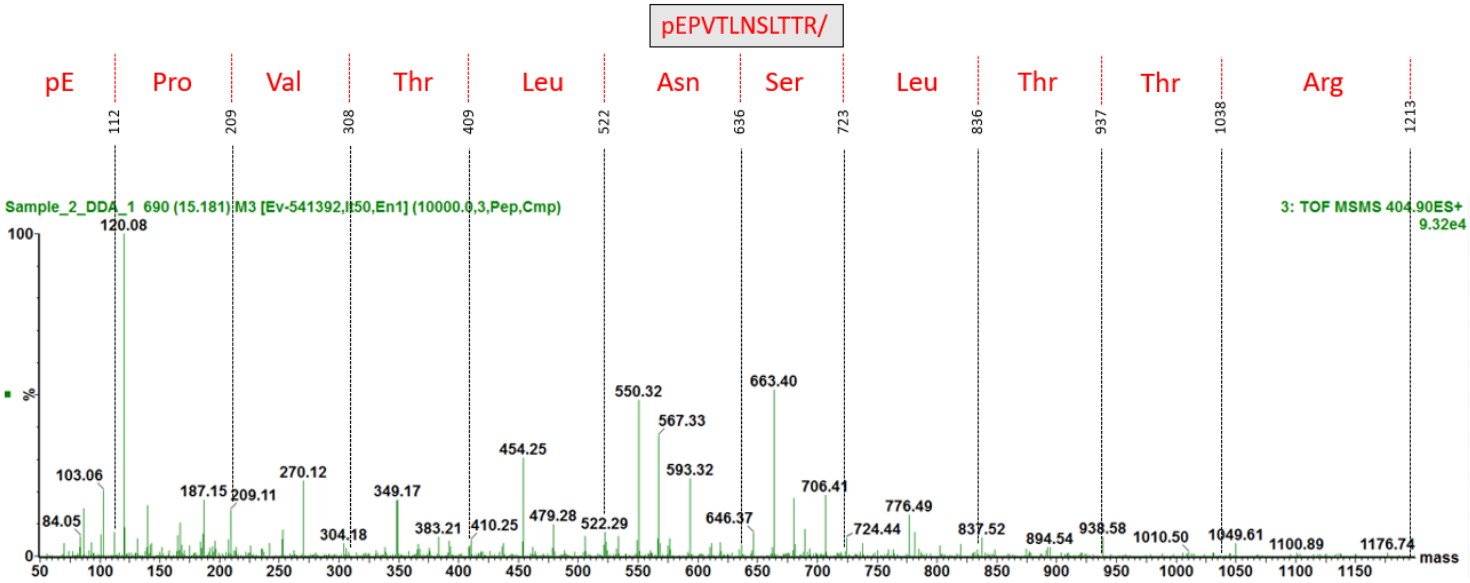

Figure 19 : MSMS fragmentation spectrum of the +3 peptide (m/z = 404.9). The grey box represents the unexpected sequence of the N-ter part of the S1(pGlu) protein. The mass of the amino acids is cumulative throughout the mass spectrum until the total mass of our peptide which is 1212.7 Da.

The proportion of +3 peptide at retention time 15.3min is much higher than at time 15.98min and inversely for +2 peptide (See Appendix 12). The presence of two elution times suggests the presence of two isomers of this peptide interacting differently with the column. This may be indicative of the presence of a peptidyl-prolyl bond (Xaa-Pro) in this peptide undergoing slow cis/trans isomerization.

Based on these observations and automatic de novo sequence prediction based on the fragmentation spectrum (See Appendix 13), we found that the observed peptide is compatible with the unexpected pEPVTLNSLTTR sequence (See Figure 18C & 19). If true, this means that the pyroglutamate is present at the N-terminus but its primary sequence does not correspond to the SARS-CoV-2 spike protein.

After these analyses, we realized that a NxT glycosylation site was present at the N-termini of expected S1(Val) and S1(pGlu) proteins (not in the unexpected sequence discussed above) and that glycosylation of Asn17 was indeed reported in the literature. A quantitative MS analysis on recombinant S1 protein produced in HEK293 cells indicated that the major glycan on Asn17 was composed of 4 hexoses, 4 N-acetylated hexoses and one sialic acid corresponding to an additional mass of 1751 Da. [28]

Since our commercial proteins are produced in similar HEK293 cells, it is probable that this glycosylation is also present on our proteins but we were unable to distinctively detect its presence in none of our proteins with the conditions used to perform the MS. Moreover, the glycosylation would only occur on the expected peptides thanks to the presence of the consensus sequence (N-X-S/T) but not in the unexpected sequence mentioned above for the S1(pGlu) protein.

4.1.2 Evaluation of the S1-ACE2 interaction with BLI

Within this part of this master thesis, we used BLI to study S1-ACE2 interaction. However, this technique is quite new in the laboratory (acquired early last year). In order to validate the accuracy and reproducibility of the data, we have performed several tests to find the best experimental conditions and performed triplicates for each experiment.

The main limitation of this technique is the cost of purified proteins due to the high concentration at which we must work. It was important to us to do as many runs as possible with one sample of proteins or to reuse them between experiments.

Optimisation of the experiment setup was done and we were able to test up to three separate conditions per row in a 96well plate, reaching up to 24 different sensograms. However, the length of such an experiment was of almost 12 hours leading to evaporation of the solutions. As a result, the recording of 6 sensograms during a ~3hours experiment at 30°C leads to almost 25% of solution evaporation while performing the same experiment at 20°C leads to a solution evaporation of less than 15%. Interestingly, the recording of 12 sensograms (~6hours) at the lower temperature leads to less than 20% of evaporation.

We tested also to re-use our proteins after an experiment by freezing them again and reusing them later on. Until now, proteins were used after only one congelation due to the aliquots production (these are subsequently referred to as fresh proteins). The results obtained after comparison between fresh and reused proteins were not convincing enough and we preferred to set aside this possibility even though the higher the concentration of the protein, the less pronounced the effects of freeze/thaw cycles.

To avoid possible non-specific interaction with the Ni-NTA biosensor, we tried also to add 0.02% Tween and 0.1% BSA in our buffer solution. Due to unusual results, we decided to stop using BSA because there seems to have residual IgG in the BSA solution reacting with the Fc-tag of our ACE2 protein and so other experiments were performed with only Tween 0.02%. However, it turns out that the presence of Tween 0.02% in the solution seems to impact the interaction due to an association and dissociation steps that are too fast compared to the condition without Tween 0.02%. For the rest of our experiments, we decided to use nothing but PBS for our solution.

With ProteinA biosensors, we performed two experiments:

1) We investigated the specific interaction between ACE2-Fc protein immobilized on the sensor and the soluble S1 protein of SARS-CoV-2 with or without pGlu (S1pGlu or S1Val).

2) We evaluated an eventual effect of Lactavir on the *in vitro* interaction between ACE2 and each purified S1.

4.1.2.1 S1-ACE2 interaction

In a first experiment, we decided to measure and compare the binding forces of S1(Val) and S1(pGlu) with the ACE2 receptor. This experiment will enable us to determine if the S1 N-terminus is contributing to the interaction.

Practically, we ran a BLI experiment detailed in Figure 15 and obtained a complete sensogram as shown in Figure 20. Also, the kinetic graph of the first replicate is represented in Figure 21A while the kinetic graph of the triplicate is represented in Figure 21B.

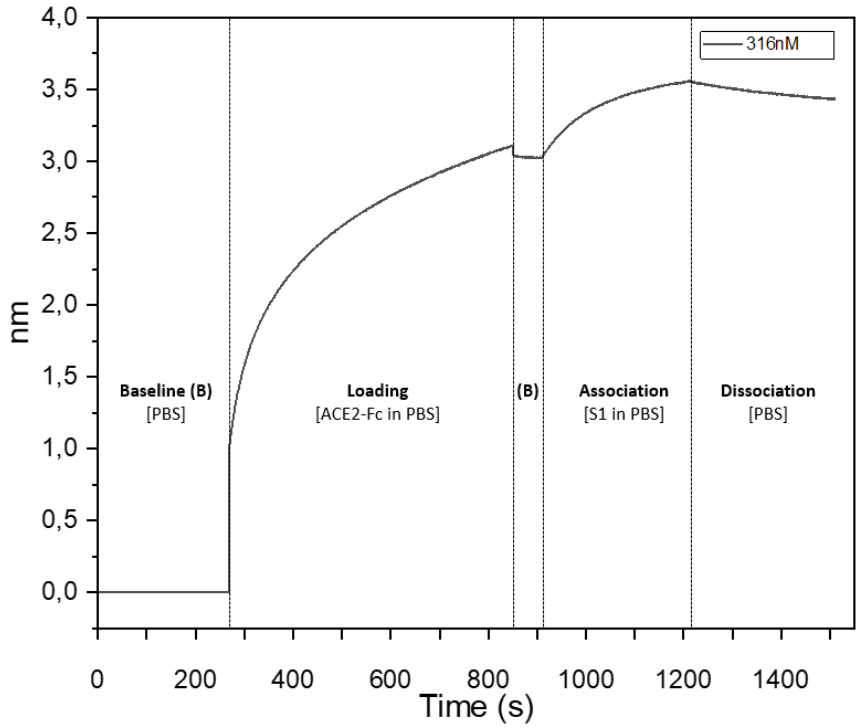

Figure 20 : Complete sensogram of a BLI experiment with the S1Val at 316nM as analyte and ACE2-Fc at 632nM as ligand. All the steps for a BLI experiment were previously explained and consists in the following steps: A first baseline followed by the loading step and a second baseline (B). The kinetic part of the experiment includes the association and dissociation steps and is further developed in Figure 24A.

With this experiment, we highlight that our measurements are reproducible. We also provided a sufficient number of repetitions to get a good precision in our results (See Figure 22). Also, we can compare them to the literature and our results are in the same nanomolar range which suggests a good accuracy. [56,98]

We realised this experiment in triplicates but we have to aggregate the K_D values obtained for the different concentrations in analytes (316nM, 253,2nM, 126,6nM and 63,29nM) from the triplicate to obtain an average K_D value corresponding to the affinity between our ligand and our analyte of interest.

As seen in Figure 22, both K_D values are around 21nM and there is no significant difference between S1(Val) and S1(pGlu). It is certain that the sensitivity of the machine is high on large orders of magnitude but this also implies a more complicated distinction on very small scales of magnitude. A significant difference of interaction between two proteins is evidenced by one or two orders of magnitude variation.

It is however difficult to definitely conclude that the pGlu is not contributing since the mass analysis raised some concern about the N-terminus of S1(pGlu) (See section 5).

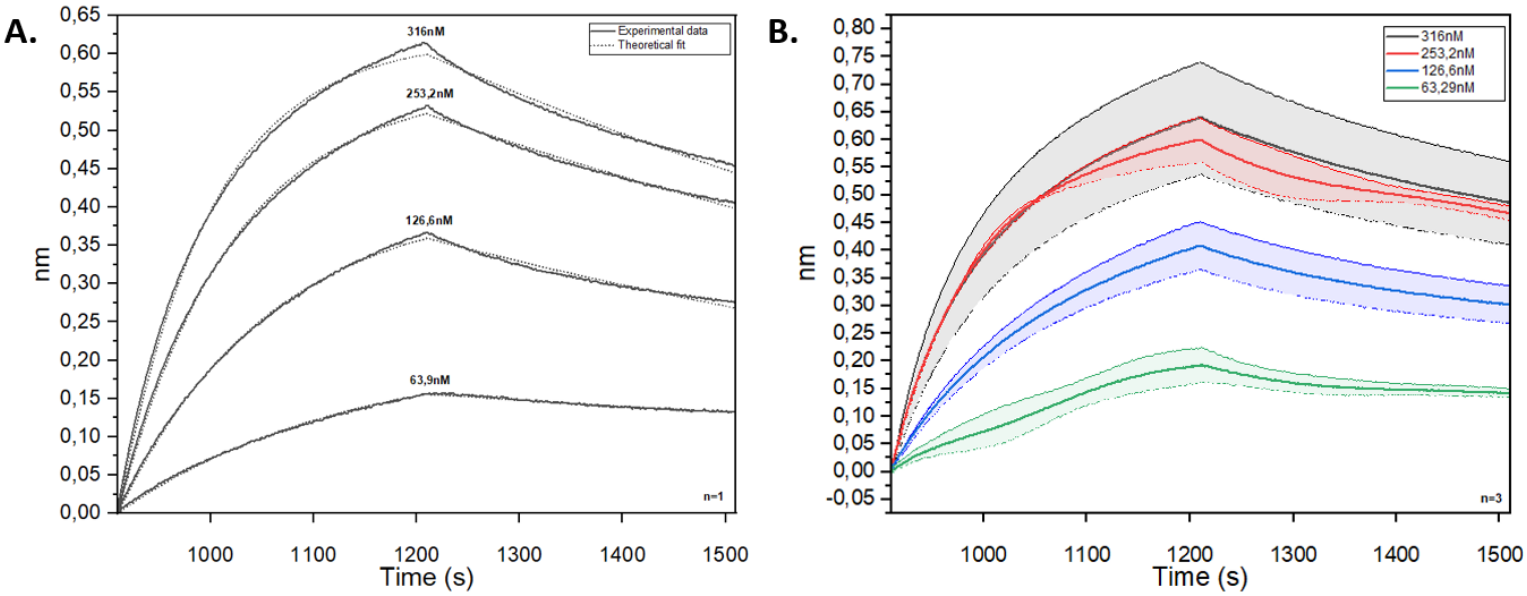

Figure 21 : Kinetic graph of the ACE2-S1(Val) interaction by BLI with four concentration of S1(Val) tested (316nM, 253,2nM, 126,6nM and 63,29nM). ***A.*** *Kinetic graph of one replicate where the short dashes represent the fit proposed by the software while the solid lines are the measured data.* ***B.*** *Kinetic graph of the triplicate where the bold line represents the mean of three separate experiments and the coloured area represent the standard deviation (SD).*

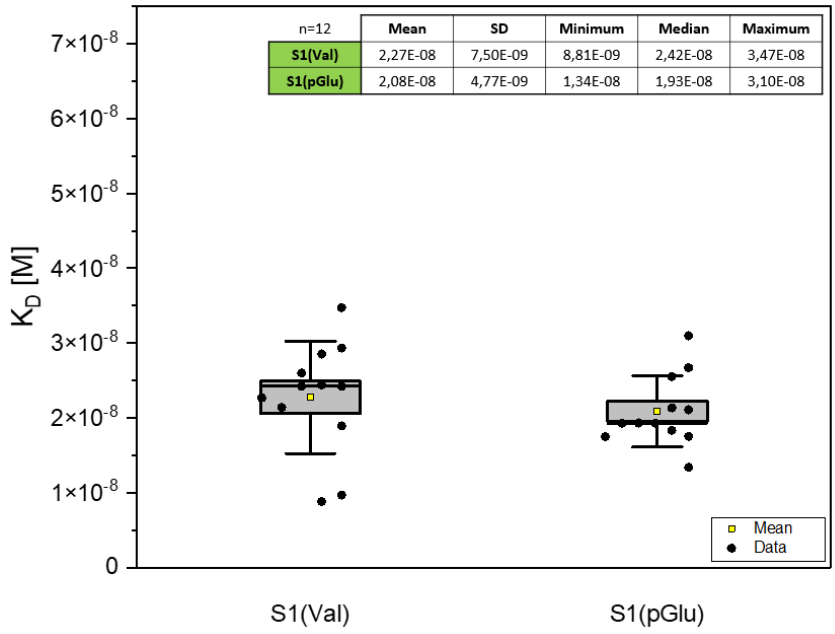

Figure 22 : Interval plot of K_D values between ACE2 and either S1(Val) or S1(pGlu). Those data were obtained by performing the experiment detailed in Figure 15 on a total of 12 samples.

4.1.2.2 Effect of Lactavir

Next, we measured the binding forces of S1(Val) and S1(pGlu) toward the ACE2 receptor in presence of various concentration of Lactavir ranging from 0,1µM to 1mM (0,1µM, 1µM, 10µM, 100µM, 1mM) at a fix concentration of the S1 analyte (20µg/mL corresponding to ≈ 250nM). The objective here is to evaluate a potential impact of Lactavir on the binding interaction between the ACE2 receptor and the S1(Val) or S1(pGlu).

Prior to start, we had to attest if the addition of Lactavir in solution could be detected during the experiment and if our compound was aggregating against our ligand prior or after its attachment to the biosensor, leading to disturbances in the signal. We added 1mM of Lactavir in every well (starting from the first baseline) and we compared it with a condition without Lactavir. No differences were observed during this test which indicates that our compound cannot be detected and that it does not disturb the binding of the ligand to the biosensor.

As represented on Figure 23, we can assess that the S1-ACE2 interaction seems not affected by Lactavir in the tested concentration range. Even though there is sometimes a higher variability than during the first experiment without Lactavir (up to 50nM of difference with Lactavir), we have to highlight that this experiment was only reproduced 3 times and that the high variation observed is due to outliers.

For the S1Val, we can make abstraction of one outlier (K_D value = 47nM in Figure 23A) and the visual trend is similar across all tested Lactavir concentrations. Moreover, by comparing the mean K_D values for the S1(Val) from each Lactavir concentration (See Table 2), the trend is almost identical and the standard deviation (SD) highlight well the presence of an outlier at 1µM of Lactavir.

Table 2 : K_D values between ACE2 and either S1(Val) or S1(pGlu)in presence of Lactavir. SD= Standard Deviation

n=3		S1(Val)		S1(pGlu)	
		Mean	SD	Mean	SD
[Lactavir]	1mM	3,72E-08	2,15E-09	4,36E-08	2,08E-08
	100µM	3,68E-08	2,26E-09	4,28E-08	9,78E-09
	10µM	3,74E-08	2,76E-09	3,28E-08	1,43E-08
	1µM	4,02E-08	6,10E-09	3,59E-08	6,03E-09
	0.1µM	3,66E-08	1,95E-09	3,02E-08	2,76E-09

Concerning the S1pGlu, there are also some outliers but in greater numbers (K_D value ± 67nM in 1mM condition, K_D value ± 54nM in 100µM condition and K_D value ± 49nM in 10µM condition) (See Figure 23B). To date, we do not have a single explanation to address those outliers and we don't know why they are higher with this S1pGlu.

Is it due to the intrinsic difference between the two S1? Is it because of a defective biosensor? Is it due to an operating error? It is most likely a combination of those and more experiments should be performed to completely lift the veil on this result.

However, the visual tendency is similar across Lactavir concentration and no significant differences can be highlighted (See Figure 23B). Again, by comparing the mean K_D values for the S1pGlu from each Lactavir concentration (See Table 2), the trend is almost the same and the difference in the K_D values is at the maximum of ±15nM, which is not significant to determine an impact on the binding affinity.

One possible explanation for this is that the impact of Lactavir occurs at a lower concentration than 0.1µM since antiviral effects were already detected from 50nM with the team of Prof. Boulant on Caco-2 cells (See Appendix 1). Assuming that we are at saturation of the system with the concentrations of Lactavir used, we can pool all the data obtained in the presence of Lactavir and compare them with those obtained without Lactavir.

If this hypothesis is correct, we can state that there is indeed an effect of Lactavir on S1-ACE2 interaction by performing a t test on these data (See Figure 24). However, given that the measured K_D remains in the nanomolar range, the biological relevance of this observed difference should be taken with caution.

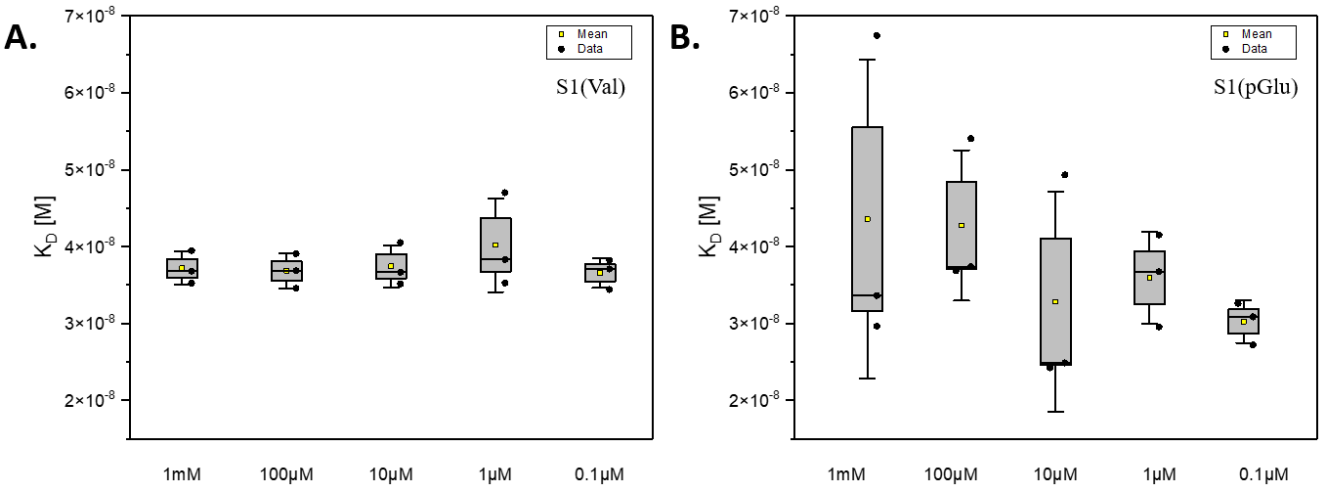

Figure 23 : Interval plot of K_D values between ACE2 and either S1(Val) ***[A]*** *or S1 (pGlu)* ***[B]*** *at 20µg/mL (±250nM) in presence of a Lactavir range of concentration (0.1µM, 1µM, 10µM, 100µM, 1mM)*

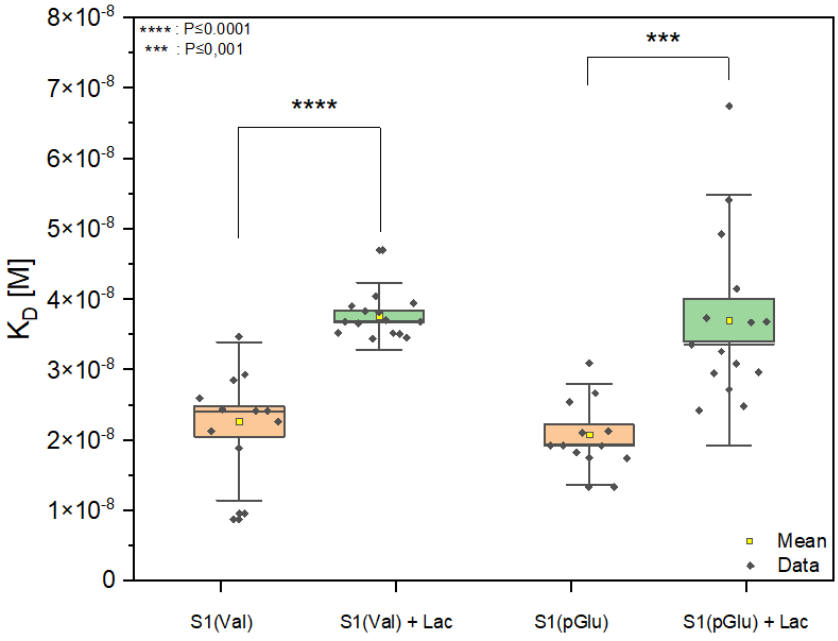

Figure 24 : Interval plot of K_D values between ACE2 and either S1(Val) (orange) or S1 (pGlu) (green) in presence or absence of a Lactavir concentration higher than 0,1µM.

To summarise these two experiments, we can state that the presence or absence of pGlu at the N-ter part of S1 is not impacting the affinity constant of the interaction between ACE2 and the S1. Also, the addition of Lactavir above 0,1µM has no concentration-dependent impact on the affinity constant with the two S1. With the tested concentration of Lactavir, we cannot state that there is an impact from the compound on the K_D values. However, if we assume that we have a system at saturation and that we decide to compare this saturation tray with the absence of Lactavir, we detect a significant but modest decrease of the S1-ACE2 affinity. This observed decrease in affinity should be taken with caution as we still are in a nanomolar range of measurement.

4.1.3 ACE2 enzymatic assays

Given the limited knowledge we have about the antiviral mechanism of Lactavir, we do not know for sure where it interacts and how it interacts. Structural evidences shows that ACE2 catalytic site and ACE2 binding site with S protein are different and one study using pseudotyped retroviruses has shown that the enzymatic activity and the S protein-mediated infection are distinct processes with no influence from one to the other. [24,55,99]

However, another study highlighted also a large hinge-bending motion by comparing the X-Ray structures of the native ACE2 to an inhibitor (MLN-4760)-bound ACE2.[100] The MLN-4760 possess two carboxylates that binds inside the catalytic pocket and the binding motion of the whole inhibitor impacts the key helix for S binding on ACE2 (Highlighted in Figure 9) and may influence directly the specific S-ACE2 interaction (See Figure 25).

Our postulate is that Lactavir, being a carboxylate, might bind to ACE2 in the catalytic pocket and modulate the S1-ACE2 interaction.

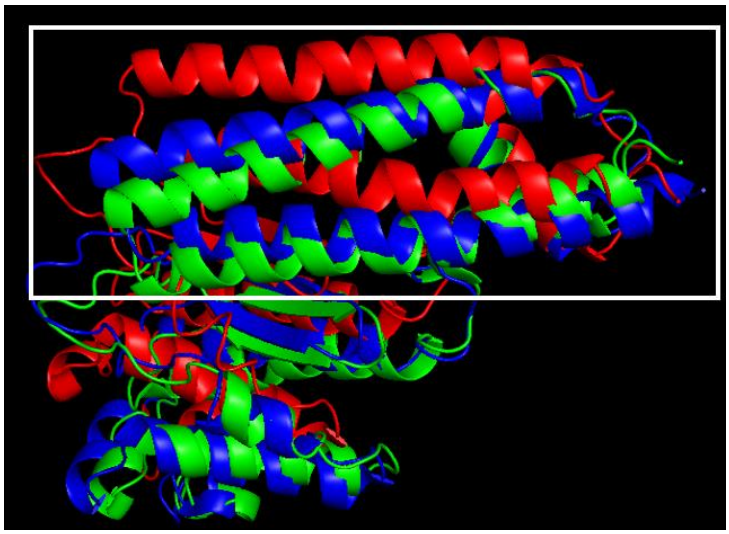

Figure 25 : Superposition of three structures of ACE2. Green ribbon: Native ACE2 (PDB:1R42); Blue ribbon: ACE2-S1 complex (PDB: 7KNB); Red ribbon: ACE2-MLN-4760 complex (PDB: 1R4L). The key helix for S binding on ACE2 moves when an inhibitor is bind to ACE2.

Enzymatic assays were performed for two reasons:

The first reason is to assure ourselves that the freezing/thawing process of ACE2 is not deleterious to its structural conformation. By testing this, we can ensure that the conformational structure is not impacted which is very important for the BLI experiments we performed previously.

The second reason is to better understand the antiviral impact of Lactavir and assess if the presence of Lactavir disrupts the enzymatic activity of ACE2. This action could lead to a destabilization of the S1-ACE2 interaction due to a bending motion as it has been highlighted for an inhibitor.[100] If an impact is demonstrated, more experiments should be done to attest how this disruption occurs.

By recovering ACE2 enzymatic activity, we were able to determine that the freezing/thawing process of ACE2 did not deteriorate the protein to the point of preventing enzymatic activity up to a maximum of two cycles, at which point we observed a significant decrease in enzymatic activity (See Appendix 14).

After a screening of several Lactavir concentrations (0,1µM; 0,5µM; 1µM; 2µM; 4µM; 8µM; 16µM; 50µM) on ACE2 inhibition assay, two concentrations were replicated three times (0,1µM and 1µM) during the same day to avoid any freezing/thawing cycle (See Figure 26).

For this experiment, we used two important control:

a) The negative control (without ACE2) highlight the low fluorescence to the substrate when no enzymatic activity is noticed.
b) The positive control (with ACE2 and 0µM of Lactavir) illustrate the expected enzymatic activity without any external influence of a compound. By enlarging the graphs, we can highlight the early steps of the reaction before reaching the tray and illustrate a potential difference in the rate of reaction.

Overall, there seems to be no significant difference between the positive control and the two Lactavir concentrations tested even though it has been replicated three times. Based on this experiment, we can conclude that Lactavir does not act as an inhibitor of ACE2 nor as a disruptive factor and, therefore, does not impact the S1-ACE2 interaction through the bending motion induced by the presence of an inhibitor in ACE2 catalytic site as explained above.

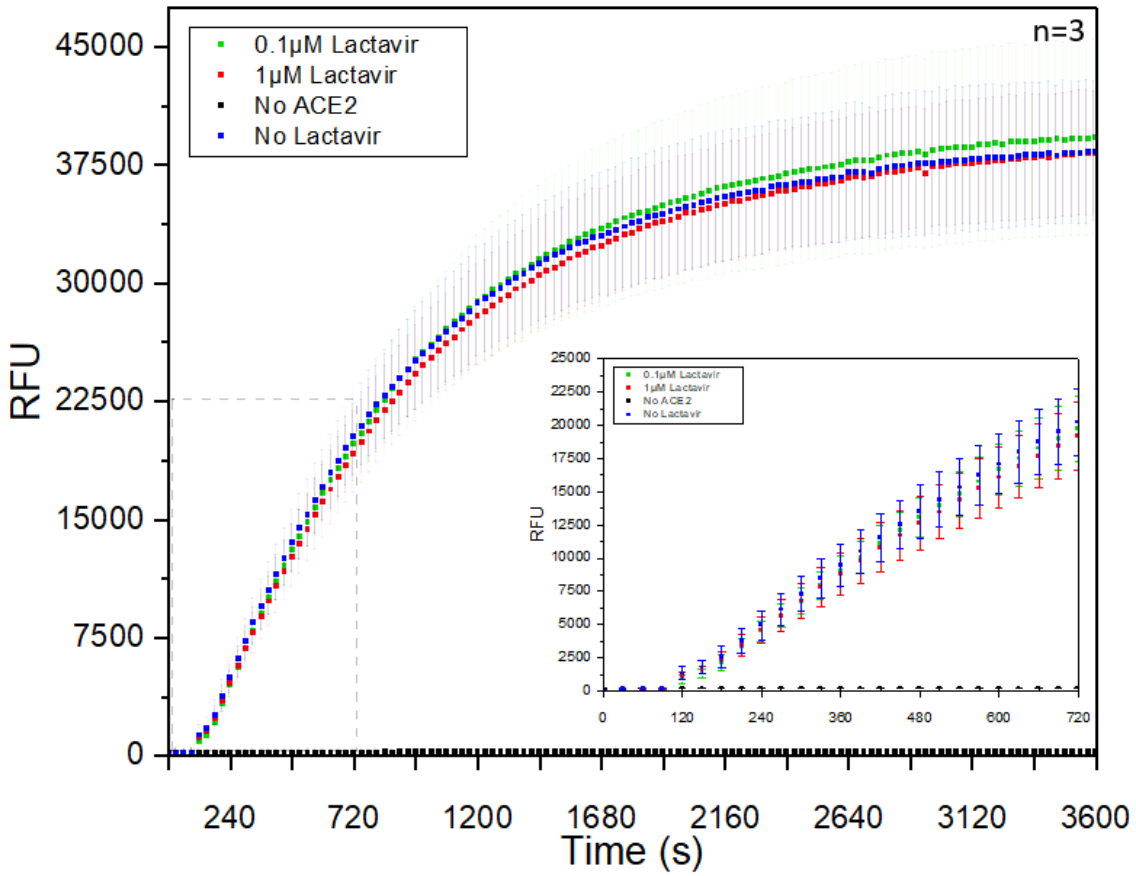

Figure 26 : ACE2 enzymatic experiment in presence of 10µM of $ZnCl_2$. The negative control is without ACE2 (Black dots). Three concentrations of Lactavir were tested (0µM - 0,1µM - 1µM). The whole length of the experiment is shown (3600s) and the early minutes of the experiment are enlarged (length=720s)

4.2 *In cellular* experiments

4.2.1 VSV production

VSV production proved to be challenging and the optimised production protocol is described in Section 3.2.2. Initially, we tried to concentrate VSVs by using PEG precipitation without success as we lost all infectivity from our VSVs in a further infectivity assay. This result is probably due to the omission of flash freezing the samples before putting them in the -80°C, since it is known that slow freezing could be deleterious to biological material.

Afterwards, we stopped trying to concentrate our production as it was easier for us to use them freshly. Theoretically, the VSVs stored at 4°C can be use up to two weeks after production even though we tested after one month and still found signs of infectivity. However, for the experiments presented afterwards, the two weeks period of storage was not exceeded.

As the technique was developed by Kimberley Durlet for the research team, she was in charge of the optimisation of the production and this will not be discussed here. Still, she was able to improve the production of VSVs to obtain a higher Infectious Units per millilitre (IU/mL) from $1\text{-}2x10^5$ IU/mL up to $3x10^8$ IU/mL with the optimised protocol.

Besides concentration, another challenge is the limited volume of VSV production which is correlated to the culture conditions of the HEK293T cells. The volume recovered from the production is of approximately 9,5mL but with the high volume required to infect one plate and the use by several researchers, the volume production needs to be further improved.

For the later experiments showed in this part, we assessed the $TCID_{50}$ (See Box 1) of the virus batch used for the infectivity assay performed the same day. To realise one $TCID_{50}$ test, you need 400µL of fresh viruses while for an infectivity assay, you need 4200µL of fresh viruses. This amount represents almost 50% of our total VSV production so we always diluted our viruses (two- five- or ten-times) to perform an infectivity assay.

4.2.2 Infectivity assays

As the infectivity tests were directly dependent on the production of VSVs, their frequencies had to be adapted according to the quantities of VSVs produced and the periods of production. We tested three different VSV expressing the S protein of various VOCs (Wuhan, Delta and Omicron). However, we failed to validate the infectivity of the Omicron VSV and only did further experiments with the VSV expressing the Wuhan (S(Wuhan)*VSV-ΔG) or Delta S protein (S(Delta)*VSV-ΔG).

Next, we used both VSVs to test the influence of either Lactavir or pyroglutamic acid as it has been shown that both have a similar antiviral effect (See section 1.3). Due to the high number of conditions tested, the number of biological replicates is low (See Appendix 15) and their distribution is scattered which makes it difficult to identify a potential impact of the two antiviral compounds.

The variability of these results motivated us to decrease the number of conditions in order to increase the number of replicates. To do so, we focused the infectivity tests on the impact of Lactavir at three concentrations (1 µM, 10µM and 100µM) and we performed the next tests only with the Wuhan S protein as the Delta S protein was not more produced for the same reason as above.

The following experiment allows us to highlight the interest of increasing the number of biological replicates. Despite the inability to insert a positive control due to a shortage of virus, this experiment indicates that while Lactavir has an effect on the infectivity of pseudotyped VSV, it is not concentration dependent (See Appendix 16)

In total, we realised a dozen of infectivity assays to improve the protocol and our two lasts experiments were obtained by using the optimised protocol presented in Section 3.2.3.

To perform the second to last experiment, we were able to use fresh S(Wuhan)*VSV-ΔG at a high infectivity titer ($3x10^8$ IU/mL) when produced. In only 4 days, the calculated infectivity titer for this batch stored at 4°C dropped to $1,1x10^5$ IU/mL which is not consistent with the literature.[101] However, A549 (ACE2+TMPRSS2) were infected and we can compare the impact of a gradient of Lactavir to our positive control (See Figure 27).

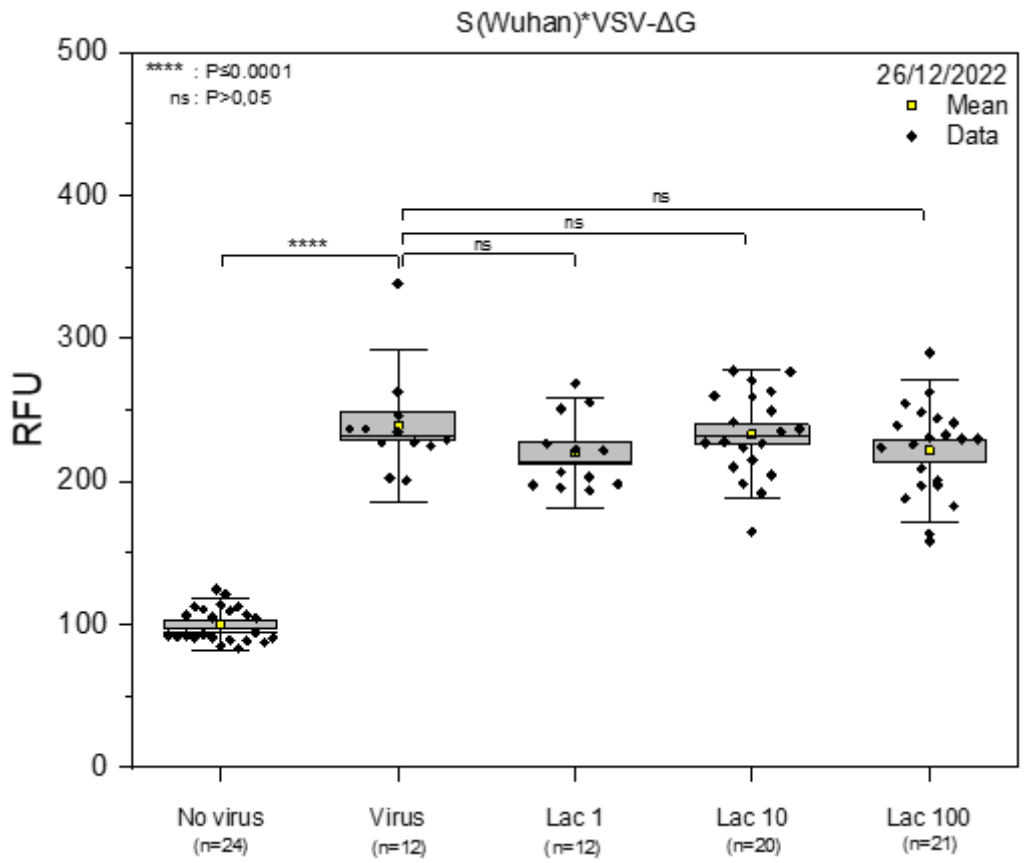

*Figure 27 : Impact of a Lactavir range of concentration (1µM – 10µM – 100µM) on infected A549 cells expressing ACE2 and TMPRSS2 S(Wuhan)*VSV-ΔG. Y axis is Relative Fluorescent Unit (RFU). The infectivity titer for the VSVs used is $1,1x10^5$ IU/mL. A t Test was performed on the raw data and represented on the interval plot.*

A similar conclusion can be drawn, even with a higher number of biological replicates there seems to be no significant impact of Lactavir on the infectivity of our Wuhan S pseudotyped VSVs.

Despite these results, and to make sure we were not missing something, we decided to do a final experiment, this time using freshly prepared Lactavir. Indeed, the Lactavir used for the previous tests had been prepared several months earlier, frozen and thawed several times.

We used a frozen stock of VSVs at a high infectivity titer ($7{,}2x10^7$ IU/mL) before freezing and used it to perform our last infectivity assay. Again, the infectivity titer from this batch dropped to an even lower concentration of $2{,}3x10^3$ IU/mL but A549 (ACE2+TMPRSS2) were still infected (See Appendix 7).

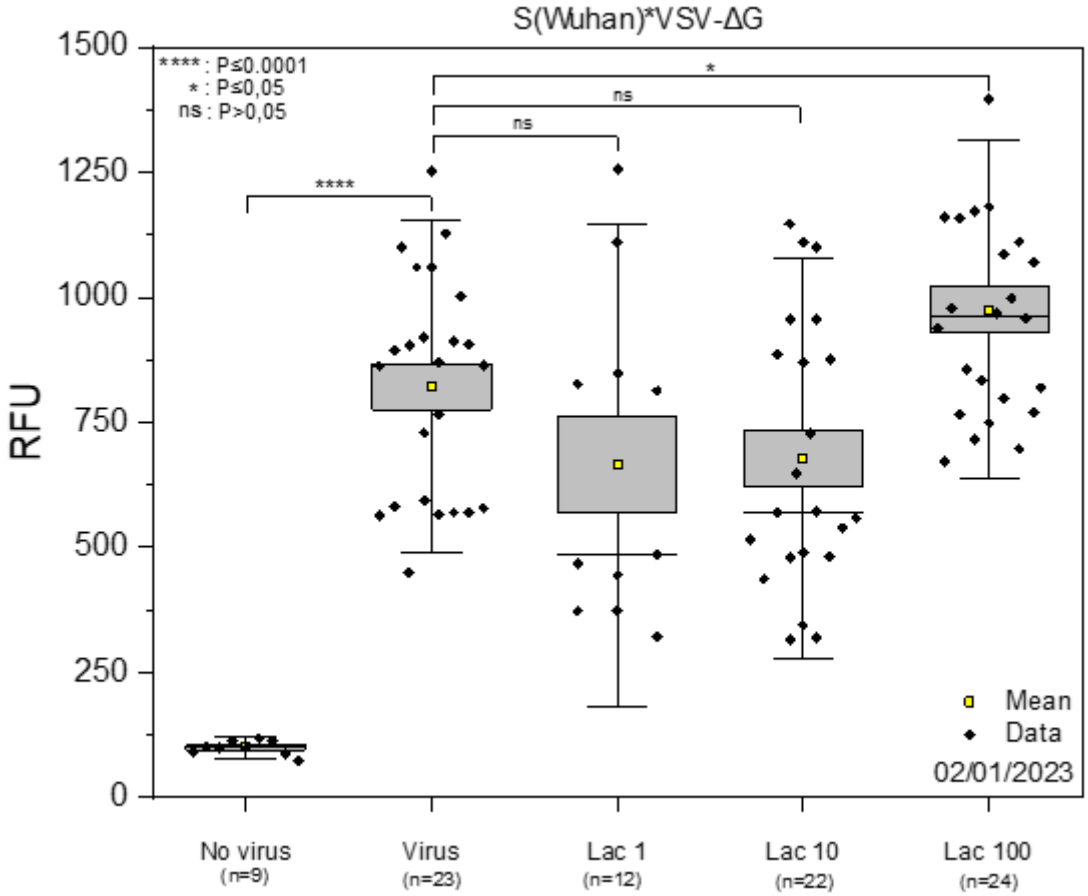

*Figure 28 : Impact of a Lactavir range of concentration (1µM – 10µM – 100µM) on infected A549 cells expressing ACE2 and TMPRSS2 S(Wuhan)*VSV-ΔG. Y axis is Relative Fluorescent Unit (RFU). The infectivity titer for the VSVs used is $2{,}3x10^3$ IU/mL. A t Test was performed on the raw data and represented on the interval plot.*

Even with a greater number of positive controls, we can notice a high variability in our replicates while the values obtained for the negative control are particularly clustered which indicates that a low infectivity titer makes the analysis harder (See Figure 29). Indeed, the high variability observed can be due to a greater disparity of S(Wuhan)*VSV-ΔG within the different wells due to the low infectivity titer obtained after freezing.

To conclude, no significant effects of Lactavir are observed on the infectivity of fresh or frozen S(Wuhan)*VSV-ΔG on A549 cells (ACE2+TMRPSS2). For production reasons, it was unfortunately not possible to compare the effect of Lactavir on the infectivity of pseudotyped VSVs with the S protein of two other VOCs (Delta and Omicron). However, we were able to optimise VSV production and confirm a robust protocol with a high number of replicates for infectivity testing.

5. Conclusion and perspectives

The aim of this master's thesis was to characterize the antiviral effect of Lactavir with *in vitro* and *in cellular* experiments and to obtain more insights concerning the N-terminal pGlu function present on the S protein of the SARS-CoV-2. To do so, we worked through two main axes:

The first axis focused on *in vitro* experiments by using two techniques: BLI and ACE2 inhibition assays.

Due to the use of commercial proteins and our interest in the N-terminal pGlu residue, an MS analysis was carried out with these proteins while performing *in vitro* experiments. We were able to validate the N-ter sequence of S1(Val) which is truncated by two amino terminal residues (deletion of Q14 and C15) but we did not find the N-terminus sequence of S1(pGlu) as proposed by the supplier. However, we detected a peptide present in the S1(pGlu) sample but absent in the S1(Val) sample, and featuring an expected -LTTR C-terminal signature. This signature corresponds to the end of the first N-ter peptide in the S1(Val) which indicates that the rest of the sequence is similar between the two samples. The presence of a N-glycosylation on Asn17 is expected as it has been reported in the literature. However, we were unable to distinctively detect its presence with the conditions used to perform the analysis as we did not used a PNGase which leaves an identifiable scar on the peptide as a feature of a N-glycosylation.

Interestingly, we detected well the N-ter sequence of S1(Val) with our setup which indicates that there is no Asn17 glycosylation on this sample. Both S1 were produced by the same company with HEK293 cells which means that if S1(Val) is not glycosylated, there is no reason to believe that S1(pGlu) would be. Moreover, no corresponding peptide with the additional glycan mass of 1751 Da (mentioned in Section 4.1.1) was found in further research in the MS spectrum of S1(pGlu). Based on this observation, we performed an automatic de novo sequence prediction to gain insights concerning the N-ter of S1(pGlu). We obtained an unexpected sequence that does not match the sequence provided by the supplier but with a N-ter pGlu residue (pEPVTLNSLTTR).

At this point, there are two possibilities:

1) First, there is an Asn17 glycosylation on the S1(pGlu) and not on the S1(Val) and we were unable to detect it due to the setup conditions which questions the presence of N-ter pGlu as our de novo sequencing will not match the masses found.
2) Second, the sequence given by the supplier is not correct and some modifications were done to enable a better expression of the S1 in presence of a N-ter pGlu residue. This better expression being already present in S1(Val), due to the deletion of the pGlu N-ter and a Cys, there were no need to further modify the S protein.

To address these two possibilities, it would be essential to repeat this analysis with PNGase treatment before trypsin digestion. This treatment will remove the N-glycans and allow us to confirm or refute the presence of this post-translational modification. This will allow us to directly determine the veracity of the unexpected N-ter sequence for S1(pGlu).

This analysis raises many questions about the commercial production of proteins and the accuracy of the protein sequences produced. Are these mutations random and there is no sequence check after production or are they intentional? Does the production of S1 with the unaltered sequence have a cytotoxic action on the cell?

Does the mutation of a single amino acid, leaving an N-ter Cys, have a cytotoxic action on the cells when the protein is expressed? If our unexpected sequence is assessed, why is it needed to alter the initial sequence to allow a N-ter pGlu?

Regarding BLI experiments, we investigated the interaction between ACE2-Fc immobilized on the biosensor (ligand) and the soluble S1 protein of SARS-CoV-2 (analyte) with or without pGlu [S1(pGlu) or S1(Val)]. Given the novelty of the technique in the laboratory, we were able to highlight the reproducibility of our measurements and relate them to the existing literature by retrieving K_D values in the nanomolar range.

For the S1-ACE2 interaction, two explanations can be proposed due to the uncertainties raised by the MS analysis:

1) We assume that there is an absence of pGlu at the N-ter part of S1 which indicates that we compared two proteins without any pGlu residues. It is expected that there will be no impact on the affinity constant of the S1-ACE2 interaction.

2) We assume that there is a pGlu at the N-ter part of S1 and we can state that the presence of pGlu residue does not have a significant impact on the S1-ACE2 interaction.

If we want to go further with the second explanation, it would be really important to invert the protein linked to the biosensor to confirm the affinity range for this interaction. Furthermore, it is important to consider that ACE2 also has a putative N-ter pGlu residue. It is putative because no analysis concerning ACE2 has been carried out. It would be interesting to carry the same experiments and comparing the impact of the presence or absence of pGlu on each of the proteins. We could use proteins where N-ter pGlu residue is known to be present and treat them with a pyroglutamyl aminopeptidase that removes the N-ter pyroglutamyl residue. Thanks to this enzyme, we could obtain two nearly identical proteins except for their N-ter end which will be truncated.

Concerning the impact of Lactavir on the S1-ACE2 interaction, the addition of Lactavir above 0,1µM has no concentration-dependent impact on the affinity constant regardless of the S1.

In order to ensure that an effect is not missed, it might be interesting to perform the same experiments with even lower concentrations of Lactavir as the antiviral effects of Lactavir were detected from 50nM in *in vivo* experiments (See Appendix 1). A possible assumption would be that we have a system at saturation in Lactavir where we cannot detect a concentration-dependent effect. By comparing this saturation tray with the absence of Lactavir, we detect a modest decrease of the S1-ACE2 affinity for both proteins, from 20-25nM (without Lactavir) to 35-40nM in K_D values (with Lactavir).

This observed decrease in affinity should be taken with caution as we still are in a nanomolar range of measurement and the biological relevance of it is hard to determine.

Concerning the ACE2 inhibition assay, we performed enzymatic assays in presence of Lactavir to explore its implication in a potential hinge-bending motion of ACE2. A large hinge-bending motion has been highlighted in the literature by using MLN-4760 as an inhibitor of ACE2. This inhibitor possesses two carboxylates that binds inside the catalytic pocket and the binding motion of the whole inhibitor impacts the key helix for S binding on ACE2. Lactavir, being a carboxylate, might bind to ACE2 in the catalytic pocket and this could potentially lead to a modulation of the S1-ACE2 interaction by moving the key helix for S binding to ACE2. If true, it could provide some clarification for the results obtained with *in vivo* experiments. However, we did not measure a significant difference between our positive controls and the two Lactavir concentrations. These results lead to the conclusion that Lactavir does not act as an inhibitor of ACE2 nor as a disruptive factor.

An interesting BLI experiment could be to quantify the effect on the affinity constant of the S1-ACE2 interaction by adding the MLN-4760 inhibitor as we did for Lactavir. By doing this, we could measure the implication of the hinge-bending motion on the S1-ACE2 interaction as it has already been attested for this ACE2 inhibitor in the literature.

The second axis relied on *in cellular* experiments by producing pseudotyped VSVs with the S protein of the following variants (Wuhan, Delta, Omicron). In addition, infectivity assays were performed in presence of Lactavir to attest the antiviral effects of the compound *in cellular* with a physiologically relevant environment.

The VSV production has been greatly improved in order to increase the infectivity titer but further optimizations in production volume are needed. The production limitation can be partially overcome by changing the cell culture flasks from T75 to T175 to recover more than 20mL/flask instead of the actual 9,5mL/flask. Increasing the number of flasks will finally overcome the production problems. Also, the possible long-term storage conditions for VSVs need to be fully explored in order to determine which is the most efficient for maintaining a high infectivity titer. One possibility would be to re-test the concentration of VSVs via PEG precipitation or by using a sugar gradient. However, the impacts of these manipulations need to be measured by performing $TCID_{50}$ tests at regular intervals afterwards, to ensure that the infectivity titer is maintained given the significant differences that we have identified throughout this work.

The infectivity tests were mainly carried out with the S from Wuhan because its production was optimized. Preliminary results were obtained with two VOCs (Delta and Omicron) but no conclusions can be drawn due to the non-repetition of results. No significant effects of Lactavir are observed on the infectivity of fresh or frozen S(Wuhan)*VSV-ΔG on A549 cells (ACE2+TMRPSS2). For future experiments, it would be important to perform a second negative control using A549 cells that do not express ACE2 or TMPRSS2 to ensure that the infectivity we detect is due to membrane fusion entry and not due to the endosomal pathway.

Given the limited knowledge about the mechanism of action of Lactavir, it would be interesting to produce and conduct future tests with the two other VOCs as they possess the D614G mutation that stabilizes the S protein while the Wuhan S does not. Moreover, a Q14N point mutation on each S protein should be done to investigate the importance or not of the N-ter pGlu on the protein. With this mutation, we could measure the differences between the native and modified S protein through infectivity tests.

One trail to explore regarding the analysis of infectivity tests would be to use Fluorescence Activated Cell Sorting (FACS), which has the advantage of being more accurate than performed infectivity scans. However, the ability of cells infected with VSVs to resist treatments prior to the use of the cytometer needs to be assessed.

Overall, we improved the VSV production and reinforce a protocol for infectivity tests using the VSV technique. We demonstrated also the precision and reliability of the BLI technique by improving an existing protocol and adapting it to our subject. More importantly, relevant insights into the *in vitro* effect of Lactavir on S1-ACE2 interaction and into the *in cellular* infectivity assays using S(Wuhan)*VSV-ΔG were gained. We improved the existing knowledge concerning Lactavir and these results can be used for further research to identify future antiviral compounds.

6. Appendix

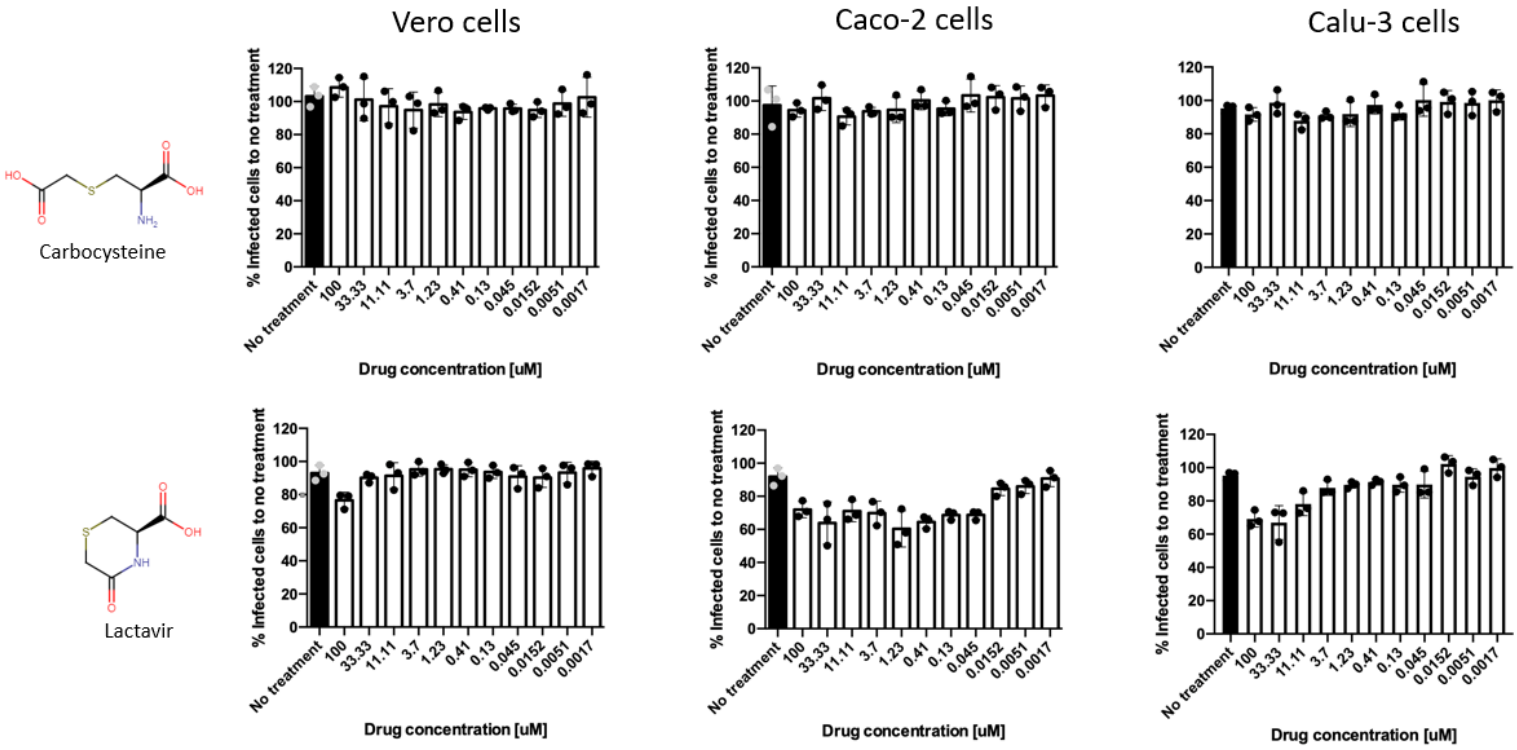

Appendix 1 : First set of experiment performed at Heidelberg using Carbocysteine as a drug for the first row and Lactavir as a drug for the second row. Three cell lines were used (Vero cells; Caco-2 cells and Calu-3 cells) to mimic different types of tissues. For more information on the cell lines, see Box 1.

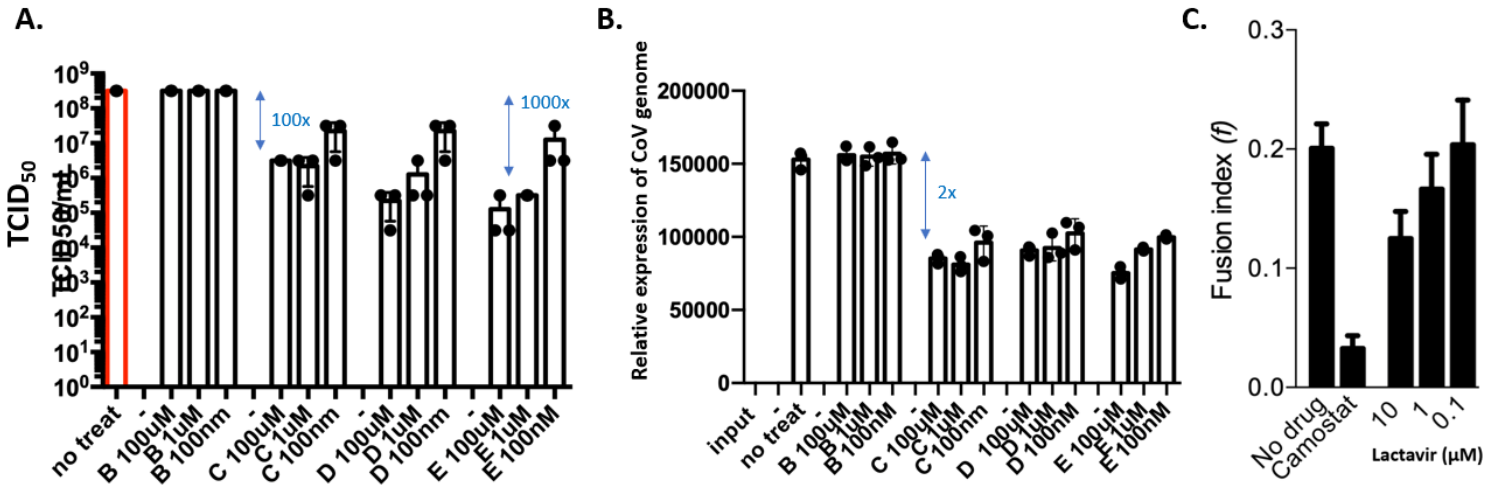

Appendix 2 : Second set of experiment performed in collaboration with Heidelberg. B: carbocysteine; C: Lactavir; D: Lactam 3; E: Pyroglutamate ***A.*** *Quantification of produced viruses 24h post-infection in Caco-2 cells. A decrease of two order of magnitude is observed with Lactavir and up to three order of magnitude with pyroglutamate.* ***B.*** *Quantification of viral RNA by qPCR 24h post-infection in Caco-2 cells. A decrease of ±50% is observed with Lactavir, pyroglutamate and Lactam 3.* ***C.*** *Measure of the fusion index for syncytia formation in presence of Lactavir or Camostat (known inhibitor of TMPRSS2).*

Appendix 3 : Classification of the possible risk groups based on Biosafety in Microbiological and Biomedical Laboratories (BMBL)

Risk Group	Risks and pathogenicity	Bio-Safety Level (BSL) of laboratory facilities:
RG 1	There is no or low individual and community risk. This includes microorganisms that are unlikely to cause human or animal disease	BSL-1
RG 2	There is a moderate individual risk and low community risk. It includes pathogens that can cause human or animal disease but is unlikely to be a serious hazard.	BSL-2
RG 3	There is a high individual risk and low community risk. It includes pathogens that usually causes serious human or animal disease but does is not ordinarily contagious.	BSL-3 also known as containment.
RG 4	There is a high individual risk and community risk. It means that the pathogens can causes serious human or animal disease, and it can be transmitted from one individual to another, directly or indirectly. Moreover, effective treatment and preventive measures are not usually available.	BSL-4 also known as maximum containment.

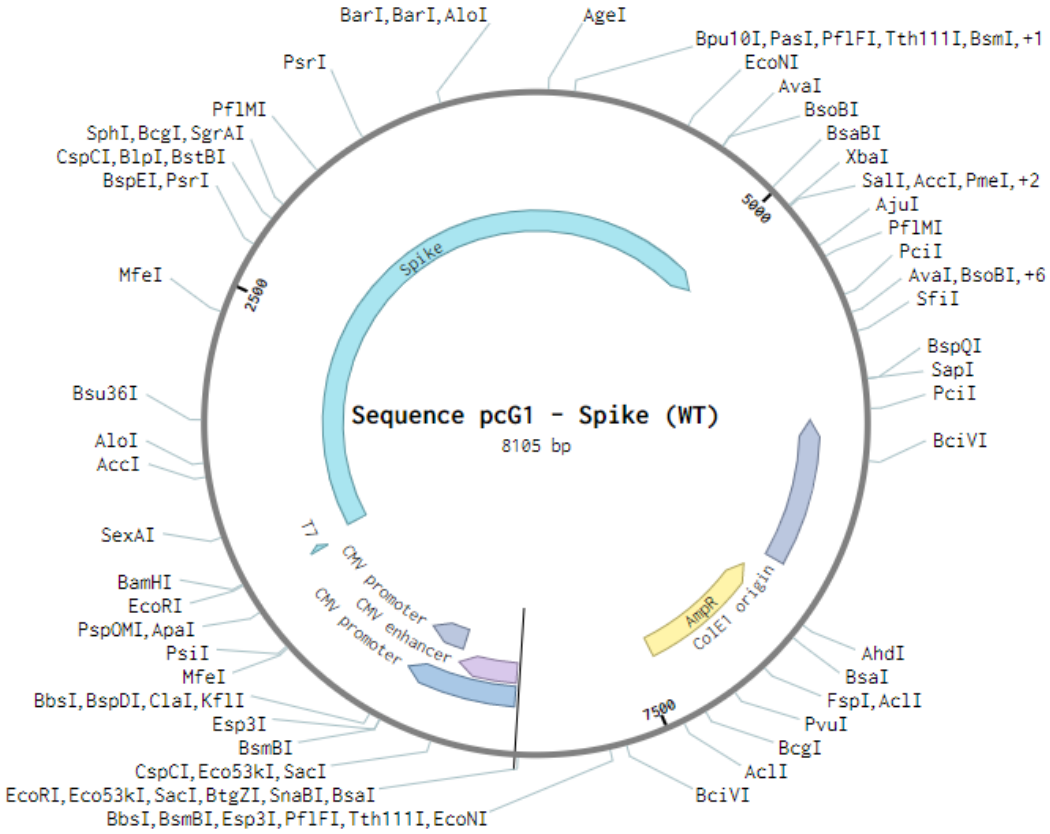

Appendix 4 :Plasmid corresponding to the Wuhan strain (pCG1)

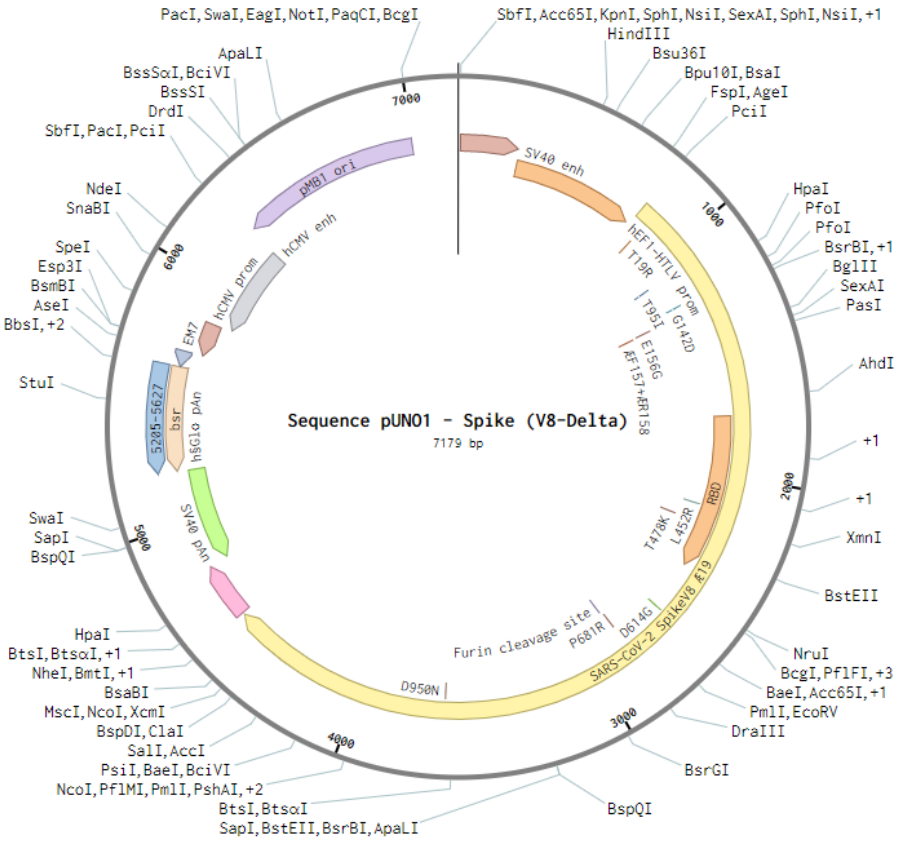

Appendix 5 : Plasmid corresponding to the Delta VOC (pUNO1)

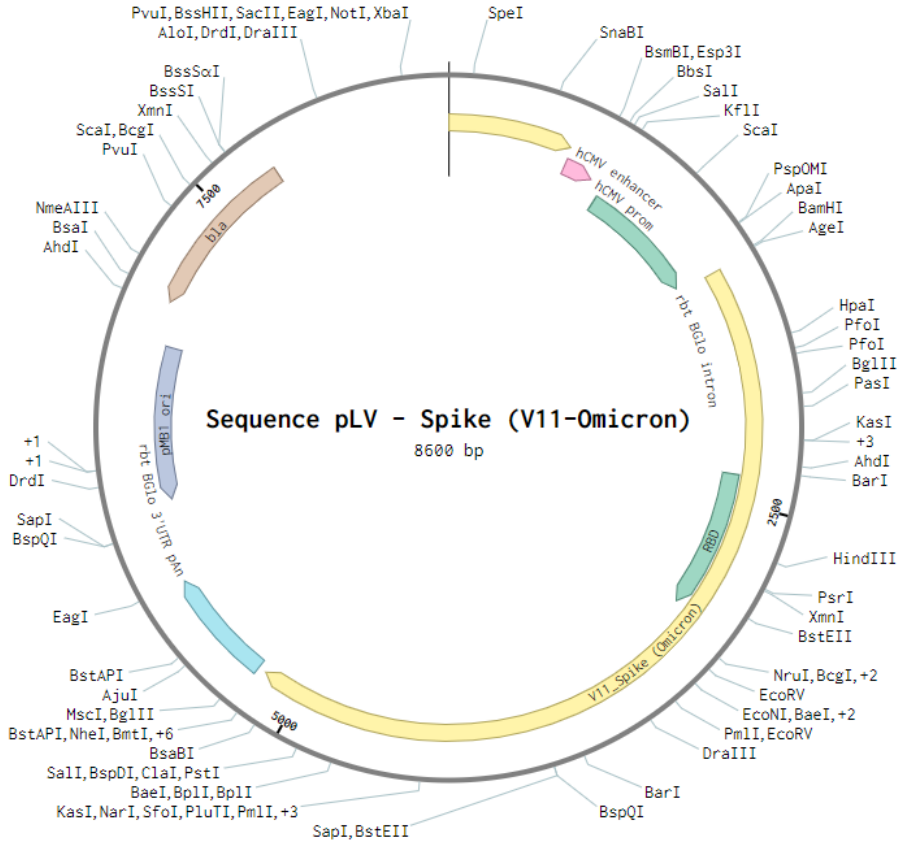

Appendix 6 : Plasmid corresponding to the Omicron VOC (pLV)

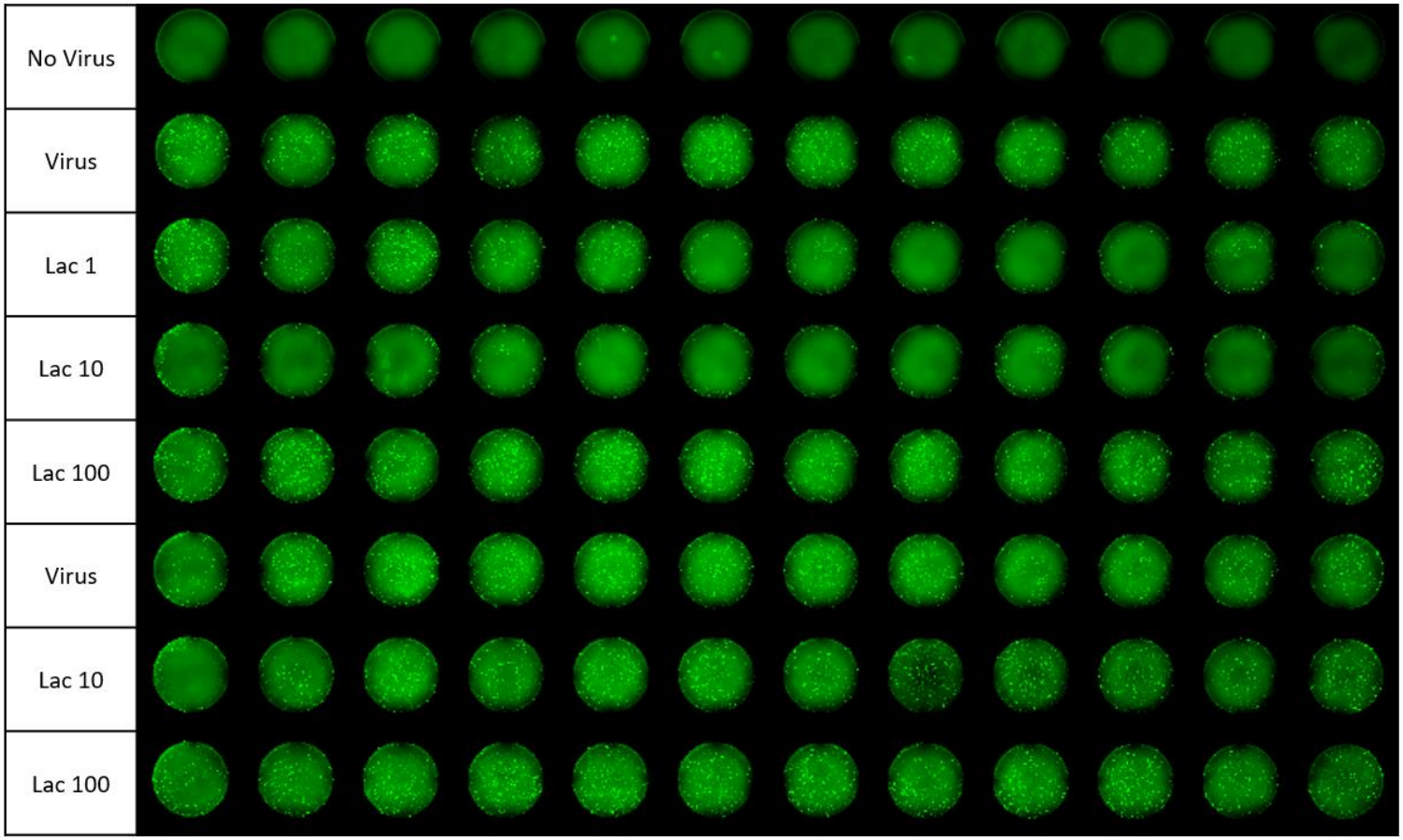

*Appendix 7 : Scan of the infectivity plate of the 02nd of January 2023 with an infectivity titer of 2,3x10³ IU/mL. Each green pixel corresponds to an infected A549 cell. The first row is our negative control without S(Wuhan)*VSV-ΔG and the second row is our positive control with S(Wuhan)*VSV-ΔG but without Lactavir. The interval plot corresponding to this plate is in Figure 33.*

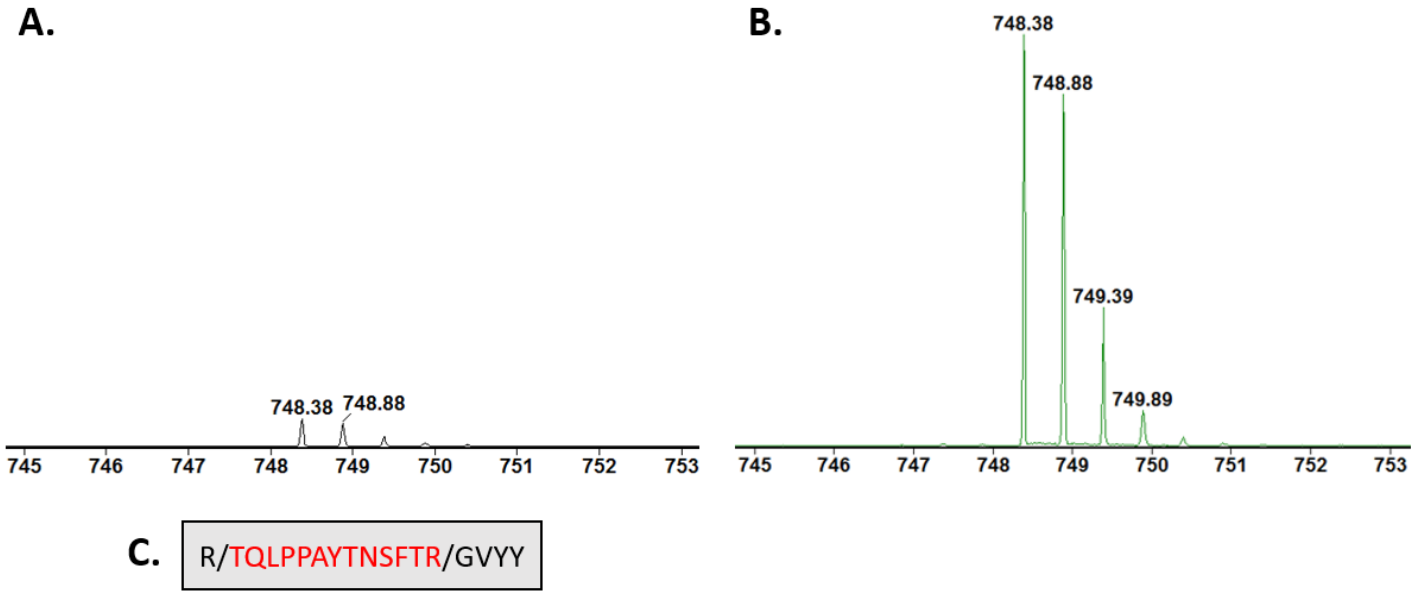

Appendix 8 : MS spectrum for the N-ter part of purchased proteins. ***A.*** *MS spectrum for S1(Val) sample.* ***B.*** *MS spectrum for S1(pGlu) sample.* ***C.*** *Red sequence correspond to the retrieved peptide charged positively two times (m/z = 748.38).*

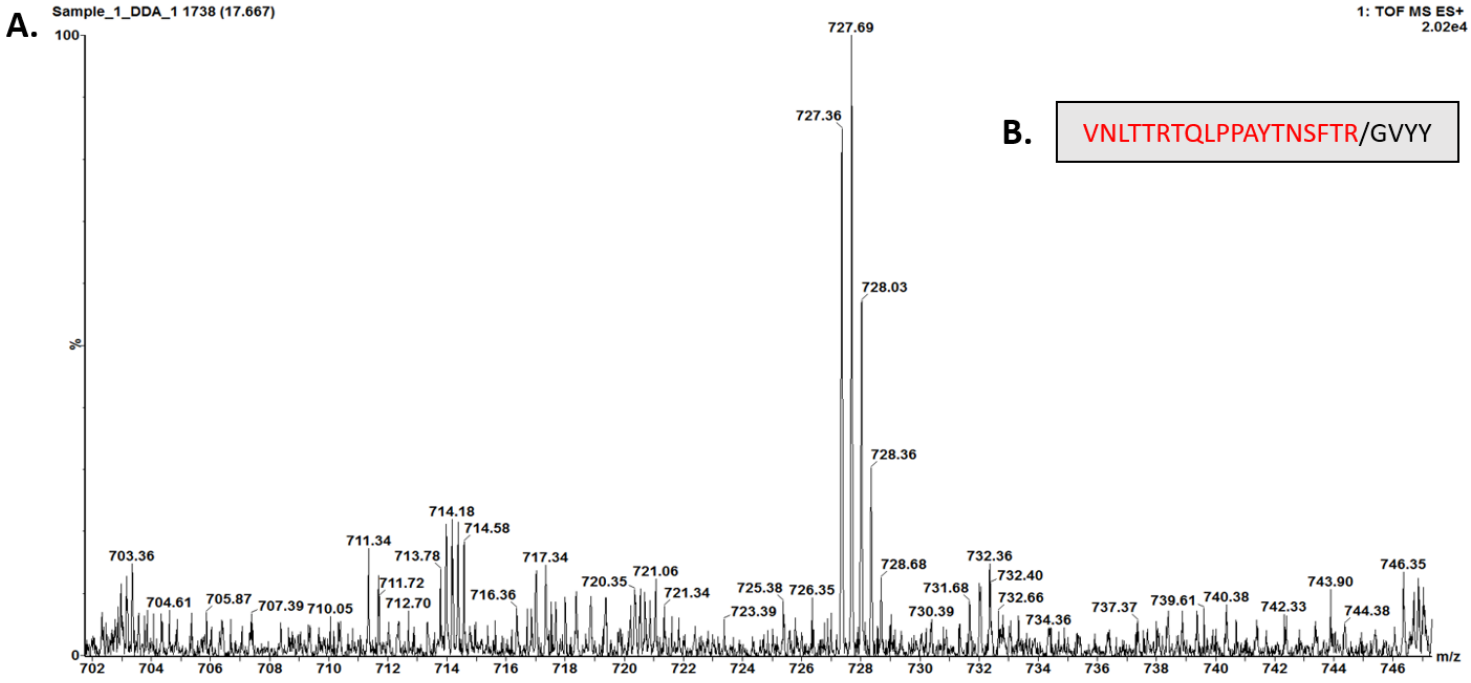

Appendix 9 : ***A.*** *MS spectrum for the N-part of the S1(Val) protein.* ***B.*** *Red sequence correspond to the retrieved peptide charged positively three times (m/z = 727.38).*

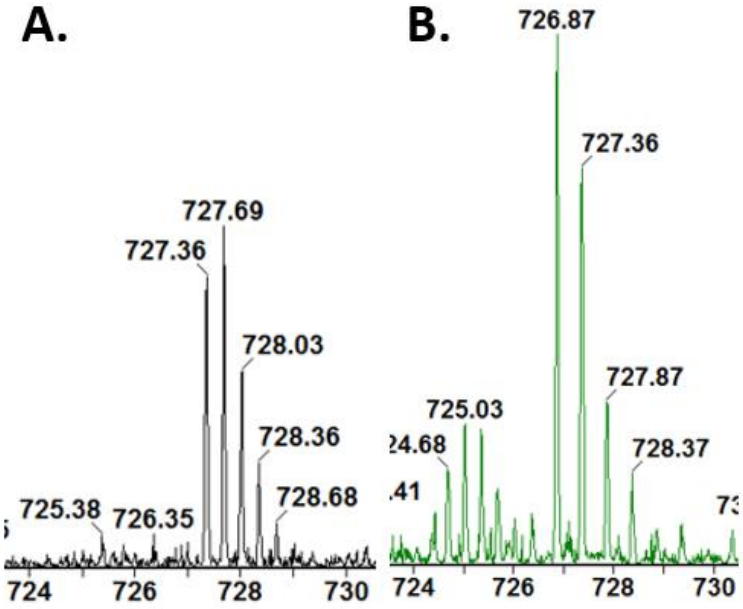

Appendix 10 : ***A.*** *MS spectrum for the N-part of the S1(Val) protein with a peptide charged three times positively (m/z = 727.38).* ***B.*** *MS spectrum for the S1(pGlu) protein. The peptide identified is two times charged positively even though the mass identified (m/z = 726.87) is close to the peptide in A.*

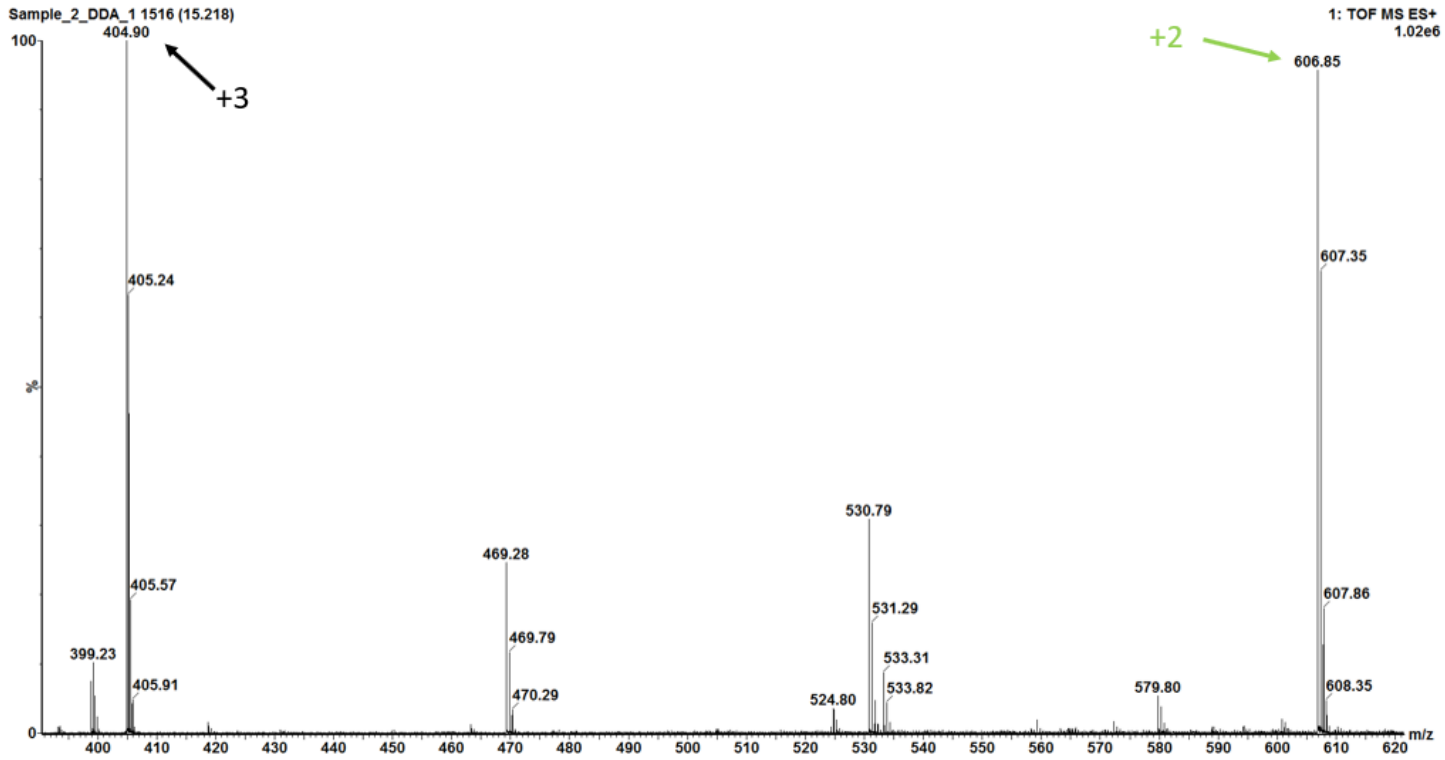

Appendix 11 : MS Spectrum of the N-ter part of the S1(pGlu) protein. We found two pics representing two peptides charged differently. The first one is three times charged (m/z = 404.9) while the second one is two times charged (m/z = 606.85).

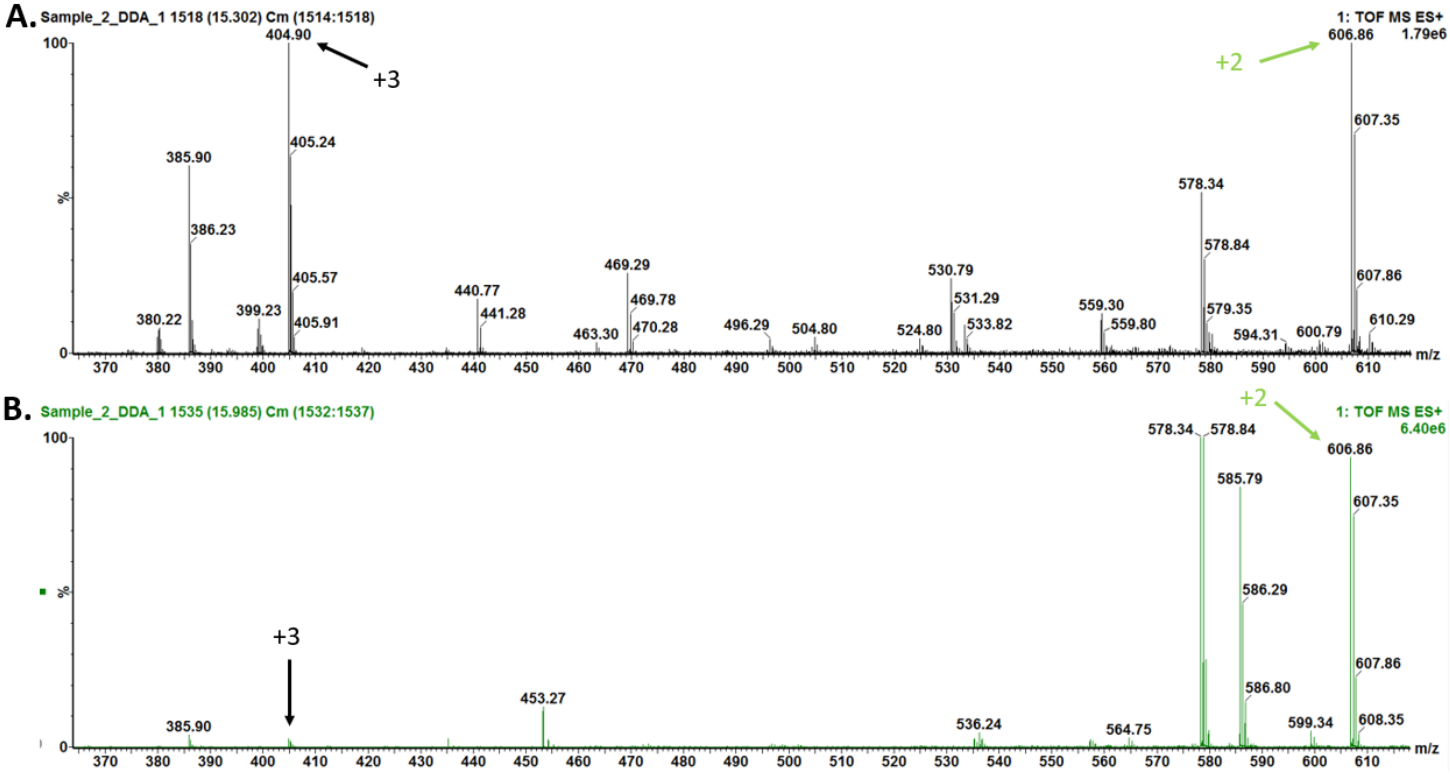

Appendix 12 : MS Spectrum of the N-ter part of the S1(pGlu) protein.
***A.** MS spectrum at elution time 15min30. **B.** MS spectrum at elution time 15min98.*

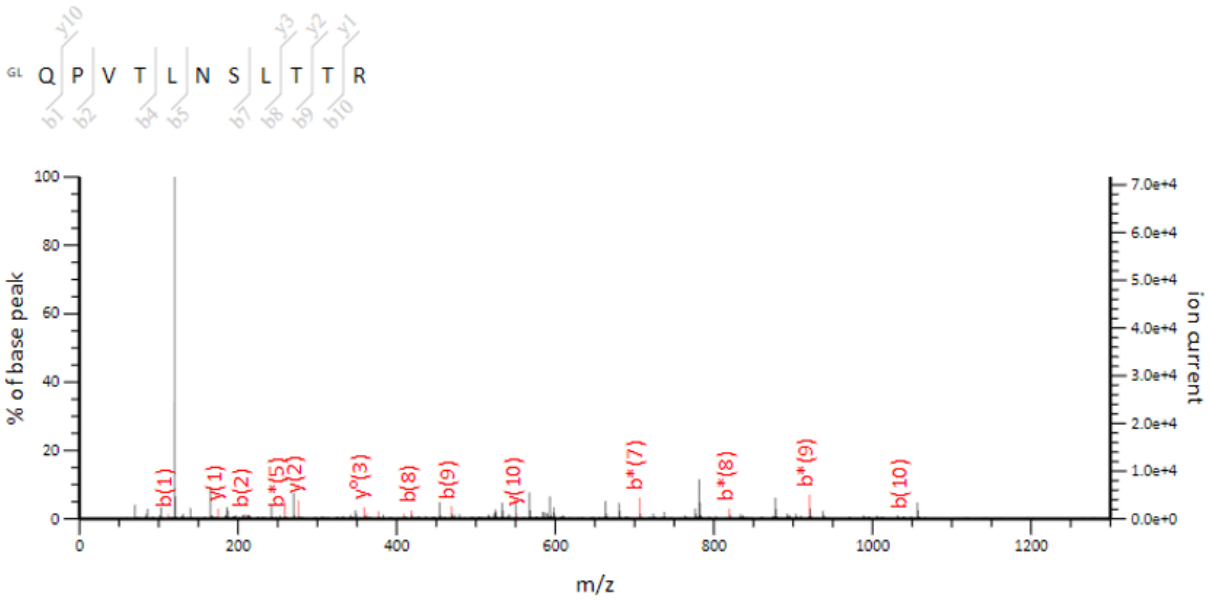

#	b	Seq.	y	#
1	112.0393	Q		11
2	209.0921	P	1101.6263	10
3	308.1605	V	1004.5735	9
4	409.2082	T	905.5051	8
5	522.2922	L	804.4574	7
6	636.3352	N	691.3733	6
7	723.3672	S	577.3304	5
8	836.4512	L	490.2984	4
9	937.4989	T	377.2143	3
10	1038.5466	T	276.1666	2
11		R	175.1190	1

Appendix 13 : Fragmentation spectrum of the N-ter part of the S1(pGlu) protein obtained by using the MASCOT software and identification table of the b and y ions analyzed from the fragmentation spectrum. The monoisotopic mass of neutral peptide is 1211.6510, a fixed modification (Carbamidomethyl) and a variable modification (N-ter: Gln->pE) have been inserted in the software to obtain this unexpected sequence.

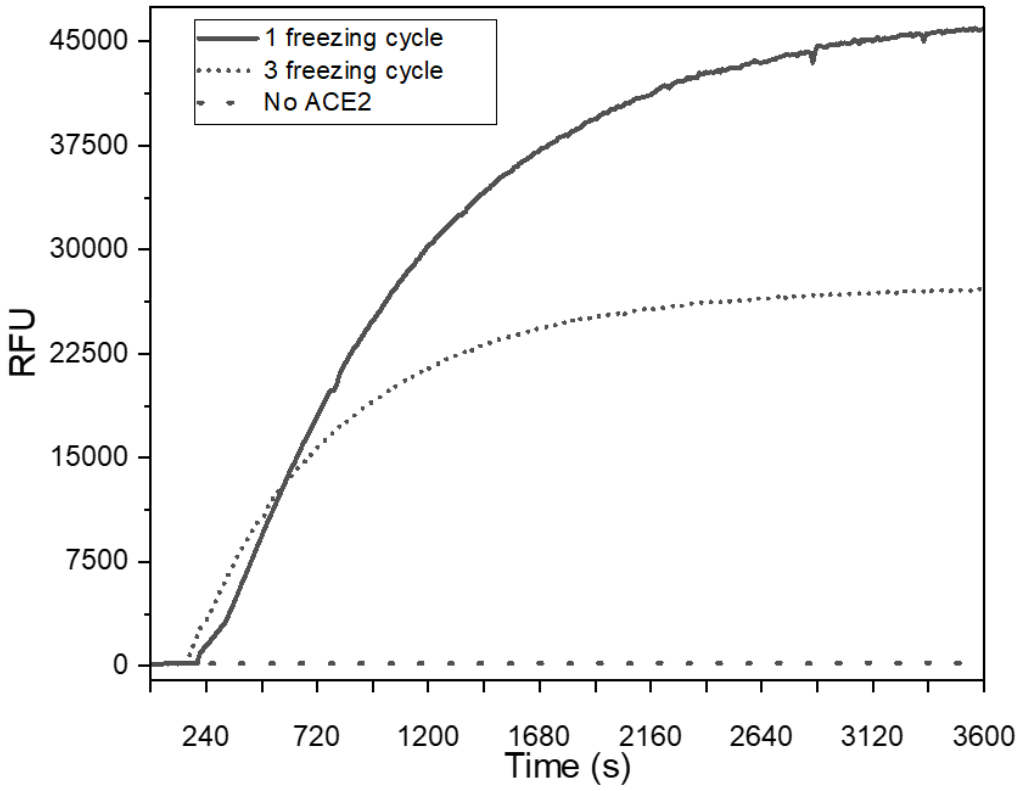

Appendix 14 : Evaluation of the impact of freezing cycles on the enzymatic activity of ACE2 with a fluorogenic substrate Mca-APK(Dnp)-OH. The first freezing cycle describe here correspond to the realization of aliquots and their long-term storage at -20°C after solubilization of the purified powder of the compound. The curve corresponding to the three freezing cycle correspond to two thawing/freezing cycle after the first freezing cycle.

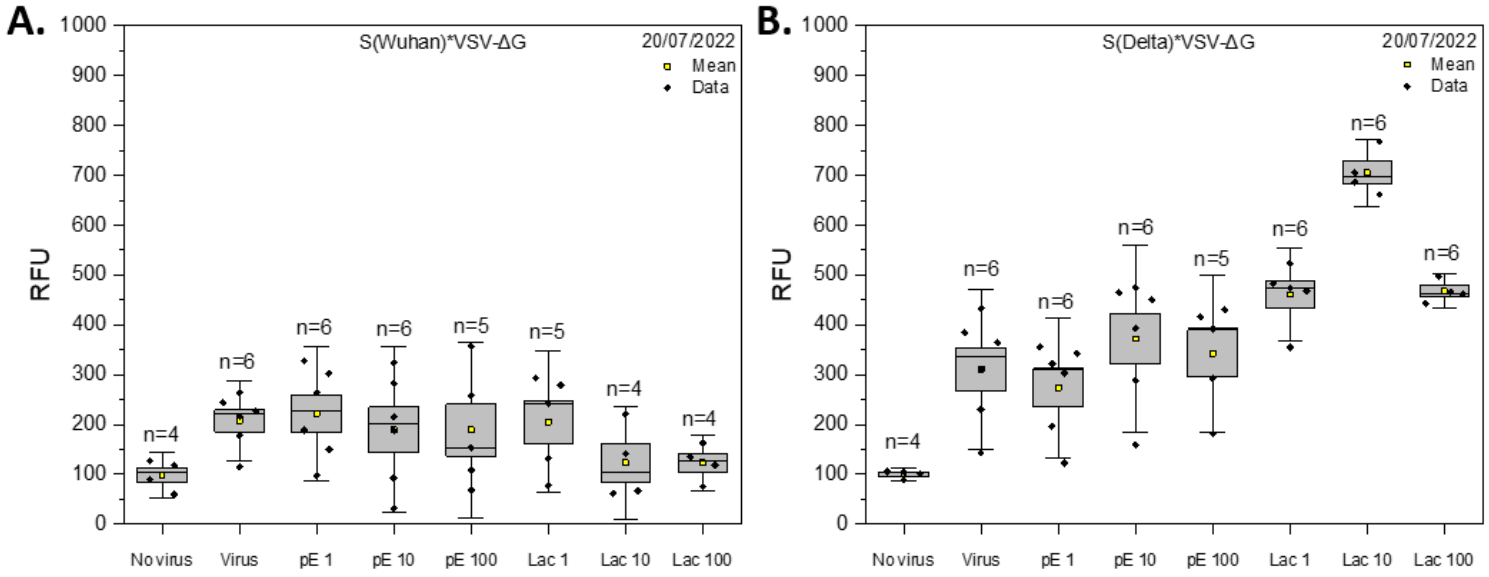

*Appendix 15 : Impact of antiviral compounds on infected A549 cells expressing ACE2 and TMPRSS2 by S(Wuhan)*VSV-ΔG* ***[A]*** *or S(Delta)*VSV-ΔG* ***[B].*** *pE: Pyroglutamic acid (1µM – 10µM – 100µM); Lac: Lactavir (1µM – 10µM – 100µM). Y axis is Relative Fluorescent Unit (RFU)*

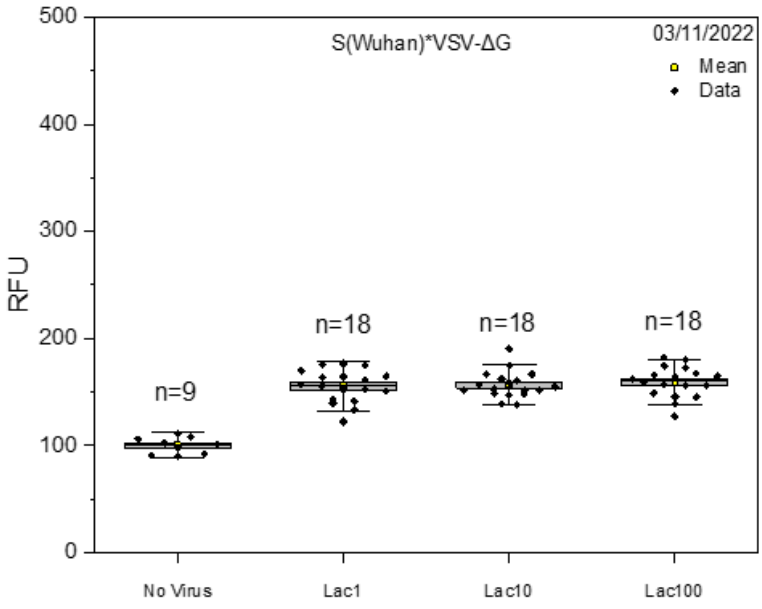

*Appendix 16 : Impact of a Lactavir range of concentration (1µM – 10µM – 100µM) on infected A549 cells expressing ACE2 and TMPRSS2 by S(Wuhan)*VSV-ΔG. Y axis is Relative Fluorescent Unit (RFU)*

7. Bibliography

(1) Chen, Y.; Liu, Q.; Guo, D. Emerging Coronaviruses: Genome Structure, Replication, and Pathogenesis. *J Med Virol* **2020**, *92* (4), 418–423. https://doi.org/10.1002/jmv.25681.

(2) V'kovski, P.; Kratzel, A.; Steiner, S.; Stalder, H.; Thiel, V. Coronavirus Biology and Replication: Implications for SARS-CoV-2. *Nat Rev Microbiol* **2021**, *19* (3), 155–170. https://doi.org/10.1038/s41579-020-00468-6.

(3) Baggen, J.; Vanstreels, E.; Jansen, S.; Daelemans, D. Cellular Host Factors for SARS-CoV-2 Infection. *Nat Microbiol* **2021**, *6* (10), 1219–1232. https://doi.org/10.1038/s41564-021-00958-0.

(4) ICTV. Taxonomy. zimmer.

(5) Saberiyan, M.; Karimi, E.; Khademi, Z.; Movahhed, P.; Safi, A.; Mehri-Ghahfarrokhi, A. SARS-CoV-2: Phenotype, Genotype, and Characterization of Different Variants. *Cell Mol Biol Lett* **2022**, *27* (1), 50. https://doi.org/10.1186/s11658-022-00352-6.

(6) Kesheh, M. M.; Hosseini, P.; Soltani, S.; Zandi, M. An Overview on the Seven Pathogenic Human Coronaviruses. *Reviews in Medical Virology* **2022**, *32* (2). https://doi.org/10.1002/rmv.2282.

(7) Salian, V. S.; Wright, J. A.; Vedell, P. T.; Nair, S.; Li, C.; Kandimalla, M.; Tang, X.; Carmona Porquera, E. M.; Kalari, K. R.; Kandimalla, K. K. COVID-19 Transmission, Current Treatment, and Future Therapeutic Strategies. *Mol. Pharmaceutics* **2021**, *18* (3), 754–771. https://doi.org/10.1021/acs.molpharmaceut.0c00608.

(8) Hu, B.; Guo, H.; Zhou, P.; Shi, Z.-L. Characteristics of SARS-CoV-2 and COVID-19. *Nat Rev Microbiol* **2021**, *19* (3), 141–154. https://doi.org/10.1038/s41579-020-00459-7.

(9) Ali, I.; Alharbi, O. M. L. COVID-19: Disease, Management, Treatment, and Social Impact. *Science of The Total Environment* **2020**, *728*, 138861. https://doi.org/10.1016/j.scitotenv.2020.138861.

(10) Tang, S.; Mao, Y.; Jones, R. M.; Tan, Q.; Ji, J. S.; Li, N.; Shen, J.; Lv, Y.; Pan, L.; Ding, P.; Wang, X.; Wang, Y.; MacIntyre, C. R.; Shi, X. Aerosol Transmission of SARS-CoV-2? Evidence, Prevention and Control. *Environment International* **2020**, *144*, 106039. https://doi.org/10.1016/j.envint.2020.106039.

(11) Zimmer, C.; Wu, J., K.; Corum, J. Coronavirus Drug and Treatment Tracker. August 31, 2022. https://www.nytimes.com/interactive/2020/science/coronavirus-drugs-treatments.html (accessed 2022-11-28).

(12) World Health Organization. https://www.who.int/en/activities/tracking-SARS-CoV-2-variants (accessed 2022-11-25).

(13) COVID-19 Treatment Guidelines. https://www.covid19treatmentguidelines.nih.gov/therapies/antivirals-including-antibody-products/summary-recommendations/.

(14) O'Toole, Á.; Pybus, O. G.; Abram, M. E.; Kelly, E. J.; Rambaut, A. Pango Lineage Designation and Assignment Using SARS-CoV-2 Spike Gene Nucleotide Sequences. *BMC Genomics* **2022**, *23* (1), 121. https://doi.org/10.1186/s12864-022-08358-2.

(15) Starr, T. N.; Greaney, A. J.; Dingens, A. S.; Bloom, J. D. Complete Map of SARS-CoV-2 RBD Mutations That Escape the Monoclonal Antibody LY-CoV555 and Its Cocktail with LY-CoV016. *Cell Reports Medicine* **2021**, *2* (4), 100255. https://doi.org/10.1016/j.xcrm.2021.100255.

(16) Chan, K. C.; Song, Y.; Xu, Z.; Shang, C.; Zhou, R. SARS-CoV-2 Delta Variant: Interplay between Individual Mutations and Their Allosteric Synergy. *Biomolecules* **2022**, *12* (12), 1742. https://doi.org/10.3390/biom12121742.

(17) McCallum, M.; Walls, A. C.; Sprouse, K. R.; Bowen, J. E.; Rosen, L. E.; Dang, H. V.; De Marco, A.; Franko, N.; Tilles, S. W.; Logue, J.; Miranda, M. C.; Ahlrichs, M.; Carter, L.; Snell, G.; Pizzuto, M. S.; Chu, H. Y.; Van Voorhis, W. C.; Corti, D.; Veesler, D. Molecular Basis of Immune Evasion by the Delta and Kappa SARS-CoV-2 Variants. *Science* **2021**, *374* (6575), 1621–1626. https://doi.org/10.1126/science.abl8506.

(18) He, X.; He, C.; Hong, W.; Zhang, K.; Wei, X. The Challenges of COVID-19 Delta Variant: Prevention and Vaccine Development. *MedComm* **2021**, *2* (4), 846–854. https://doi.org/10.1002/mco2.95.
(19) Laenen, L.; Cuypers, L.; Baele, G.; Dellicour, S.; Maes, P.; André, E. *Genomic Surveillance of SARS-CoV-2 in Belgium*; National Rference Center for Coronaviruses: UZ Leuven, 2022. https://www.uzleuven.be/nl/laboratoriumgeneeskunde/genomic-surveillance-sars-cov-2-belgium/genomic-surveillance-sars-cov-2-belgium-graphs (accessed 2022-12-16).
(20) Fang, F. "Flora"; Shi, P.-Y. Omicron: A Drug Developer's Perspective. *Emerging Microbes & Infections* **2022**, *11* (1), 208–211. https://doi.org/10.1080/22221751.2021.2023330.
(21) Zheng, C.; Shao, W.; Chen, X.; Zhang, B.; Wang, G.; Zhang, W. Real-World Effectiveness of COVID-19 Vaccines: A Literature Review and Meta-Analysis. *International Journal of Infectious Diseases* **2022**, *114*, 252–260. https://doi.org/10.1016/j.ijid.2021.11.009.
(22) Hayawi, K.; Shahriar, S.; Serhani, M. A.; Alashwal, H.; Masud, M. M. Vaccine versus Variants (3Vs): Are the COVID-19 Vaccines Effective against the Variants? A Systematic Review. *Vaccines* **2021**, *9* (11), 1305. https://doi.org/10.3390/vaccines9111305.
(23) Huang, Y.; Yang, C.; Xu, X.; Xu, W.; Liu, S. Structural and Functional Properties of SARS-CoV-2 Spike Protein: Potential Antivirus Drug Development for COVID-19. *Acta Pharmacol Sin* **2020**, *41* (9), 1141–1149. https://doi.org/10.1038/s41401-020-0485-4.
(24) Jackson, C. B.; Farzan, M.; Chen, B.; Choe, H. Mechanisms of SARS-CoV-2 Entry into Cells. *Nat Rev Mol Cell Biol* **2022**, *23* (1), 3–20. https://doi.org/10.1038/s41580-021-00418-x.
(25) Petitjean, S. J. L.; Chen, W.; Koehler, M.; Jimmidi, R.; Yang, J.; Mohammed, D.; Juniku, B.; Stanifer, M. L.; Boulant, S.; Vincent, S. P.; Alsteens, D. Multivalent 9-O-Acetylated-Sialic Acid Glycoclusters as Potent Inhibitors for SARS-CoV-2 Infection. *Nat Commun* **2022**, *13* (1), 2564. https://doi.org/10.1038/s41467-022-30313-8.
(26) Wang, M.-Y.; Zhao, R.; Gao, L.-J.; Gao, X.-F.; Wang, D.-P.; Cao, J.-M. SARS-CoV-2: Structure, Biology, and Structure-Based Therapeutics Development. *Front. Cell. Infect. Microbiol.* **2020**, *10*, 587269. https://doi.org/10.3389/fcimb.2020.587269.
(27) Meng, B.; Abdullahi, A.; Ferreira, I. A. T. M.; Goonawardane, N.; Saito, A.; Kimura, I.; Yamasoba, D.; Gerber, P. P.; Fatihi, S.; Rathore, S.; Zepeda, S. K.; Papa, G.; Kemp, S. A.; Ikeda, T.; Toyoda, M.; Tan, T. S.; Kuramochi, J.; Mitsunaga, S.; Ueno, T.; Shirakawa, K.; Takaori-Kondo, A.; Brevini, T.; Mallery, D. L.; Charles, O. J.; The CITIID-NIHR BioResource COVID-19 Collaboration; Baker, S.; Dougan, G.; Hess, C.; Kingston, N.; Lehner, P. J.; Lyons, P. A.; Matheson, N. J.; Ouwehand, W. H.; Saunders, C.; Summers, C.; Thaventhiran, J. E. D.; Toshner, M.; Weekes, M. P.; Maxwell, P.; Shaw, A.; Bucke, A.; Calder, J.; Canna, L.; Domingo, J.; Elmer, A.; Fuller, S.; Harris, J.; Hewitt, S.; Kennet, J.; Jose, S.; Kourampa, J.; Meadows, A.; O'Brien, C.; Price, J.; Publico, C.; Rastall, R.; Ribeiro, C.; Rowlands, J.; Ruffolo, V.; Tordesillas, H.; Bullman, B.; Dunmore, B. J.; Gräf, S.; Hodgson, J.; Huang, C.; Hunter, K.; Jones, E.; Legchenko, E.; Matara, C.; Martin, J.; Mescia, F.; O'Donnell, C.; Pointon, L.; Shih, J.; Sutcliffe, R.; Tilly, T.; Treacy, C.; Tong, Z.; Wood, J.; Wylot, M.; Betancourt, A.; Bower, G.; Cossetti, C.; De Sa, A.; Epping, M.; Fawke, S.; Gleadall, N.; Grenfell, R.; Hinch, A.; Jackson, S.; Jarvis, I.; Krishna, B.; Nice, F.; Omarjee, O.; Perera, M.; Potts, M.; Richoz, N.; Romashova, V.; Stefanucci, L.; Strezlecki, M.; Turner, L.; De Bie, E. M. D. D.; Bunclark, K.; Josipovic, M.; Mackay, M.; Butcher, H.; Caputo, D.; Chandler, M.; Chinnery, P.; Clapham-Riley, D.; Dewhurst, E.; Fernandez, C.; Furlong, A.; Graves, B.; Gray, J.; Hein, S.; Ivers, T.; Le Gresley, E.; Linger, R.; Kasanicki, M.; King, R.; Kingston, N.; Meloy, S.; Moulton, A.; Muldoon, F.; Ovington, N.; Papadia, S.; Penkett, C. J.; Phelan, I.; Ranganath, V.; Paraschiv, R.; Sage, A.; Sambrook, J.; Scholtes, I.; Schon, K.; Stark, H.; Stirrups, K. E.; Townsend, P.; Walker, N.; Webster, J.; The Genotype to Phenotype Japan (G2P-Japan) Consortium; Butlertanaka, E. P.; Tanaka, Y. L.; Ito, J.; Uriu, K.; Kosugi, Y.; Suganami, M.; Oide, A.; Yokoyama, M.; Chiba, M.; Motozono, C.; Nasser, H.; Shimizu, R.; Kitazato, K.; Hasebe, H.; Irie, T.; Nakagawa, S.; Wu, J.; Takahashi, M.; Fukuhara, T.; Shimizu, K.; Tsushima, K.; Kubo, H.; Kazuma, Y.; Nomura, R.; Horisawa, Y.; Nagata, K.; Kawai, Y.; Yanagida, Y.; Tashiro, Y.; Tokunaga, K.; Ozono, S.; Kawabata, R.; Morizako, N.; Sadamasu, K.; Asakura, H.; Nagashima, M.; Yoshimura, K.; Ecuador-COVID19 Consortium;

Cárdenas, P.; Muñoz, E.; Barragan, V.; Márquez, S.; Prado-Vivar, B.; Becerra-Wong, M.; Caravajal, M.; Trueba, G.; Rojas-Silva, P.; Grunauer, M.; Gutierrez, B.; Guadalupe, J. J.; Fernández-Cadena, J. C.; Andrade-Molina, D.; Baldeon, M.; Pinos, A.; Bowen, J. E.; Joshi, A.; Walls, A. C.; Jackson, L.; Martin, D.; Smith, K. G. C.; Bradley, J.; Briggs, J. A. G.; Choi, J.; Madissoon, E.; Meyer, K. B.; Mlcochova, P.; Ceron-Gutierrez, L.; Doffinger, R.; Teichmann, S. A.; Fisher, A. J.; Pizzuto, M. S.; de Marco, A.; Corti, D.; Hosmillo, M.; Lee, J. H.; James, L. C.; Thukral, L.; Veesler, D.; Sigal, A.; Sampaziotis, F.; Goodfellow, I. G.; Matheson, N. J.; Sato, K.; Gupta, R. K. Altered TMPRSS2 Usage by SARS-CoV-2 Omicron Impacts Infectivity and Fusogenicity. *Nature* **2022**, *603* (7902), 706–714. https://doi.org/10.1038/s41586-022-04474-x.

(28) Gong, Y.; Qin, S.; Dai, L.; Tian, Z. The Glycosylation in SARS-CoV-2 and Its Receptor ACE2. *Sig Transduct Target Ther* **2021**, *6* (1), 396. https://doi.org/10.1038/s41392-021-00809-8.

(29) Casas-Sanchez, A.; Romero-Ramirez, A.; Hargreaves, E.; Ellis, C. C.; Grajeda, B. I.; Estevao, I. L.; Patterson, E. I.; Hughes, G. L.; Almeida, I. C.; Zech, T.; Acosta-Serrano, Á. Inhibition of Protein *N*- Glycosylation Blocks SARS-CoV-2 Infection. *mBio* **2022**, *13* (1), e03718-21. https://doi.org/10.1128/mbio.03718-21.

(30) Wang, D.; Zhou, B.; Keppel, T. R.; Solano, M.; Baudys, J.; Goldstein, J.; Finn, M. G.; Fan, X.; Chapman, A. P.; Bundy, J. L.; Woolfitt, A. R.; Osman, S. H.; Pirkle, J. L.; Wentworth, D. E.; Barr, J. R. N-Glycosylation Profiles of the SARS-CoV-2 Spike D614G Mutant and Its Ancestral Protein Characterized by Advanced Mass Spectrometry. *Sci Rep* **2021**, *11* (1), 23561. https://doi.org/10.1038/s41598-021-02904-w.

(31) Zhang, Y.; Zhao, W.; Mao, Y.; Chen, Y.; Zheng, S.; Cao, W.; Zhu, J.; Hu, L.; Gong, M.; Cheng, J.; Yang, H. O-Glycosylation Landscapes of SARS-CoV-2 Spike Proteins. *Front. Chem.* **2021**, *9*, 689521. https://doi.org/10.3389/fchem.2021.689521.

(32) Marcon, C. Deciphering the Single Molecule Interaction between the DC-/L-SIGN and the Severe Acute Respiratory Syndrome Coronavirus 2 (SARS-CoV-2) S1 Protein Using Atomic Force Microscopy (AFM), 2022.

(33) Zhang, J.; Cai, Y.; Xiao, T.; Lu, J.; Peng, H.; Sterling, S. M.; Walsh, R. M.; Rits-Volloch, S.; Zhu, H.; Woosley, A. N.; Yang, W.; Sliz, P.; Chen, B. Structural Impact on SARS-CoV-2 Spike Protein by D614G Substitution. *Science* **2021**, *372* (6541), 525–530. https://doi.org/10.1126/science.abf2303.

(34) Takeda, M. Proteolytic Activation of SARS-CoV-2 Spike Protein. *Microbiology and Immunology* **2022**, *66* (1), 15–23. https://doi.org/10.1111/1348-0421.12945.

(35) Ozono, S.; Zhang, Y.; Ode, H.; Sano, K.; Tan, T. S.; Imai, K.; Miyoshi, K.; Kishigami, S.; Ueno, T.; Iwatani, Y.; Suzuki, T.; Tokunaga, K. SARS-CoV-2 D614G Spike Mutation Increases Entry Efficiency with Enhanced ACE2-Binding Affinity. *Nat Commun* **2021**, *12* (1), 848. https://doi.org/10.1038/s41467-021-21118-2.

(36) Letko, M.; Marzi, A.; Munster, V. Functional Assessment of Cell Entry and Receptor Usage for SARS-CoV-2 and Other Lineage B Betacoronaviruses. *Nat Microbiol* **2020**, *5* (4), 562–569. https://doi.org/10.1038/s41564-020-0688-y.

(37) Klinakis, A.; Cournia, Z.; Rampias, T. N-Terminal Domain Mutations of the Spike Protein Are Structurally Implicated in Epitope Recognition in Emerging SARS-CoV-2 Strains. *Computational and Structural Biotechnology Journal* **2021**, *19*, 5556–5567. https://doi.org/10.1016/j.csbj.2021.10.004.

(38) Soh, W. T.; Liu, Y.; Nakayama, E. E.; Ono, C.; Torii, S.; Nakagami, H.; Matsuura, Y.; Shioda, T.; Arase, H. *The N-Terminal Domain of Spike Glycoprotein Mediates SARS-CoV-2 Infection by Associating with L-SIGN and DC-SIGN*; preprint; Microbiology, 2020. https://doi.org/10.1101/2020.11.05.369264.

(39) Benton, D. J.; Wrobel, A. G.; Xu, P.; Roustan, C.; Martin, S. R.; Rosenthal, P. B.; Skehel, J. J.; Gamblin, S. J. Receptor Binding and Priming of the Spike Protein of SARS-CoV-2 for Membrane Fusion. *Nature* **2020**, *588* (7837), 327–330. https://doi.org/10.1038/s41586-020-2772-0.

(40) Gur, M.; Taka, E.; Yilmaz, S. Z.; Kilinc, C.; Aktas, U.; Golcuk, M. Conformational Transition of SARS-CoV-2 Spike Glycoprotein between Its Closed and Open States. *J. Chem. Phys.* **2020**, *153* (7), 075101. https://doi.org/10.1063/5.0011141.
(41) Ning, S.; Yu, B.; Wang, Y.; Wang, F. SARS-CoV-2: Origin, Evolution, and Targeting Inhibition. *Front. Cell. Infect. Microbiol.* **2021**, *11*, 676451. https://doi.org/10.3389/fcimb.2021.676451.
(42) Essalmani, R.; Jain, J.; Susan-Resiga, D.; Andréo, U.; Evagelidis, A.; Derbali, R. M.; Huynh, D. N.; Dallaire, F.; Laporte, M.; Delpal, A.; Sutto-Ortiz, P.; Coutard, B.; Mapa, C.; Wilcoxen, K.; Decroly, E.; NQ Pham, T.; Cohen, É. A.; Seidah, N. G. Distinctive Roles of Furin and TMPRSS2 in SARS-CoV-2 Infectivity. *J Virol* **2022**, *96* (8), e00128-22. https://doi.org/10.1128/jvi.00128-22.
(43) Yao, H.; Song, Y.; Chen, Y.; Wu, N.; Xu, J.; Sun, C.; Zhang, J.; Weng, T.; Zhang, Z.; Wu, Z.; Cheng, L.; Shi, D.; Lu, X.; Lei, J.; Crispin, M.; Shi, Y.; Li, L.; Li, S. Molecular Architecture of the SARS-CoV-2 Virus. *Cell* **2020**, *183* (3), 730-738.e13. https://doi.org/10.1016/j.cell.2020.09.018.
(44) Cai, Y.; Zhang, J.; Xiao, T.; Peng, H.; Sterling, S. M.; Walsh, R. M.; Rawson, S.; Rits-Volloch, S.; Chen, B. Distinct Conformational States of SARS-CoV-2 Spike Protein. *Science* **2020**, *369* (6511), 1586–1592. https://doi.org/10.1126/science.abd4251.
(45) Tai, L.; Zhu, G.; Yang, M.; Cao, L.; Xing, X.; Yin, G.; Chan, C.; Qin, C.; Rao, Z.; Wang, X.; Sun, F.; Zhu, Y. Nanometer-Resolution in Situ Structure of the SARS-CoV-2 Postfusion Spike Protein. *Proc. Natl. Acad. Sci. U.S.A.* **2021**, *118* (48), e2112703118. https://doi.org/10.1073/pnas.2112703118.
(46) Tortorici, M. A.; Walls, A. C.; Lang, Y.; Wang, C.; Li, Z.; Koerhuis, D.; Boons, G.-J.; Bosch, B.-J.; Rey, F. A.; de Groot, R. J.; Veesler, D. Structural Basis for Human Coronavirus Attachment to Sialic Acid Receptors. *Nat Struct Mol Biol* **2019**, *26* (6), 481–489. https://doi.org/10.1038/s41594-019-0233-y.
(47) Glowacka, I.; Bertram, S.; Müller, M. A.; Allen, P.; Soilleux, E.; Pfefferle, S.; Steffen, I.; Tsegaye, T. S.; He, Y.; Gnirss, K.; Niemeyer, D.; Schneider, H.; Drosten, C.; Pöhlmann, S. Evidence That TMPRSS2 Activates the Severe Acute Respiratory Syndrome Coronavirus Spike Protein for Membrane Fusion and Reduces Viral Control by the Humoral Immune Response. *J Virol* **2011**, *85* (9), 4122–4134. https://doi.org/10.1128/JVI.02232-10.
(48) Limburg, H.; Harbig, A.; Bestle, D.; Stein, D. A.; Moulton, H. M.; Jaeger, J.; Janga, H.; Hardes, K.; Koepke, J.; Schulte, L.; Koczulla, A. R.; Schmeck, B.; Klenk, H.-D.; Böttcher-Friebertshäuser, E. TMPRSS2 Is the Major Activating Protease of Influenza A Virus in Primary Human Airway Cells and Influenza B Virus in Human Type II Pneumocytes. *J Virol* **2019**, *93* (21), e00649-19. https://doi.org/10.1128/JVI.00649-19.
(49) Walls, A. C.; Tortorici, M. A.; Snijder, J.; Xiong, X.; Bosch, B.-J.; Rey, F. A.; Veesler, D. Tectonic Conformational Changes of a Coronavirus Spike Glycoprotein Promote Membrane Fusion. *Proc. Natl. Acad. Sci. U.S.A.* **2017**, *114* (42), 11157–11162. https://doi.org/10.1073/pnas.1708727114.
(50) Liu, S.; Xiao, G.; Chen, Y.; He, Y.; Niu, J.; Escalante, C. R.; Xiong, H.; Farmar, J.; Debnath, A. K.; Tien, P.; Jiang, S. Interaction between Heptad Repeat 1 and 2 Regions in Spike Protein of SARS-Associated Coronavirus: Implications for Virus Fusogenic Mechanism and Identification of Fusion Inhibitors. *The Lancet* **2004**, *363* (9413), 938–947. https://doi.org/10.1016/S0140-6736(04)15788-7.
(51) Luchini, A.; Micciulla, S.; Corucci, G.; Batchu, K. C.; Santamaria, A.; Laux, V.; Darwish, T.; Russell, R. A.; Thepaut, M.; Bally, I.; Fieschi, F.; Fragneto, G. Lipid Bilayer Degradation Induced by SARS-CoV-2 Spike Protein as Revealed by Neutron Reflectometry. *Sci Rep* **2021**, *11* (1), 14867. https://doi.org/10.1038/s41598-021-93996-x.
(52) Correa, Y.; Waldie, S.; Thépaut, M.; Micciulla, S.; Moulin, M.; Fieschi, F.; Pichler, H.; Trevor Forsyth, V.; Haertlein, M.; Cárdenas, M. SARS-CoV-2 Spike Protein Removes Lipids from Model Membranes and Interferes with the Capacity of High Density Lipoprotein to Exchange Lipids. *Journal of Colloid and Interface Science* **2021**, *602*, 732–739. https://doi.org/10.1016/j.jcis.2021.06.056.

(53) Davidson, A. M.; Wysocki, J.; Batlle, D. Interaction of SARS-CoV-2 and Other Coronavirus With ACE (Angiotensin-Converting Enzyme)-2 as Their Main Receptor: Therapeutic Implications. *Hypertension* **2020**, *76* (5), 1339–1349. https://doi.org/10.1161/HYPERTENSIONAHA.120.15256.
(54) Yan, R.; Zhang, Y.; Li, Y.; Xia, L.; Guo, Y.; Zhou, Q. Structural Basis for the Recognition of SARS-CoV-2 by Full-Length Human ACE2. *Science* **2020**, *367* (6485), 1444–1448. https://doi.org/10.1126/science.abb2762.
(55) Ali, A.; Vijayan, R. Dynamics of the ACE2–SARS-CoV-2/SARS-CoV Spike Protein Interface Reveal Unique Mechanisms. *Sci Rep* **2020**, *10* (1), 14214. https://doi.org/10.1038/s41598-020-71188-3.
(56) Yang, J.; Petitjean, S. J. L.; Koehler, M.; Zhang, Q.; Dumitru, A. C.; Chen, W.; Derclaye, S.; Vincent, S. P.; Soumillion, P.; Alsteens, D. Molecular Interaction and Inhibition of SARS-CoV-2 Binding to the ACE2 Receptor. *Nat Commun* **2020**, *11* (1), 4541. https://doi.org/10.1038/s41467-020-18319-6.
(57) Lan, J.; Ge, J.; Yu, J.; Shan, S.; Zhou, H.; Fan, S.; Zhang, Q.; Shi, X.; Wang, Q.; Zhang, L.; Wang, X. Structure of the SARS-CoV-2 Spike Receptor-Binding Domain Bound to the ACE2 Receptor. *Nature* **2020**, *581* (7807), 215–220. https://doi.org/10.1038/s41586-020-2180-5.
(58) Shang, J.; Ye, G.; Shi, K.; Wan, Y.; Luo, C.; Aihara, H.; Geng, Q.; Auerbach, A.; Li, F. Structural Basis of Receptor Recognition by SARS-CoV-2. *Nature* **2020**, *581* (7807), 221–224. https://doi.org/10.1038/s41586-020-2179-y.
(59) Shang, J.; Wan, Y.; Luo, C.; Ye, G.; Geng, Q.; Auerbach, A.; Li, F. Cell Entry Mechanisms of SARS-CoV-2. *Proc. Natl. Acad. Sci. U.S.A.* **2020**, *117* (21), 11727–11734. https://doi.org/10.1073/pnas.2003138117.
(60) Hou, Y. J.; Okuda, K.; Edwards, C. E.; Martinez, D. R.; Asakura, T.; Dinnon, K. H.; Kato, T.; Lee, R. E.; Yount, B. L.; Mascenik, T. M.; Chen, G.; Olivier, K. N.; Ghio, A.; Tse, L. V.; Leist, S. R.; Gralinski, L. E.; Schäfer, A.; Dang, H.; Gilmore, R.; Nakano, S.; Sun, L.; Fulcher, M. L.; Livraghi-Butrico, A.; Nicely, N. I.; Cameron, M.; Cameron, C.; Kelvin, D. J.; de Silva, A.; Margolis, D. M.; Markmann, A.; Bartelt, L.; Zumwalt, R.; Martinez, F. J.; Salvatore, S. P.; Borczuk, A.; Tata, P. R.; Sontake, V.; Kimple, A.; Jaspers, I.; O'Neal, W. K.; Randell, S. H.; Boucher, R. C.; Baric, R. S. SARS-CoV-2 Reverse Genetics Reveals a Variable Infection Gradient in the Respiratory Tract. *Cell* **2020**, *182* (2), 429-446.e14. https://doi.org/10.1016/j.cell.2020.05.042.
(61) Ahn, J. H.; Kim, J.; Hong, S. P.; Choi, S. Y.; Yang, M. J.; Ju, Y. S.; Kim, Y. T.; Kim, H. M.; Rahman, M. T.; Chung, M. K.; Hong, S. D.; Bae, H.; Lee, C.-S.; Koh, G. Y. Nasal Ciliated Cells Are Primary Targets for SARS-CoV-2 Replication in the Early Stage of COVID-19. *Journal of Clinical Investigation* **2021**, *131* (13), e148517. https://doi.org/10.1172/JCI148517.
(62) Wang, Y.; Wang, Y.; Luo, W.; Huang, L.; Xiao, J.; Li, F.; Qin, S.; Song, X.; Wu, Y.; Zeng, Q.; Jin, F.; Wang, Y. A Comprehensive Investigation of the MRNA and Protein Level of ACE2, the Putative Receptor of SARS-CoV-2, in Human Tissues and Blood Cells. *Int. J. Med. Sci.* **2020**, *17* (11), 1522–1531. https://doi.org/10.7150/ijms.46695.
(63) Liu, L.; Chopra, P.; Li, X.; Bouwman, K. M.; Tompkins, S. M.; Wolfert, M. A.; de Vries, R. P.; Boons, G.-J. Heparan Sulfate Proteoglycans as Attachment Factor for SARS-CoV-2. *ACS Cent. Sci.* **2021**, *7* (6), 1009–1018. https://doi.org/10.1021/acscentsci.1c00010.
(64) Clausen, T. M.; Sandoval, D. R.; Spliid, C. B.; Pihl, J.; Perrett, H. R.; Painter, C. D.; Narayanan, A.; Majowicz, S. A.; Kwong, E. M.; McVicar, R. N.; Thacker, B. E.; Glass, C. A.; Yang, Z.; Torres, J. L.; Golden, G. J.; Bartels, P. L.; Porell, R. N.; Garretson, A. F.; Laubach, L.; Feldman, J.; Yin, X.; Pu, Y.; Hauser, B. M.; Caradonna, T. M.; Kellman, B. P.; Martino, C.; Gordts, P. L. S. M.; Chanda, S. K.; Schmidt, A. G.; Godula, K.; Leibel, S. L.; Jose, J.; Corbett, K. D.; Ward, A. B.; Carlin, A. F.; Esko, J. D. SARS-CoV-2 Infection Depends on Cellular Heparan Sulfate and ACE2. *Cell* **2020**, *183* (4), 1043-1057.e15. https://doi.org/10.1016/j.cell.2020.09.033.
(65) Wei, C.; Wan, L.; Yan, Q.; Wang, X.; Zhang, J.; Yang, X.; Zhang, Y.; Fan, C.; Li, D.; Deng, Y.; Sun, J.; Gong, J.; Yang, X.; Wang, Y.; Wang, X.; Li, J.; Yang, H.; Li, H.; Zhang, Z.;

Wang, R.; Du, P.; Zong, Y.; Yin, F.; Zhang, W.; Wang, N.; Peng, Y.; Lin, H.; Feng, J.; Qin, C.; Chen, W.; Gao, Q.; Zhang, R.; Cao, Y.; Zhong, H. HDL-Scavenger Receptor B Type 1 Facilitates SARS-CoV-2 Entry. *Nat Metab* **2020**, *2* (12), 1391–1400. https://doi.org/10.1038/s42255-020-00324-0.

(66) Amraei, R.; Yin, W.; Napoleon, M. A.; Suder, E. L.; Berrigan, J.; Zhao, Q.; Olejnik, J.; Chandler, K. B.; Xia, C.; Feldman, J.; Hauser, B. M.; Caradonna, T. M.; Schmidt, A. G.; Gummuluru, S.; Muhlberger, E.; Chitalia, V.; Costello, C. E.; Rahimi, N. *CD209L/L-SIGN and CD209/DC-SIGN Act as Receptors for SARS-CoV-2*; preprint; Cell Biology, 2020. https://doi.org/10.1101/2020.06.22.165803.

(67) Thépaut, M.; Luczkowiak, J.; Vivès, C.; Labiod, N.; Bally, I.; Lasala, F.; Grimoire, Y.; Fenel, D.; Sattin, S.; Thielens, N.; Schoehn, G.; Bernardi, A.; Delgado, R.; Fieschi, F. DC/L-SIGN Recognition of Spike Glycoprotein Promotes SARS-CoV-2 Trans-Infection and Can Be Inhibited by a Glycomimetic Antagonist. *PLoS Pathog* **2021**, *17* (5), e1009576. https://doi.org/10.1371/journal.ppat.1009576.

(68) Rahimi, N. C-Type Lectin CD209L/L-SIGN and CD209/DC-SIGN: Cell Adhesion Molecules Turned to Pathogen Recognition Receptors. *Biology* **2020**, *10* (1), 1. https://doi.org/10.3390/biology10010001.

(69) Cantuti-Castelvetri, L.; Ojha, R.; Pedro, L. D.; Djannatian, M.; Franz, J.; Kuivanen, S.; van der Meer, F.; Kallio, K.; Kaya, T.; Anastasina, M.; Smura, T.; Levanov, L.; Szirovicza, L.; Tobi, A.; Kallio-Kokko, H.; Österlund, P.; Joensuu, M.; Meunier, F. A.; Butcher, S. J.; Winkler, M. S.; Mollenhauer, B.; Helenius, A.; Gokce, O.; Teesalu, T.; Hepojoki, J.; Vapalahti, O.; Stadelmann, C.; Balistreri, G.; Simons, M. Neuropilin-1 Facilitates SARS-CoV-2 Cell Entry and Infectivity. *Science* **2020**, *370* (6518), 856–860. https://doi.org/10.1126/science.abd2985.

(70) Daly, J. L.; Simonetti, B.; Klein, K.; Chen, K.-E.; Williamson, M. K.; Antón-Plágaro, C.; Shoemark, D. K.; Simón-Gracia, L.; Bauer, M.; Hollandi, R.; Greber, U. F.; Horvath, P.; Sessions, R. B.; Helenius, A.; Hiscox, J. A.; Teesalu, T.; Matthews, D. A.; Davidson, A. D.; Collins, B. M.; Cullen, P. J.; Yamauchi, Y. Neuropilin-1 Is a Host Factor for SARS-CoV-2 Infection. *Science* **2020**, *370* (6518), 861–865. https://doi.org/10.1126/science.abd3072.

(71) Gu, Y.; Cao, J.; Zhang, X.; Gao, H.; Wang, Y.; Wang, J.; He, J.; Jiang, X.; Zhang, J.; Shen, G.; Yang, J.; Zheng, X.; Hu, G.; Zhu, Y.; Du, S.; Zhu, Y.; Zhang, R.; Xu, J.; Lan, F.; Qu, D.; Xu, G.; Zhao, Y.; Gao, D.; Xie, Y.; Luo, M.; Lu, Z. Receptome Profiling Identifies KREMEN1 and ASGR1 as Alternative Functional Receptors of SARS-CoV-2. *Cell Res* **2022**, *32* (1), 24–37. https://doi.org/10.1038/s41422-021-00595-6.

(72) Lea, T. Caco-2 Cell Line. In *The Impact of Food Bioactives on Health*; Verhoeckx, K., Cotter, P., López-Expósito, I., Kleiveland, C., Lea, T., Mackie, A., Requena, T., Swiatecka, D., Wichers, H., Eds.; Springer International Publishing: Cham, 2015; pp 103–111. https://doi.org/10.1007/978-3-319-16104-4_10.

(73) Zhu, Y.; Chidekel, A.; Shaffer, T. H. Cultured Human Airway Epithelial Cells (Calu-3): A Model of Human Respiratory Function, Structure, and Inflammatory Responses. *Critical Care Research and Practice* **2010**, *2010*, 1–8. https://doi.org/10.1155/2010/394578.

(74) Desmyter, J.; Melnick, J. L.; Rawls, W. E. Defectiveness of Interferon Production and of Rubella Virus Interference in a Line of African Green Monkey Kidney Cells (Vero). *J Virol* **1968**, *2* (10), 955–961. https://doi.org/10.1128/jvi.2.10.955-961.1968.

(75) Thomas, P.; Smart, T. G. HEK293 Cell Line: A Vehicle for the Expression of Recombinant Proteins. *Journal of Pharmacological and Toxicological Methods* **2005**, *51* (3), 187–200. https://doi.org/10.1016/j.vascn.2004.08.014.

(76) Foster, K. A.; Oster, C. G.; Mayer, M. M.; Avery, M. L.; Audus, K. L. Characterization of the A549 Cell Line as a Type II Pulmonary Epithelial Cell Model for Drug Metabolism. *Experimental Cell Research* **1998**, *243* (2), 359–366. https://doi.org/10.1006/excr.1998.4172.

(77) Buchrieser, J.; Dufloo, J.; Hubert, M.; Monel, B.; Planas, D.; Rajah, M. M.; Planchais, C.; Porrot, F.; Guivel-Benhassine, F.; Van der Werf, S.; Casartelli, N.; Mouquet, H.; Bruel, T.; Schwartz, O. Syncytia Formation by SARS-CoV-2-infected Cells. *The EMBO Journal* **2020**, *39* (23). https://doi.org/10.15252/embj.2020106267.

(78) Liu, Y. D.; Goetze, A. M.; Bass, R. B.; Flynn, G. C. N-Terminal Glutamate to Pyroglutamate Conversion in Vivo for Human IgG2 Antibodies. *Journal of Biological Chemistry* **2011**, *286* (13), 11211–11217. https://doi.org/10.1074/jbc.M110.185041.
(79) Mozdzanowski, J.; Bongers, J.; Anumula, K. High-Yield Deblocking of Amino Termini of Recombinant Immunoglobulins with Pyroglutamate Aminopeptidase. *Analytical Biochemistry* **1998**, *260* (2), 183–187. https://doi.org/10.1006/abio.1998.2690.
(80) Yang, Y. Intramolecular Cyclization Side Reactions. In *Side Reactions in Peptide Synthesis*; Elsevier, 2016; pp 119–161. https://doi.org/10.1016/B978-0-12-801009-9.00006-9.
(81) Vijayan, D. K.; Zhang, K. Y. J. Human Glutaminyl Cyclase: Structure, Function, Inhibitors and Involvement in Alzheimer's Disease. *Pharmacological Research* **2019**, *147*, 104342. https://doi.org/10.1016/j.phrs.2019.104342.
(82) Kehlen, A.; Haegele, M.; Böhme, L.; Cynis, H.; Hoffmann, T.; Demuth, H.-U. N-Terminal Pyroglutamate Formation in CX3CL1 Is Essential for Its Full Biologic Activity. *Bioscience Reports* **2017**, *37* (4), BSR20170712. https://doi.org/10.1042/BSR20170712.
(83) GOREN, H. J.; BAUCE, L. G.; VALE, W. Forces and Structural Limitations of Binding of Thyrotrophin-Releasing Factor to the Thyrotrophin-Releasing Receptor: The Pyroglutamic Acid Moiety. *Mol Pharmacol* **1977**, *13* (4), 606.
(84) The UniProt Consortium; Bateman, A.; Martin, M.-J.; Orchard, S.; Magrane, M.; Agivetova, R.; Ahmad, S.; Alpi, E.; Bowler-Barnett, E. H.; Britto, R.; Bursteinas, B.; Bye-A-Jee, H.; Coetzee, R.; Cukura, A.; Da Silva, A.; Denny, P.; Dogan, T.; Ebenezer, T.; Fan, J.; Castro, L. G.; Garmiri, P.; Georghiou, G.; Gonzales, L.; Hatton-Ellis, E.; Hussein, A.; Ignatchenko, A.; Insana, G.; Ishtiaq, R.; Jokinen, P.; Joshi, V.; Jyothi, D.; Lock, A.; Lopez, R.; Luciani, A.; Luo, J.; Lussi, Y.; MacDougall, A.; Madeira, F.; Mahmoudy, M.; Menchi, M.; Mishra, A.; Moulang, K.; Nightingale, A.; Oliveira, C. S.; Pundir, S.; Qi, G.; Raj, S.; Rice, D.; Lopez, M. R.; Saidi, R.; Sampson, J.; Sawford, T.; Speretta, E.; Turner, E.; Tyagi, N.; Vasudev, P.; Volynkin, V.; Warner, K.; Watkins, X.; Zaru, R.; Zellner, H.; Bridge, A.; Poux, S.; Redaschi, N.; Aimo, L.; Argoud-Puy, G.; Auchincloss, A.; Axelsen, K.; Bansal, P.; Baratin, D.; Blatter, M.-C.; Bolleman, J.; Boutet, E.; Breuza, L.; Casals-Casas, C.; de Castro, E.; Echioukh, K. C.; Coudert, E.; Cuche, B.; Doche, M.; Dornevil, D.; Estreicher, A.; Famiglietti, M. L.; Feuermann, M.; Gasteiger, E.; Gehant, S.; Gerritsen, V.; Gos, A.; Gruaz-Gumowski, N.; Hinz, U.; Hulo, C.; Hyka-Nouspikel, N.; Jungo, F.; Keller, G.; Kerhornou, A.; Lara, V.; Le Mercier, P.; Lieberherr, D.; Lombardot, T.; Martin, X.; Masson, P.; Morgat, A.; Neto, T. B.; Paesano, S.; Pedruzzi, I.; Pilbout, S.; Pourcel, L.; Pozzato, M.; Pruess, M.; Rivoire, C.; Sigrist, C.; Sonesson, K.; Stutz, A.; Sundaram, S.; Tognolli, M.; Verbregue, L.; Wu, C. H.; Arighi, C. N.; Arminski, L.; Chen, C.; Chen, Y.; Garavelli, J. S.; Huang, H.; Laiho, K.; McGarvey, P.; Natale, D. A.; Ross, K.; Vinayaka, C. R.; Wang, Q.; Wang, Y.; Yeh, L.-S.; Zhang, J.; Ruch, P.; Teodoro, D. UniProt: The Universal Protein Knowledgebase in 2021. *Nucleic Acids Research* **2021**, *49* (D1), D480–D489. https://doi.org/10.1093/nar/gkaa1100.
(85) Rich, R. L.; Myszka, D. G. Higher-Throughput, Label-Free, Real-Time Molecular Interaction Analysis. *Analytical Biochemistry* **2007**, *361* (1), 1–6. https://doi.org/10.1016/j.ab.2006.10.040.
(86) Lad, L.; Clancy, S.; Kovalenko, M.; Liu, C.; Hui, T.; Smith, V.; Pagratis, N. High-Throughput Kinetic Screening of Hybridomas to Identify High-Affinity Antibodies Using Bio-Layer Interferometry. *SLAS Discovery* **2015**, *20* (4), 498–507. https://doi.org/10.1177/1087057114560123.
(87) Syahir, A.; Usui, K.; Tomizaki, K.; Kajikawa, K.; Mihara, H. Label and Label-Free Detection Techniques for Protein Microarrays. *Microarrays* **2015**, *4* (2), 228–244. https://doi.org/10.3390/microarrays4020228.
(88) Nirschl, M.; Reuter, F.; Vörös, J. Review of Transducer Principles for Label-Free Biomolecular Interaction Analysis. *Biosensors (Basel)* **2011**, *1* (3), 70–92. https://doi.org/10.3390/bios1030070.
(89) Kamat, V.; Rafique, A. Designing Binding Kinetic Assay on the Bio-Layer Interferometry (BLI) Biosensor to Characterize Antibody-Antigen Interactions. *Analytical Biochemistry* **2017**, *536*, 16–31. https://doi.org/10.1016/j.ab.2017.08.002.

(90) Frenzel, D.; Willbold, D. Kinetic Titration Series with Biolayer Interferometry. *PLOS ONE* **2014**, *9* (9), e106882. https://doi.org/10.1371/journal.pone.0106882.
(91) Shah, N. B.; Duncan, T. M. Bio-Layer Interferometry for Measuring Kinetics of Protein-Protein Interactions and Allosteric Ligand Effects. *JoVE* **2014**, No. 84, 51383. https://doi.org/10.3791/51383.
(92) *Biosafety in Microbiological and Biomedical Laboratories—6th Edition*, 6th ed.; U.S. Department of Health and Human Services, 2020.
(93) Li, Q.; Liu, Q.; Huang, W.; Li, X.; Wang, Y. Current Status on the Development of Pseudoviruses for Enveloped Viruses. *Rev Med Virol* **2018**, *28* (1). https://doi.org/10.1002/rmv.1963.
(94) Chen, M.; Zhang, X.-E. Construction and Applications of SARS-CoV-2 Pseudoviruses: A Mini Review. *Int. J. Biol. Sci.* **2021**, *17* (6), 1574–1580. https://doi.org/10.7150/ijbs.59184.
(95) Salazar-García, M.; Acosta-Contreras, S.; Rodríguez-Martínez, G.; Cruz-Rangel, A.; Flores-Alanis, A.; Patiño-López, G.; Luna-Pineda, V. M. Pseudotyped Vesicular Stomatitis Virus-Severe Acute Respiratory Syndrome-Coronavirus-2 Spike for the Study of Variants, Vaccines, and Therapeutics Against Coronavirus Disease 2019. *Front Microbiol* **2021**, *12*, 817200. https://doi.org/10.3389/fmicb.2021.817200.
(96) Whelan, S. P. J. Vesicular Stomatitis Virus. In *Encyclopedia of Virology*; Elsevier, 2008; pp 291–299. https://doi.org/10.1016/B978-012374410-4.00529-X.
(97) Wessel, D.; Flügge, U. I. A Method for the Quantitative Recovery of Protein in Dilute Solution in the Presence of Detergents and Lipids. *Analytical Biochemistry* **1984**, *138* (1), 141–143. https://doi.org/10.1016/0003-2697(84)90782-6.
(98) Tian, X.; Li, C.; Huang, A.; Xia, S.; Lu, S.; Shi, Z.; Lu, L.; Jiang, S.; Yang, Z.; Wu, Y.; Ying, T. Potent Binding of 2019 Novel Coronavirus Spike Protein by a SARS Coronavirus-Specific Human Monoclonal Antibody. *Emerging Microbes & Infections* **2020**, *9* (1), 382–385. https://doi.org/10.1080/22221751.2020.1729069.
(99) Moore, M. J.; Dorfman, T.; Li, W.; Wong, S. K.; Li, Y.; Kuhn, J. H.; Coderre, J.; Vasilieva, N.; Han, Z.; Greenough, T. C.; Farzan, M.; Choe, H. Retroviruses Pseudotyped with the Severe Acute Respiratory Syndrome Coronavirus Spike Protein Efficiently Infect Cells Expressing Angiotensin-Converting Enzyme 2. *J Virol* **2004**, *78* (19), 10628–10635. https://doi.org/10.1128/JVI.78.19.10628-10635.2004.
(100) Towler, P.; Staker, B.; Prasad, S. G.; Menon, S.; Tang, J.; Parsons, T.; Ryan, D.; Fisher, M.; Williams, D.; Dales, N. A.; Patane, M. A.; Pantoliano, M. W. ACE2 X-Ray Structures Reveal a Large Hinge-Bending Motion Important for Inhibitor Binding and Catalysis. *Journal of Biological Chemistry* **2004**, *279* (17), 17996–18007. https://doi.org/10.1074/jbc.M311191200.
(101) Zimmer, B.; Summermatter, K.; Zimmer, G. Stability and Inactivation of Vesicular Stomatitis Virus, a Prototype Rhabdovirus. *Veterinary Microbiology* **2013**, *162* (1), 78–84. https://doi.org/10.1016/j.vetmic.2012.08.023.

UNIVERSITÉ CATHOLIQUE DE LOUVAIN
Faculté des sciences
Place des sciences, 2 bte L6.06.01, 1348 Louvain-la-Neuve, Belgique | **www.uclouvain.be/sc**